GEOLOGIE • UMWELT • ROHSTOFFE • BAUGRUND

JENA-GEOS®-Ingenieurbüro GmbH · Saalbahnhofstraße 25 c · 07743 Jena

Fachbeiträge der JENA-GEOS® Nº 01/2019

JG	STAUNER, M.: The Impact of Climate Change on the Potentials of Regenerative Energy Systems in Lower Franconia, Bavaria – JENA-GEOS, Fachbeiträge, Jg. 2019, Band 1	2019/01

TECHNISCHE UNIVERSITÄT MÜNCHEN

MASTER THESIS

The Impact of Climate Change on the Potentials of Regenerative Energy Systems in Lower Franconia, Bavaria

SCIENTIFIC WORK OF THE STUDY PROGRAM
MASTER OF SCIENCE IN ENVIRONMENTAL ENGINEERING
IN COLLABORATION WITH THE CHAIR OF ECOCLIMATOLOGY
OF THE DEPARTMENT OF CIVIL, GEO AND ENVIRONMENTAL ENGINEERING
OF THE TECHNICAL UNIVERSITY OF MUNICH
AND THE CHAIR OF GEOGRAPHY
OF THE DEPARTMENT OF GEOSCIENCE
OF THE LUDWIG–MAXIMILIANS-UNIVERVITY MUNICH

Supervised by

Prof. Dr. Ralf Ludwig, Ludwig–Maximilians–University Munich
Prof. Dr. Anette Menzel, Technical University of Munich

Submitted by

Manoel Stauner
Student ID: 03634050
Email: mano.stauner@gmx.de

Date of Submission *06.12.2019*

Declaration of Academic Honesty

I, Manoel Stauner, hereby declare that the thesis submitted, titled "*The Impact of Climate Change on the Potentials of Regenerative Energy Systems in Lower Franconia, Bavaria*", is solely my own unaided work and that every text passage, figure or diagram from books, papers, the web or any other source copied or in any other way used has been acknowledged and fully cited.

I am aware that the thesis in digital form can be examined for the use of unauthorized aid and in order to determine whether the thesis as a whole or parts incorporated in it may be deemed as plagiarism. For the comparison of my work with existing sources I agree that it shall be entered in a database where it shall also remain after examination, to enable comparison with future theses submitted. Further rights of reproduction and usage, however, are not granted here.

This thesis was not previously presented to another examination board and has not been published.

First and last name City, Date and Signature

Acknowledgments

First of all, I particularly would like to thank Prof. Dr. Ralf Ludwig at the Chair of Geography, Ludwig-Maximilians-University Munich for giving me the opportunity on working on this interesting and enriching project. I am convinced that this topic will be very relevant for the future.

I am also grateful to Prof. Dr. Ralf Ludwig for giving me the chance visiting Alberta, Canada and being part of Abby-Net in which I could extend my knowledge in energy systems under changing environmental conditions by interdisciplinary people and topics.

I also would like to express my warmest gratitude to my life partner Jana Müller who encouraged me with nice words and supported me whenever it was needed.

In addition, I would like to acknowledge the cooperation with the Chair of Ecoclimatology, especially Prof. Dr. Menzel and Dr. Nicole Estrella, who took over the official supervision from the TUM side.

Table of Contents

Acronyms and Abbreviations

Table 1 Acronyms and Abbreviations in the thesis

Abbreviation	Full name
PV	Photovoltaic
CO_2	Carbon dioxide
kba	R1-r1i1p1
kbk	R2-r1i1p1
Kbm	R2-r3i1p1
Kcm	R4-r9i1p1
kbu	R3-r1i1p1
W	Würzburg
S	Schweinfurt
Ke	Kemmern
St	Steinbach
Kr	Krotzenburg
Kl	Kleinheubach
Ta	Tauberbischofsheim
Sh	Sachsenheim
Wo	Wolfsmünster
Sa	Salz
Bk	Bad Kissingen
E	Electric Energy
P	Power performance
GCM	General Circulation Model
IDW	Inverse Distance Weighting Method
EEG	Renewable Energy Law
RCM	Regional Climate Model
RCP	Representative Concentration Pathway

List of Figures

List of Tables

Abstract

Climate change is of ongoing public and scientific interest. By a continuous increase of anthropogenic trace gases in the atmosphere, resulting from conventional energy sources by a significant proportion, the radiation budget alternates and forces climate parameters to an ongoing shift enhanced by an increased accumulation of water vapour and greenhouse gases in the atmosphere (Taylor & Penner, 1994), which leads to the effect of global warming (Pvamanarhan, Barksrrom, & Harruison, 1989).

To counteract this effect and to slow down the accumulation of CO_2 in the atmosphere, renewable energies play a significant role in the concept of the energy transition, known as the 'Energiewende' (Quaschning, 2015a). Key elements for this transition, from conventional energy sources to green energy, are in progress by the expansion of regenerative energy systems combined with the construction of energy storages (Geoffrey, Hammond, & Pearson, 2013). It could be said, "Renewable energy is the fastest growing energy source of Europe" (Teske, personal communication, October 2012).

The scope of this master thesis covers comprehensive analysis of climate parameters and the technology of renewable energy systems within the study area of Lower Franconia, which was carried out to assess and evaluate the future energy generation by regenerative systems. Climate parameters were analysed not only with respect to the present time period but also with respect to modelled future scenarios regarding different initial conditions. By the creation of individual power plans for the systems photovoltaic (PV), wind turbines and run – of – river plants, a comparison could be made between present and future energy generation.

The results of the thesis revealed that most of the climate parameters will change in the future. In general, an increase in global radiation as well as in temperature will occur, whereas the discharge and water level will decline. Regarding the wind speed only a slight shift to decreased wind forces was determined. However, the size of these climate changes depends locally. By analysing the values of present climate parameters and differentiating the study area into characteristic climate catchment areas, depending on geographical, climatological and energetic conditions, power plans for the determination of the energy generation of the single renewable systems could be created. In regard of the energy output, these power plans compared the energy generation from the present and future state. Hence, it could be stated, that a slightly increase in power generation by PV-modules will occur, whereas a dramatically drop in energy generation by run–of–river plants within the study area will appear. In terms of wind power also a slightly decrease in power generation will arise. Beside the change of climate parameters regarding global radiation, temperature, wind speed, discharge and water level, the technology of existing regenerative systems supposed to be a main cause for the energy generation change. Finally, based on these findings, and outlook and recommendations for a possible future were presented.

Zusammenfassung

Der Klimawandel ist von anhaltendem öffentlichem und wissenschaftlichem Interesse. Durch einen kontinuierlichen Anstieg der anthropogenen Spurengase in der Atmosphäre, der unter anderem durch konventionelle Energiequellen verursacht wird, ändert sich das Strahlungsbudget und zwingt die Klimaparameter zu einer kontinuierlichen Verschiebung, die durch eine erhöhte Anreicherung von Wasserdampf und Treibhausgasen in der Atmosphäre verstärkt wird (Taylor & Penner, 1994). Dies führt zu einer globalen Erwärmung (Pvamanarhan et al., 1989).

Um diesem Effekt entgegenzuwirken und die Ansammlung von CO_2 in der Atmosphäre zu verlangsamen, nehmen die erneuerbare Energien eine wichtige Rolle im Konzept der Energiewende inne. Der Begriff der sogenannten "Energiewende" wurde geboren (Volker Quaschning, 2015). Schlüsselelemente für diesen Übergang von konventionellen Energiequellen zu Ökostrom sind der Ausbau regenerativer Energiesysteme in Verbindung mit dem Bau von Energiespeichern (Geoffrey et al., 2013). Man könnte sagen: "Erneuerbare Energien sind die am schnellsten wachsende Energiequelle Europas" (Teske, 2012).

Im Rahmen dieser Masterarbeit wird sich mit einer umfassende Analyse der Klimaparameter und der Technologien erneuerbarer Energiesysteme im Untersuchungsgebiet Unterfranken befasst, die zur Beurteilung und Bewertung der zukünftigen Energieerzeugung durch regenerative Energiesysteme durchgeführt wurde. Klimaparameter wurden nicht nur in Bezug auf den aktuellen Zeitraum, sondern auch in Bezug auf modellierte Zukunftsszenarien zu unterschiedlichen Ausgangsbedingungen analysiert. Durch die Erstellung individueller Leistungspläne für die Systeme Photovoltaik, Windkraftanlagen und Laufwasserkraftwerken konnte ein Vergleich zwischen aktueller und zukünftiger Energieerzeugung durchgeführt werden.

Die Ergebnisse der Arbeit zeigten, dass sich die meisten Klimaparameter in der Zukunft ändern werden. Im Allgemeinen kommt es zu einem Anstieg der Globalstrahlung und der Temperatur, während der Abfluss und der Wasserstand sinken. Bezüglich der Windgeschwindigkeit wurde nur eine leichte Verschiebung zu geringeren Windkräften festgestellt. Das Ausmaß dieser Klimaänderungen hängt jedoch von lokalen Gegebenheiten ab. Durch die Analyse der Werte der aktuellen Klimaparameter und die Differenzierung des Untersuchungsgebietes in charakteristische Klimaeinzugsgebiete, abhängig von den geografischen, klimatologischen und energetischen Bedingungen, konnten Leistungspläne zur Bestimmung der Energieerzeugung der einzelnen erneuerbaren Systeme erstellt werden. Im Hinblick auf die Energieausbeute verglichen diese Leistungspläne die Energieerzeugung aus dem gegenwärtigen und zukünftigen Zustand. Ergo, könnte es zu einem leichten Anstieg der Stromerzeugung durch Photovoltaik - Module kommen, während ein drastischer Rückgang in der Energieerzeugung durch den Betrieb von Flusskraftwerken zu verzeichnen sein wird. Bei der Windenergie wird sich ebenfalls ein leichter Rückgang der Stromerzeugung ergeben. Neben den sich ändernden Größen der Klimaparameter Globalstrahlung, Temperatur, Windgeschwindigkeit, Abfluss und Wasserstand soll die Technologie bestehender regenerativer Systeme eine weitere Ursache für den Wandel der Energieerzeugung sein. Schließlich wurden auf der Grundlage dieser Ergebnisse Perspektiven und Empfehlungen für eine mögliche Zukunft vorgestellt.

1 Introduction

The rapid increase of human population coupled with the increase in energy consumption is a paradox to future climate targets imposed by almost every government. In the past, energy for heating and electricity came from conventional energy sources, as fossil fuels. Due to the urgency in the climate crisis, the approach to energy production shifted. The energy transition, known as the 'Energiewende' was born. The origin of the 'Energiewende' resulted from the anti-nuclear power program in 1970, but gained a rapid progress under the government of the red and green party (1998–2005) (Jacobsson & Lauber, 2006). The cost allocation of the renewable energy law drove the green energy sector and the share of renewable energies rose from 29 TWh (1999) to 161 TWh (2014) in gross electricity generation, while the nuclear power and coal power production sank (AGEB Arbeitsgemeinschaft Energiebilanzen, 2015). Figure 1 shows the net electricity generation in the first half of the year 2019. It was noticeable, that in comparison between the first halfs of the year 2018 and 2019, the proportion of conventional energy sources as nuclear energy (- 0,1 TWh; - 0,3 %), brown coal (- 13,8 TWh; - 20,7 %) and hard coal (- 8,2 TWh; - 23,7 %) decreased, whereas renewable energies yielded, as for wind power an increase of 10,8 TWh (+ 19,2 % and for solar power 1,8 TWh (+ 5,6 %) could be stated. In general, the share of net electricity generation makes out almost the half of the total (125,3 TWh; 47,3 %) in the first half of the year 2019 (Burger, 2019).

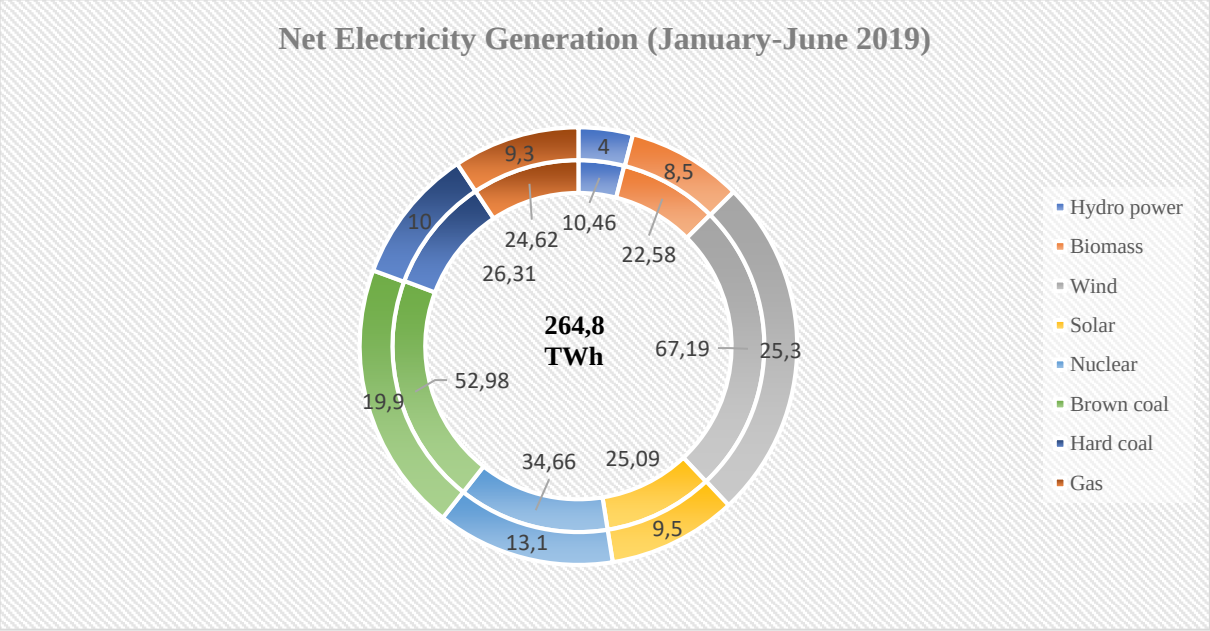

Figure 1 Net electricity generation within the first half of the year 2019 (January-June) (Burger, 2019).

Looking at the electricity generation, the share of renewable energies is growing fast. Between 2000 – 2017 the electricity generation of renewables put on 27 % in Germany, while the increase was limited to 6 % worldwide. Therefore, in the year 2017 wind power contributed the highest share, 49 % of electricity generation from renewable energies and kept the most important regenerative energy source, followed by photovoltaic with 18 % and hydropower, which contributed 9 %. Figure 2 displays the rise of proportion of wind power and photovoltaic within the period 2000 – 2017 (BDEW Bundesverband der Energie- und Wasserwirtschaft, 2018).

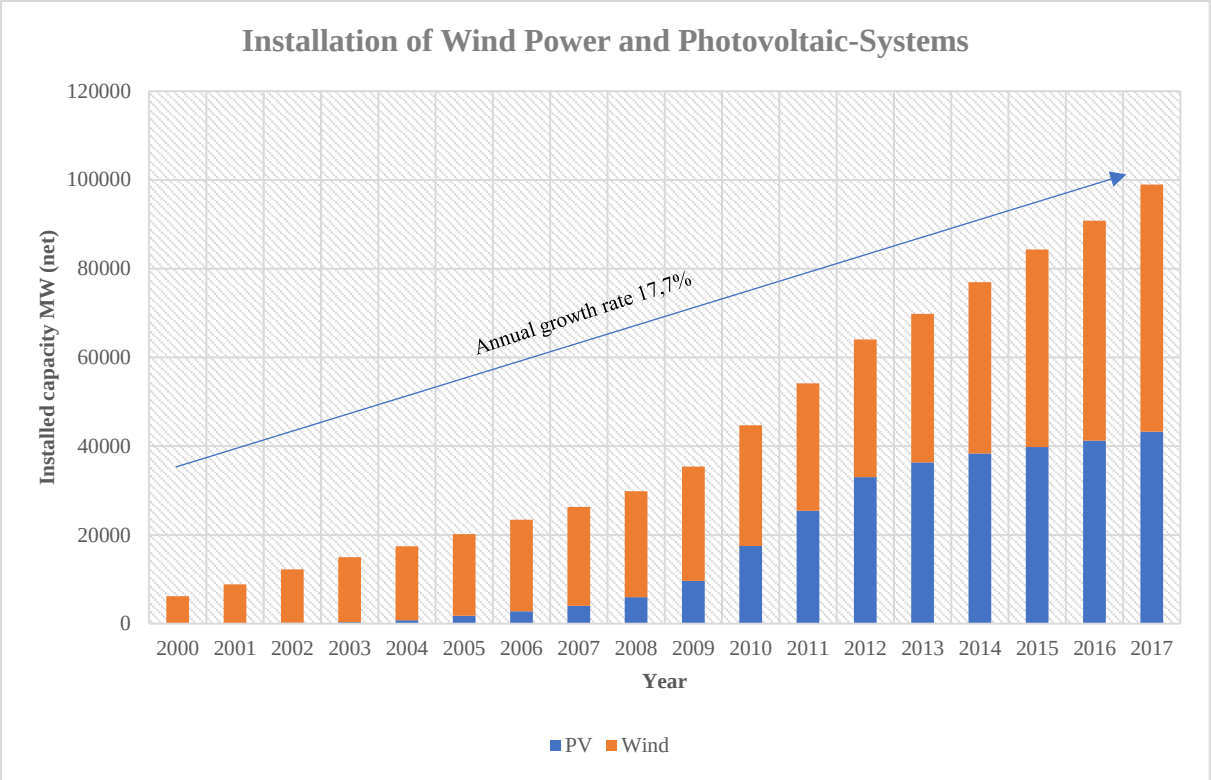

Figure 2 Expansion of installed capacity of PV and wind turbines within the time period 2000 – 2017 (BDEW Bundesverband der Energie- und Wasserwirtschaft, 2018).

This effect could be accounted to the renewable energy law ('EEG'). Picked out as a central theme in this stated law were the distribution effects as well as the integration of wind- and solar energy into the power supply (Schiffer, 2019). Beside the steady growth rate, renewable energies must deal with challenges, which needed to be stated. The generation of renewable energies suffer from temporal fluctuations. As an example, hydropower depends on the quantities of precipitation and evaporation in the catchment area and other physical and geographical conditions. Solar- and wind energy are exposed to irregularities and strongly depend on the geographical area as well as on climate parameters as radiation, temperature and wind force. Thus, those energy forms offer a low secured performance. By an increasing expansion of wind turbines, the supply of wind energy exceeds the receptivity of the power grid, which leads to an urgency of expansion of the power grid in north and south direction in Germany. The same challenge occurs by photovoltaic. Furthermore, technological solutions needed to be found to challenge the volatility of the electricity generation from renewable energies, especially mentioned wind power and photovoltaic. If it is possible in the future to ensure a steady renewable electricity generation by the expansion of the power grid and storage technologies, renewable energies could fully replace conventional energy forms (Schiffer, 2019).

Renewable energies directly depend on climate parameters. How will they evolve in the future? Controlled by the global radiation, atmospheric and thermohaline circulations underly an ongoing process and determine, amongst others, the climate. Natural trace gases absorb and emit radiation at certain wave lengths and ensure the increase of the average earth temperature from - 18°C to + 15°C. In an historical point of view, an alteration of cold- and warm phases, including a natural greenhouse effect, took place on earth. However, nowadays anthropogenic greenhouse gases are added to the natural ones and enhancing the warming of the atmosphere

(Niebert, 2010). Hence, future climate will be affected by climate change. “Climate change refers to any change in climate over time, whether due to natural variability or as a result on human activity” (IPCC, 2007). Therefore, climate change and global warming will determine certain climate parameters as radiation, temperature, wind force and precipitation, which in turn directly affect the potential of renewable energies.

Within the scope of this thesis a link between climate parameters and energy generation by regenerative energy system applied to the study area Lower Franconia was drawn. The region was subdivided into several climate catchment areas depending on their geographical, climatological and energetic attributes. Climate parameters were analysed within three 20 – year cycles. On the one hand, parameters were determined within a present period (2000 – 2019), which was based on observations and measurements and on the other hand within a reference (1991 – 2010) and future period (2071 – 2090) based on a general circulation model (GCM), known as CanESM2. Thereby, the parameters global radiation, wind speed, temperature, discharge and water level were covered by comprehensive analytics and harmonized through the different periods by adapting the different created catchment areas, area–weighting and by applying a delta method. Apart from climate parameters, an identification of installed renewable energy systems within the study area took place. Thereby, the location and technical properties of these were investigated and graphically and statistically determined. Analysed climate and technological parameters from the present period were used in establishing tailored power plans for the different researched regenerative energy systems as PV–systems, wind turbines and hydro power plants. Modelling the future climate, five members were selected, which state different initial conditions for the climate model. Hence, five scenarios were illustrated regarding a reference and two extreme situations for global radiation and a dry and wet scenario in the future based on discharge. By the application of the modelled and statistically analysed future climate parameters on the existing renewable energy systems within the study area, a statement about the future energy generation could be made and afterwards compared with the present state.

Thus, this work dealt with different techniques and potentials of renewable energy systems, the interplay of these components and both - present and future climate variables. The example of Lower Franconia finally gave an outlook for the period from 2071 to 2090.

2 Background – Description of the Study Area

As the focus of this thesis is the potential of renewable energy technologies based on present and future climate parameters, it is important to describe and understand factors which were influencing the local climate situation in addition to the locally constructed renewable energy systems. Therefore, within this section, a brief overview of geography and hydrology, climate as well as regenerative energy systems was given.

2.1 Geographical Location and Hydrology

The study area was defined as the region of under Franconia and is situated in the northwest of the state of Bavaria between ~ 49°29'58'' N – 50°33'40'' N latitude and ~ 9°2'3'' E – 10°52'35'' E longitude. Under Franconia covers an area of 8.531 km² and its capital is called 'Würzburg'. The region borders the states Baden-Wurttemberg & Hesse in the south and west, Thuringia in the north and the regions Over Franconia and Middle Franconia in the east. In general, the entire region is characterized by a mix of barren topography and major physiographic units as valley fills, the catchment area of the river Main and the mountain ranges Spessart (west), Rhön (north), Frankenwald and Steigerwald (east) (Figure 3).

Lower Franconia is intersected by the river Main, which arises from the tributaries 'Roter Main' (580 m.a.s.l.) and 'Weißer Main' (887 m.a.s.l.) with a bed slope of ~ 1,5 ‰ (Google Maps, 2019) and a catchment area of ~ 27,292 km² (Gewässerkundlicher Dienst Bayern, 2019). Within the scope of the study area the river Main runs through the ridges of 'Steigerwald', the 'Main-Franconian hill country plates' and the 'Spessart'. It borders the catchment area of 'Weser' in the north and connects upstream to the catchment area 'Upper Main' (catchment area ~ 4.400 km²). The rivers Regnitz (~ 7000 km²) and Tauber (~ 1800 km²) flow into the Main in the south. The area covers ~ 10.500 km² with a maximum in erection of ~ 170 km in east – west and ~ 100 km in north–south direction (Blasy & Overland, 2005). In accordance to the beginning of the study area in Kemmern until the outflow in Krotzenburg the following could be stated: The flow path was determined to ~ 312 km, whereas the height difference along both points was ascertained to ~ 276 hm (Google Maps, 2019). The normal dammed upstream water was valued to a height difference of ~ 135 hm. Regarding to the discharge, six water gauges were relevant within the region of Under Franconia. Therefore, the average yearly discharge within the time period (2000 – 2019) between Kemmern (45 m³/s) and Kleinheubach (175 m³/s) increased with the river flow. Contrariwise, the water level decreased starting from Kemmern (277 cm) until the gauge at Krotzenburg (145 cm) (Gewässerkundlicher Dienst Bayern, 2019).

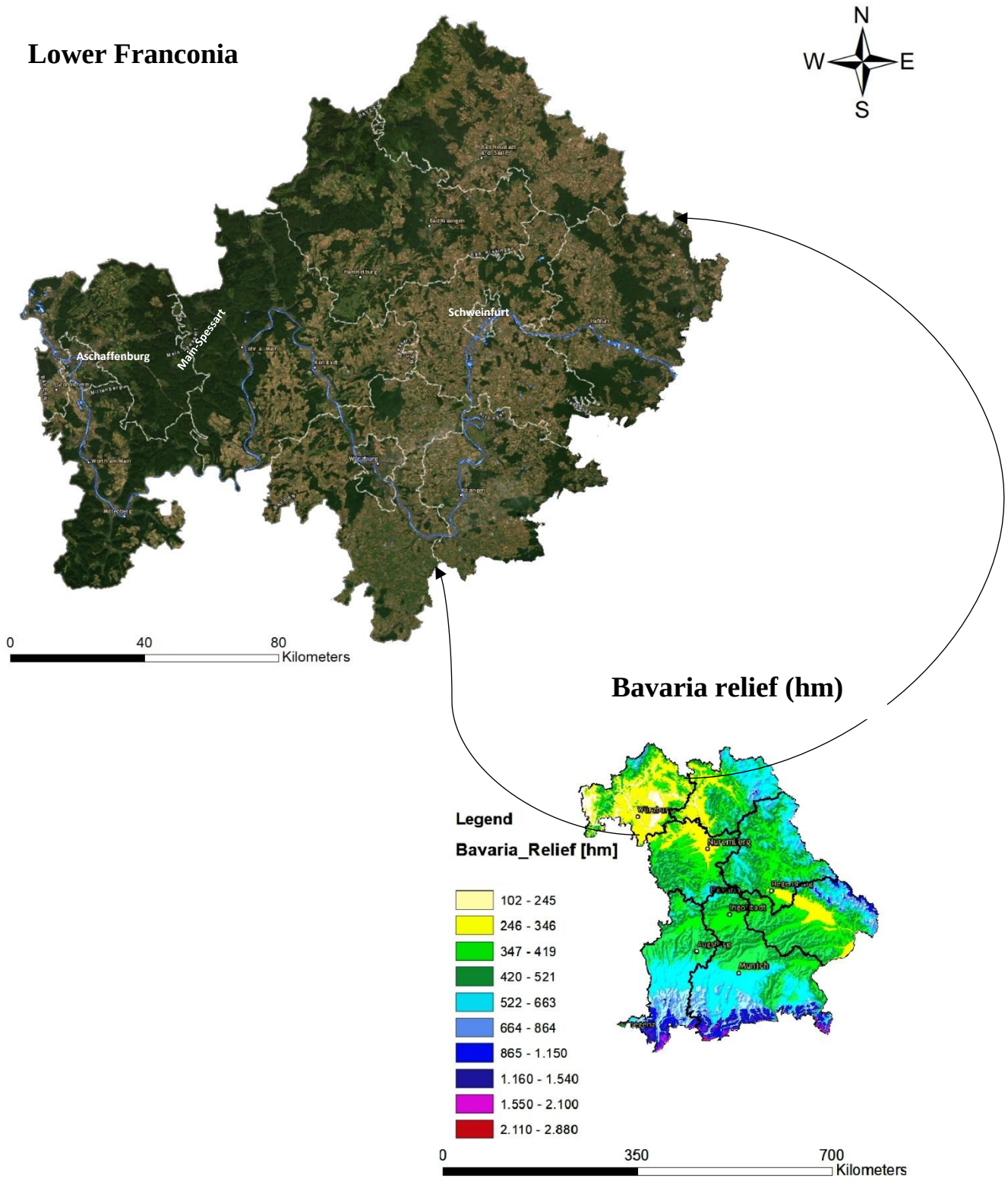

Figure 3 Location of study area Lower Franconia. Coordinate system: DHDN_3_Degree_Gauss_Zone_4; Projection: Gauss_Kruger. Source: Own figure based on Geodata: Esri, DigitalGlobe, GeoEye, Earthstar Geographics, CNES/Airbus DS, USDA, USGS, AeroGRID, IGN, and the GIS User Community (ESRI, 2019).

2.2 Theoretical Background to Climate Change

"Climate is the spatio-temporal totality of the possible instantaneous states of the atmosphere" (Gerstengarbe & Peter, 2007). Related to this, a physical law of conservation of energy applies: the radiation arriving on the surface minus the reflective component is equal to the thermal radiation emitted by the earth. With the help of the oceans and the atmosphere, the heat is distributed within the climate system and plays an important role in the regional climate. Climate change results from the changes in this energy balance, which is caused by three fundamental possibilities. First, the incoming solar radiation may vary due to changes in orbit around the sun or in the sun itself. Second, the proportion reflected into space can change. This happens due to albedo. Third, outgoing heat radiation is affected by the content of the atmosphere of absorbing gases, often greenhouse gases, and aerosols. Natural and anthropogenic processes drive the exchange of gases between the earth and the atmosphere. These include water vapor, oxygen and carbon dioxide. In the course of geological history, the climate was dominated by alternating cold and warm periods, which were mostly initiated by natural processes. However, in the recent period of geological history, especially in the history of mankind, there has been more intense warming due to greenhouse gases. "Warming of the climate system is in no doubt, and since the 1950s, many of the observed changes are unprecedented over decades to millennia ['000 years]" (Stocker, 2014). Gases such as CO_2, N_2O and CH_4 absorb radiation from the earth's surface, clouds and gas molecules and store them as heat in the lower layers of the atmosphere. Due to the increase of the world population and their activities with industrialization, agriculture, deforestation and the burning of fossil fuels, high amounts of greenhouse gases have been released. This has the effect of disrupting the natural balance between atmospheric gas and creating a general trend towards increased heat storage and hence global warming. The fact that the gases are easily distributed through the atmospheric circulation influences the whole planet. Thus, one can speak of global warming, which will be exacerbated by anthropogenic influences.

2.3 Climate of the Study Area

Lower Franconia is located within the transition region of the maritime climate of Western Europe to the continental climate of Eastern Europe. The influence of the ocean is being reduced to the southeast and the climate is taking on continental traits. While the maritime climate is rather characterized by mild winters, cool summers and higher humidity, continental climate is dominated by cold winters, hot summers and a lower humidity (Bayerisches Landesamt für Umwelt, 2018b). As mentioned in the chapter '*Geographical location and hydrology'*, Under Franconia is surrounded by low mountain ranges. As a result, the region falls characteristically under the name of the Lower Franconian dry plain. The elevations force the attracting clouds, driven by atmospheric circulation, to ascend to higher and colder strata and to downgrade due to the increasing condensation. As a result, the precipitation usually does not reach the region around Schweinfurt. Due to the warm to hot summers and the concomitant increase in evaporation, the effect of a low water supply from the river Main is enhanced (Rapp, 2000). Based on 'Würzburg' and according to the period procedure, whereas the average was recorded within the period between 2000 – 2019 and the maximum and minimum between 1947 – 2019, following could be stated: The average annual temperature was determined to 9,7 °C, whereas

the maximum was stated to 11,7 °C in 2018 and the minimum to 7,6 °C in 1956. Furthermore, it was to mention, that the highest monthly temperature (23,4 °C in August 2003) as well as the maximum temperature (39,4 °C on the 7th of August 2015) were all recorded within the 21st century. The annual sunshine hours were determined to 1640 h, while the maximum in yearly (2188,5 h in 2003) and monthly (336,1 h in July 2006) observation lay within the 21st century as well. Related to the annual rainfall, the quantity of precipitation was observed in average to 634,2 mm/year in the period of the latest 20 years (2000 – 2019). The yearly maximum was valued to 1092,4 mm (1965) and the monthly maximum 197,6 mm (June 1992) (DWD, 2019). Regarding solar radiation, it had to be distinguished between direct and diffuse radiation. The combination of both results in the global radiation. For the region Lower Franconia, the global radiation was determined to 1112,5 kWh/m² in average per year. A further important parameter is the wind force, with an ascertained value of 2,81 m/s in average per year (Chapter '*Climate Parameters*').

2.4 Background to Usage Possibilities of Renewable Energies

The supply of final energy or useful energy from regenerative energy is based on energy flows radiated by the sun. This work deals with three forms of regenerative energy supply. (1) The photovoltaic conversion of sunlight into electrical energy (photovoltaic systems). (2) The use of wind energy for power generation (wind turbines). (3) The generation of electricity from hydropower for the provision of electrical energy (hydroelectric power plants). For the utilization of the regenerative energy supply, the respective physical and technical contexts for energy conversion are decisive, described by the grade of efficiency and the degree of utilization. The efficiency is defined as the ratio between the output power and the power used, depending on the operating condition of a system and other factors that vary over a period of time. The degree of utilization is defined as the quotient of the energy that can be used in a certain period of time (e.g. breaks, idling, etc.) and the total energy supplied.

To provide energy through renewable energy systems, an economic and ecological analysis is important. For economic analysis, the cost of providing energy is an important parameter, whereas the ecological analysis is based on environmental aspects and sustainability, such as the production and dispose of installations or the visual impacts of wind turbines.

The possibilities of regenerative energy supply to meet the energy demand could be differentiated into three main potentials: The theoretical, the technical and the economic potential. The theoretical potential is defined as the regenerative energy that can theoretically and physically be harnessed within a region at a given time (e.g. the kinetic energy of the wind over the year). The technical potential describes the proportion of theoretical potential that can be used in consideration of technical possibilities. The economic potential refers to the technical share of the potential that can be used economically in the context of the given energy-economic framework conditions.

The energy flow of the earth is mainly fed from the solar energy. With 99.9 %, solar energy accounts for the largest share of the total energy converted on earth. The energy radiated from the sun to the earth is weakened within the atmosphere and partially transformed into a variety of other forms of energy and effects and is thus responsible for the evaporation and precipitation,

wind and waves (Kaltschmitt, 2006). Furthermore, over the course of millions of years, solar radiation has produced fossil fuels such as coal, oil and natural gas.

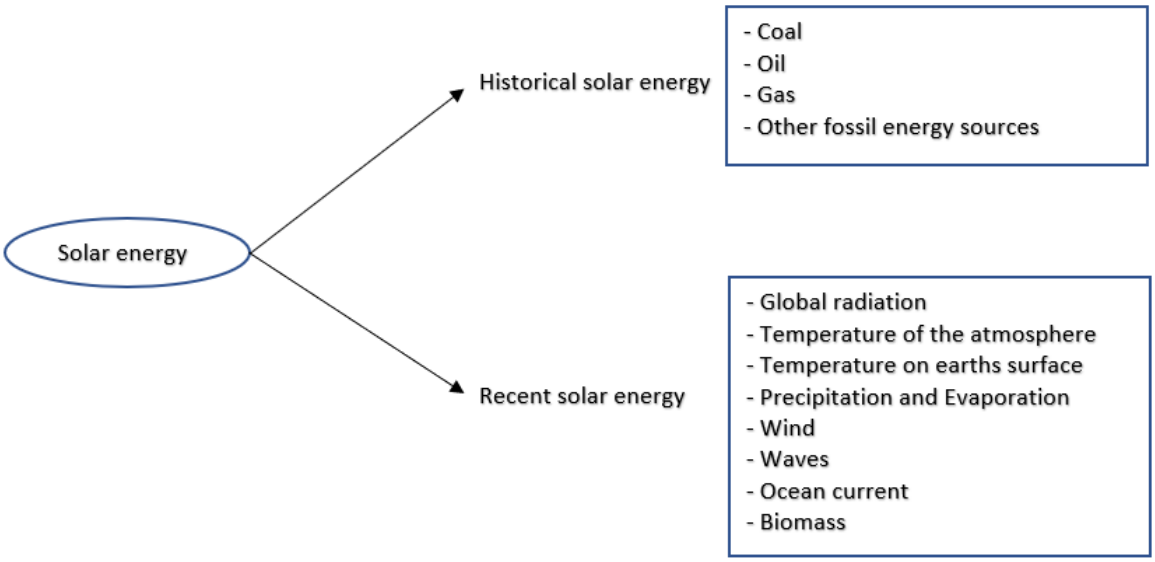

Figure 4 Energy sources and their impacts. Own figure. Source (Kaltschmitt, 2006).

Global radiation can be used in three different ways with respect to renewable energy systems. For the direct use of solar energy, solar thermal heat and photovoltaic power can be generated. The resulting wind forces can be used to generate electricity from wind energy. Furthermore, a distinction is made between hydro storage plants and run-of-river power plants with regard to hydroelectric power. Within the scope of this thesis, the focus of regenerative energy sources is on PV-modules as for solar energy, wind turbines as for wind power and on run–of–river plants for hydropower.

3 Materials and Methods

3.1 Identification of Strategic Promising Climate Parameters (Present Period)

Within the scope of this thesis, the climate parameters global radiation, temperature and wind force were determined. These parameters were based on historical values by the DWD ('Deutscher Wetterdienst') observed by 23 weather stations within the study area, which reach a time period of 131 years (1888 – 2019). Today, the stations are set up and operated according to WMO regulations. Thus, the local effects are kept very low. The further back in history, the less established such unified rules were. Depending on the application, possible local, regional and temporally changing influences should be investigated, which can be location- and parameter-specific. Uncertainty factors for long-term stability are (1) changes in station height during station shifts (especially for wind and temperature); (2) changes in the observation times from which the daily mean was calculated; (3) changes in the calculation rule. Uncertainties may also be expected from (4) changes in the instruments, and possibly also from (5) different quality control procedures (Behrendt, Penda, Finkler, Heil, & Polte-Rudolf, 2011), (6) errors in transmission or software, and (7) observation changes (Freydank, 2014).

However, getting a reliable statement, climate parameters within a period of 20 years (2000 – 2019) were used, whereas the year 2017 was used for certain calculations within a year. Due to the size of the study area, climate parameters are alternating and differ from region to region. Therefore, the study area had to be subdivided into climate districts, from where on a method was applied, known as the 'Inverse Distance Weighting Method' (IDW), receiving a secure and reliable statement about the climate values within the study area. The IDW is one of the distance-weighted interpolation methods. Hereby, it is assumed that a nearby measurement station better represents the searched value than a station farther away. The weighting factor depends on the distance between the station and the searched point. For inverse distance weighting, a inversely proportional factor to the distance is selected (formula 1). The reciprocal of the distance between the station and the searched point is used as a weighting factor (Rudolf, Hauschild, Reiss, & Schneider, 1992). As a rule, the distance is entered as a square or as an exponential function in the weighting, so that closer stations are weighted even more strongly (as with a simple reciprocal value) than more distant stations (formula 3) (Niederberger, 2000).

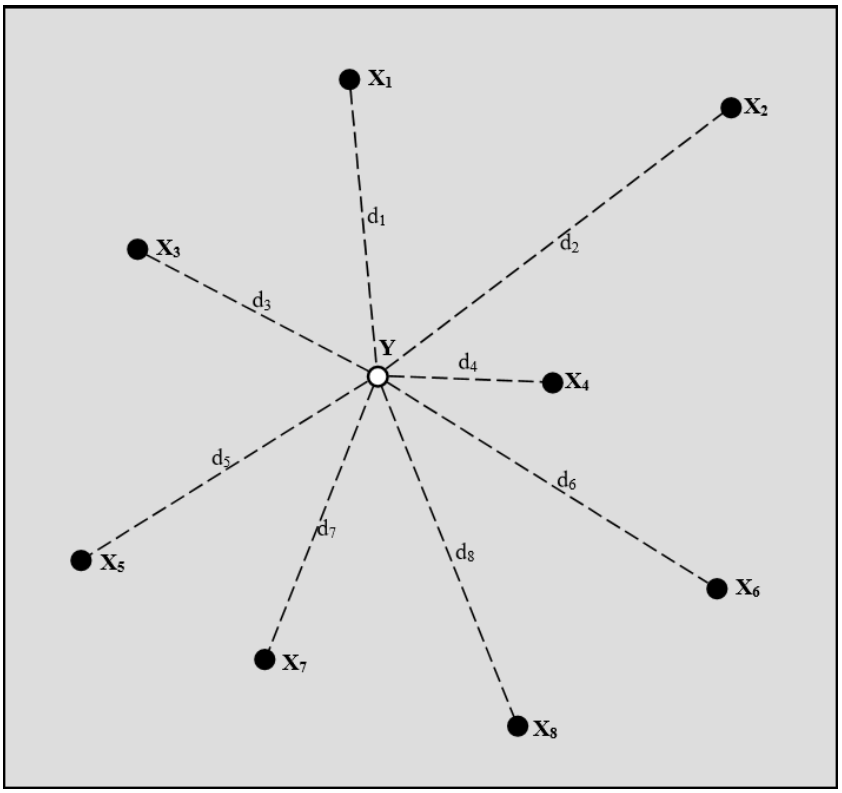

Figure 5 Schematic representation to illustrate the inverse distance weight interpolation method. Y = point to be estimated, X = known stations, and d = radial distance of the known stations to the searched point. (Niederberger, 2000)

The inverse distance weight method used was based on following formulas:

$$z(Y) = \frac{\sum_{i=1}^{n} \left(w_{X_i} \cdot z_{X_i} \right)}{\sum_{i=1}^{n} w_{X_i}}$$

With z(Y) Value on point Y [m] (1)

w Weight factor [-]

w_{xi} Weight factor on point X_i [-]

z_{xi} Value on point X_i [m]

I Index of the stations [-]

n Number of stations [-]

The weights were the reciprocals of the squared distances from the unmeasured point to the stations:

$$w_x = \frac{1}{(d_i)^2}$$

With d_i radial distance from point Y to station X [m] (2)

The radial distances from the unmeasured point to the known stations were calculated by the difference of the coordinates.

$$d_i = \sqrt{\left(r_Y - r_{X_i}\right)^2 + \left(h_y - h_{X_i}\right)^2} \quad (3)$$

With r_Y Easting at point Y [m]

r_{Xi} Easting at Station X_i [m]

h_Y Northing at Point Y [m]

h_{Xi} Northing at Station X_i [m]

The Inverse Distance Weight method is a promising method for the interpolation of meteorological data in many different projects. The method is e.g. used by the DWD, i.e. to produce climatological maps (Müller-Westermeier, 1995). Rudolph (1992) used this method to calculate the global area precipitation and the WaSiM-ETH model used this method to interpolate input data (Schulla, 1998). From the principle, this method is similar to a grid point- and grid network method but can also be used to interpolate completely irregularly set points. In the following chapters the selected climate parameters were described and implemented including their attributes into the geoinformation system ArcGIS.

3.1.1 Global Radiation

Global radiation is set together from the terms direct and diffuse radiation and holds a significant role for the energy output of PV – modules. As direct radiation, the proportion of radiation is called, which hits the earth surface unhindered and without scattering, whereas the diffuse radiation is defined as the radiation component, which is scattered, reflected or refracted by particles as clouds, aerosols and gases in the atmosphere and does not strike the earth in a straight line (Liu & Jordan, 1960). Both types of radiation occupy 50 % of the total global radiation (Quaschning, Geuder, & Ortmanns, 2002).

The DWD offers comprehensive observations regarding the global radiation in Germany (DWD Climate Data Center [CDC], 2019). The record consists of two sections. In the header section, keywords with meta-information were listed. From the "ASCII raster format" section, information in Esri ASCII raster format is available. The values of each grid cell are in a matrix of 654 columns and 866 rows. The spatial position of the grid is set to the reference point of the lower left corner of the lower left cell. The grid is arranged from north to south and is displayed in a line running from west to east with 654 values. The cell size is 1000 m x 1000 m. Unused grid cells are marked with the value - 999. The global radiation in Germany was observed between the time period 1991 – 2019.

For this study, the monthly averaged global radiation values in the period between (2000 – 2019) was brought into focus. Therefore, the IDW–method was utilized, to assign different locations and their global radiation to the belonging districts. The study area was subdivided into 14 solar districts including a centre. In total, 295 locations including values of global radiation for each month were analysed and assigned to the districts. The distribution of the mentioned locations was evaluated randomly. The values within the solar districts were averaged by the inverse distance weighting method receiving an overall global radiation within a specified district. Hence, for each district monthly mean values in global radiation could be determined and charted. Figure 6 shows the distribution of the global radiation and the solar districts with their specific centres within the frame of the study area. The map figures out the situation in June with the highest global radiation of 207,34 kWh/m² in the south and the east and the lowest value of 141,6 kWh/m² in the northwest.

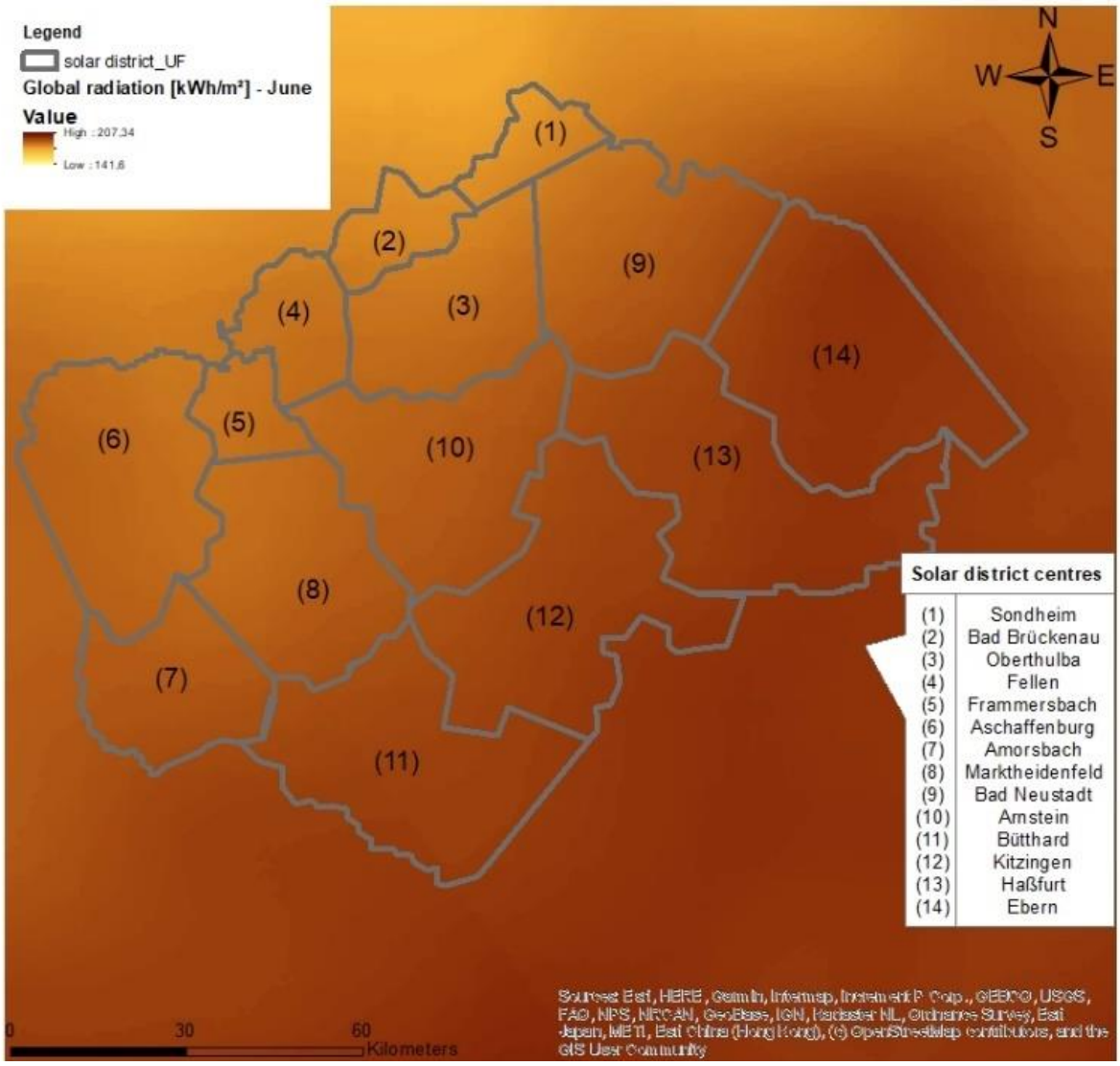

Figure 6 Assigned solar districts within the study area. The coloured background illustrates the global radiation in June. Source: Own figure based on Geodata: Esri, DigitalGlobe, GeoEye, Earthstar Geographics, CNES/Airbus DS, USDA, USGS, AeroGRID, IGN, and the GIS User Community (ESRI, 2019).

3.1.2 Wind Force

Regarding the determination of the wind force within the study area, comprehensive observations made by the 'DWD' were used. The 'DWD' offers files with metadata, which contains a portfolio of parameters measured at a selected station, with start, end, associated units, measurement rules, formulas, dates, and time units assigned to the Stations_Id and the current station name. The device history is sorted according to the meteorological parameters. It contains the chronological history of the sensor or encoder heights, device types, measuring methods and the station names (CDC, 2019).

Out of 23 weather stations only five were relevant within the study area related to a reliable time period of at least the last 20 years (2000 – 2019). Following stations were of concern (station height and coordinates were listed in brackets): 'Bamberg' (240 m; 49° 52' 27.12'' N and 10° 55' 14.16'' E), 'Lauter-Oberlauter' (344 m; 50° 18' 23,76'' N and 10° 58' 4.44'' E), 'Bad Kissingen' (282 m; 50° 13' 26.76'' N and 10° 4' 45.12'' E), 'Würzburg' (268 m; 49° 46' 13.08'' N and 9° 57' 27.72'' E) and 'Neuhütten' (339,5 m; 50° 0' 29,88'' N and 9° 25' 26,04'' E). The measurement of wind power took place at a reference height of 10 m. The measurements made by the DWD were valued in Beaufort, which is a scale to classify wind speeds into 13 wind force ranges. The transformation into a unit, which allows further calculations was made as followed (formula 4) (Meaden et al., 2007):

$$v = 0{,}836 \times B^{\frac{3}{2}} \quad (4)$$

With B Beaufort [Bft]

v Wind speed [m/s]

As a base for further calculations the study area was subdivided into eleven wind districts. Each of the districts has its own district centre, from where on the IDW–method was executed. The location of the wind districts depends on the climatological nature as well as on the location of erected wind turbines. Figure 7 shows the study area including the weather stations observing wind speeds. Furthermore, the subdivision of the wind districts and their centres are displayed. Each district has a numerated centre of which the mean monthly wind speeds could be determined.

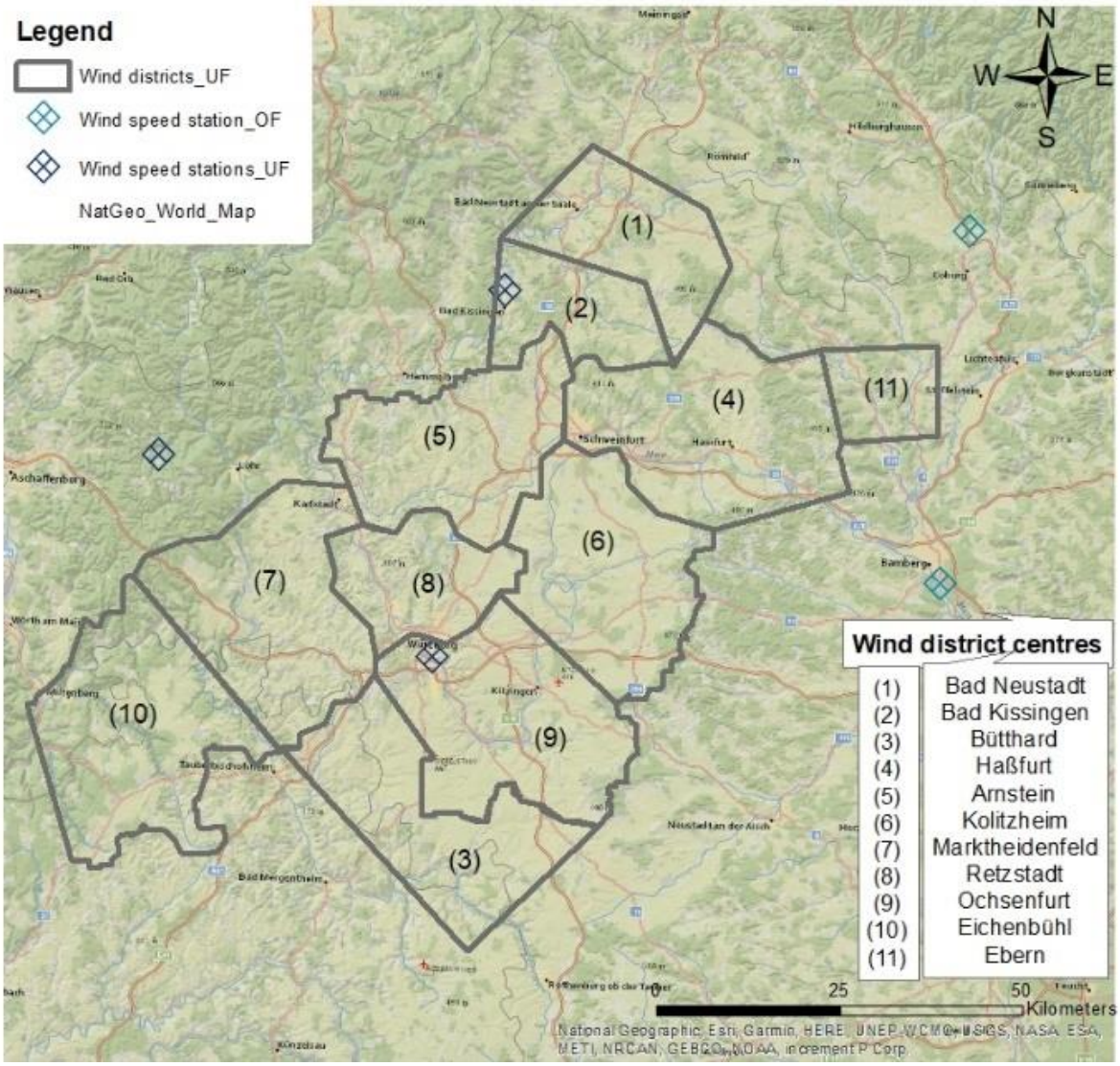

.

Figure 7 Assigned wind districts within the study area. Source: Own figure based on national geographic map. Geodata: Esri, DigitalGlobe, GeoEye, Earthstar Geographics, CNES/Airbus DS, USDA, USGS, AeroGRID, IGN, and the GIS User Community (ESRI, 2019).

3.1.3 Temperature

As for wind force, the DWD provides several metadata parameter files, which contain a list of parameters (portfolio). The observation of the parameter temperature was executed at a reference height of 2 m above surface. For further calculations, the same procedure as for wind force and global radiation was carried out, by connecting the measured temperature values to different districts within the study area. The utilization of the temperature is well related with global radiation and therefore, the same districts as for solar radiation was used (Chapter '*Global Radiation'*). Hereby, eleven weather stations regarding temperature were of concern, which were connected to the solar districts by the IDW-Method. According to the IDW-Method, each district is assigned to one or more weather stations to determine the average monthly and annual temperature. For easier allocation, the weather stations and the solar districts were marked with IDs (table 2).

Table 2 Relation between weather stations observing the parameter temperature and the according solar districts. Source: Own table

Solar district centre	***Related ID_Weather station***
1_Sondheim v. d. Rhön	1_Ostheim v. d. Rhön
2_Bad Brückenau	3_Sandberg / 4_Bad Kissingen
3_Oberthulba	4_Bad Kissingen
4_Fellen	5_Lohr a. m. Main / 6_Neuhütten
5_Frammersbach	5_Lohr a. m. Main / 6_Neuhütten
6_Aschaffenburg	7_Kahl a. m. Main / 8_Röllbach
7_Amorsbach	8_Röllbach
8_Marktheidenfeld	5_Lohr a. m. Main / 10_Würzburg
9_Bad Neustadt	1_Ostheim v. d. Rhön / 3_Sandberg
10_Arnstein	9_Schonungen / 10_Würzburg
11_Bütthard	10_Würzburg
12_Kitzingen	11_Kitzingen
13_Haßfurt	4_Bad Kissingen / 9_Schonungen
14_Ebern	2_Bad Königshofen / 9_Schonungen

3.1.4 Water Level and Discharge

Regarding parameters as discharges and water levels the river Main was taken into focus. The river Main intersects the study area and is the most important river about size and appliance within Lower Franconia. Regarding to the river Main, several water gauges were identified, but only six of them were evaluated regarding to reliability of data. From east to west along the river following gauges were of concern: Kemmern, Trunstadt, Schweinfurt, Würzburg, Steinbach and Kleinheubach. All six water gauges delivered data within the time period 2000 – 2019. Table 3 displays the location of the selected gauges including catchment area auf gauge height. The location of the selected water gauges was implemented into the geoinformation system ArcGIS including their attributes of coordinates, catchment area, gauge height and data about water level and discharge.

Table 3 Relevant gauges at river 'Main' within study area including data about coordinates, catchment area and gauge height within the study area. Source: Own table based on (Hochwassernachrichtendienst Bayern [Hnd Bayern], 2019)

Gauge	***Coordinates (WGS 84)***	***Catchment area [km²]***	***Gauge height [m.a.s.l. in m]***
Kemmern	49°57'4,2'' N – 10°52'24,5'' E	4.230	230,2
Trunstadt	49°55'46,9'' N – 10°15'18,7'' E	12.020	223,4
Schweinfurt	50°1'52,2'' N – 10°13'14,6'' E	12.717	201,2
Würzburg	49°47'45,9'' N – 9°55'32,8'' E	14.018	164,6
Steinbach	50°0'35,8'' N – 9°36'13,3'' E	17.905	146,3
Kleinheubach	49°42'59'' N – 9°13'28,3'' E	21.519	119,6

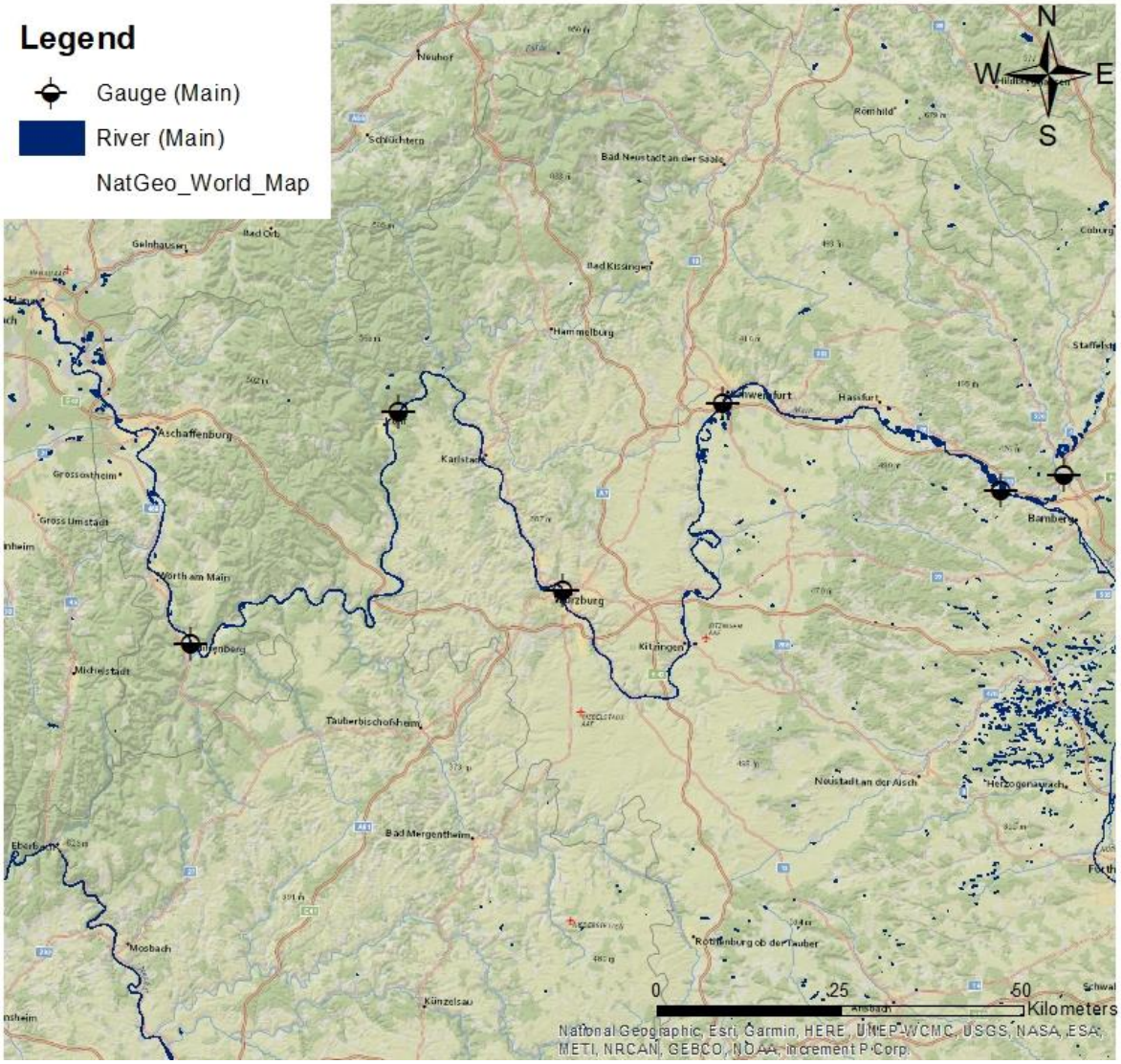

Figure 8 Gaugin stations along the river Main within the area of concern. Source: Own figure based on national geographic map. Geodata: Esri, DigitalGlobe, GeoEye, Earthstar Geographics, CNES/Airbus DS, USDA, USGS, AeroGRID, IGN, and the GIS User Community (ESRI, 2019).

3.2 Technical Potential of Regenerative Energy Systems

This work aims to compare the historical, present and future electricity production of regenerative energy systems. For this purpose, individual performance plans for the selected systems were created based on technological parameters and calculations. In the following, the selected renewable energy systems PV, wind turbines and run–of-river plants including their technical components were discussed.

3.2.1 Solar Energy

Solar energy is directly provided by the sun's energy and consists of direct, scattered and reflected radiation. This kind of energy is the driving factor for energy generation by PV – modules. The sum of direct radiation G_{Dr} and diffuse radiation G_{Df}, in each case based on the horizontal receiving surface, is referred to as global radiation G_G (formula 5).

$$G_G = G_{Dr} + G_{Df} \quad (5)$$

With G_G Global radiation [kWh/m²]

G_{Dr} Direct radiation [kWh/m²]

G_{Df} Diffuse radiation [kWh/m²]

The proportion of diffuse radiation or direct radiation on the global radiation is subject to both, daily and seasonal fluctuations. In Central European latitudes, the diffuse fraction clearly exceeds the direct share (DWD, 1989). As an example, global radiation in the winter months consists almost exclusively of diffuse radiation. In summer, the proportion of direct radiation increases but on average is always smaller than that of the diffuse radiation (Figure 9).

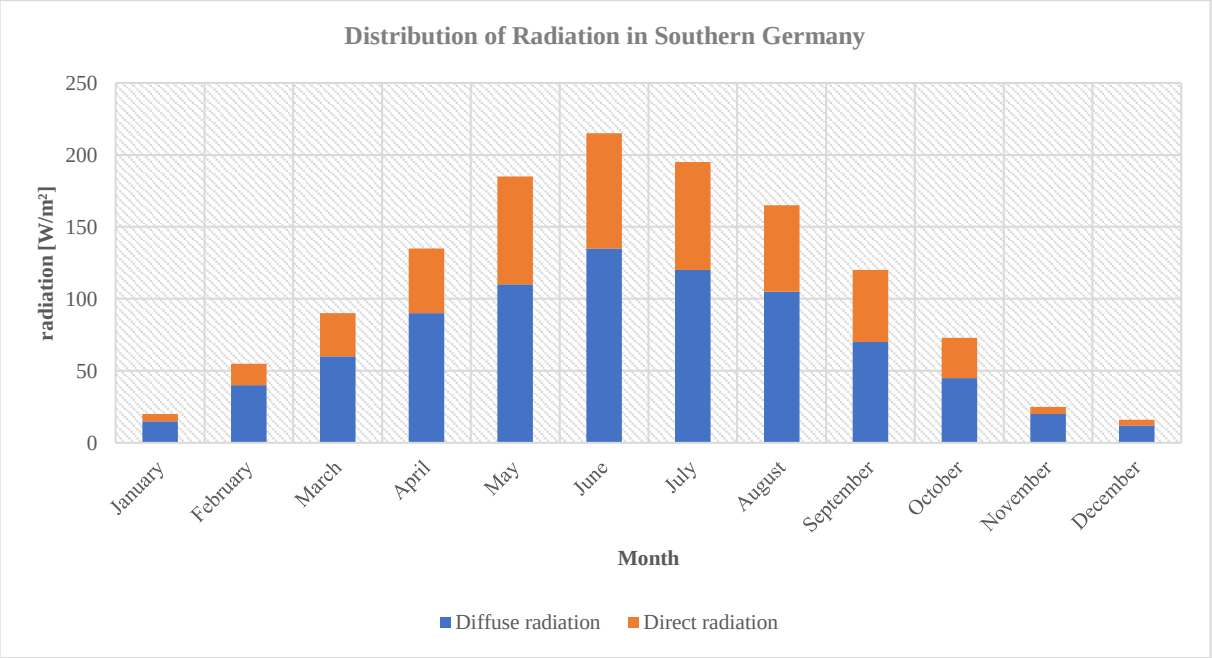

Figure 9 Global radiation differentiated in a direct fraction and a diffuse share in Southern Germany. The figure displays the course of a years. Own figure. Source: Own figure based on (DWD, 1989)

The direct radiation incident on an inclined surface is determined by the angle of incidence, which in turn depends on the orientation and location of the receiving surface and the position of the sun (formula 6).

$$cos\psi = (cos\,\alpha\,sin\,\varphi - cos\,\varphi\,cos\,\beta\,sin\,\alpha)\,sin\,\delta + (sin\,\varphi\,cos\,\beta\,sin\,\alpha + cos\,\alpha\,cos\,\varphi)\,cos\,\delta\,cos\,\omega + sin\,\beta\,sin\,\alpha\,cos\,\delta\,sin\,\omega$$

With α Tilt angle [°] (6)

β Azimuth angle [°]

φ Latitude (degree) [°]

δ Sunshine duration [h]

ω Hour angle of the sun (when sun is at highest point = 0°) [°]

ψ Angle of incidence [°]

In order to obtain direct radiation on an inclined receiving surface oriented towards a particular direction $G_{Dr,g,a}$, the direct radiation G_{Dr} incident on a horizontal receiving plane must be offset with the radiation angle of incidence ψ, the inclination angle α, the solar azimuth angle β and the orientation of the surface normal with respect to the direction γ (formula 7).

$$G_{Dr,g,a} = G_{Dr}\,(sin\,\psi\,cos\,\alpha - sin\,\alpha\,cos\,\psi\,sin(\beta - \gamma))$$

(7)

In order to obtain the diffused radiation on an inclined surface $G_{Df,g,a}$ it is assumed that the diffused radiation is evenly distributed in space and that it meets in equal parts from all directions to a certain point (isotropic model) on the earth's surface (formula 8).

$$G_{Df,g,a} = 0{,}5\,G_{Df}\,(1 + cos\ \alpha)$$

With G_{Df} Diffuse radiation on horizontal surface [kWh/m²] (8)

In addition to the diffuse and direct radiation, a certain proportion of the global radiation reflected back depending on the surface $G_{R,g,a}$ (formula 9).

$$G_{R,g,a} = A_G\,G_G sind^2(\frac{\alpha}{2})$$

With A_G Albedo effect [-] (9)

The global radiation impinging on the surface of a photovoltaic module is composed of the incoming direct radiation (formula 7), the diffuse radiation (formula 7), as well as the radiation reflected from the environment onto this receiving surface (formula 8). The total global radiation impinging on oriented radiation is calculated as follows (formula 10) (Kaltschmitt, 2006).

$$G_{G,g,a} = G_{Dr,g,a} + G_{Df,g,a} + G_{R,g,a}$$

(10)

There are generally two types of solar systems. A distinction is made between thermal solar systems and photovoltaic systems. However, this work only dedicated to PV-systems, as they can be used for electric generation. A solar cell consists of a conductive base material (p layer) and a conductive layer on top (n layer). Radiation hits the cell, causing both positive and negative charge carriers to move. In order to accomplish the release of charge carriers, semiconductors, mainly silicon, are used (Sze & Ng, 2006). For the charges to be conducted correctly, additional foreign atoms are incorporated: P- and n-doped silicon (Shockley, 1953). In this case, the p-doped silicon layer has a positive charge excess, while the n-doped layer is negatively charged. In between there is a boundary layer. The impact of both layers creates an internal electric field. With the arrival of solar radiation, electrons migrate into the n-layer, while electron holes move freely into the p-layer. Using contact layers, the electrons are dissipated and made to flow through the conductor (Kleemann & Meliß, 2013). Individual cells are combined to form a photovoltaic module consisting of electrically interconnected solar cells, embedding materials, the electrical connection cables or a connection box. The total number of available cells in a module defines the maximum module performance. In general, outputs of ~ 50 - 75 W for 36 series-connected cells is a typical size. Large-area solar modules can also achieve a standard output of over 300 W (Goetzberger & Stahl, 1985). In order to obtain the power of a PV-module, in addition to the global radiation in a specific area, the peak power of a module specified by the manufacturer, the area of a PV-system and the efficiency must be considered. The manufacturers specific nominal performance of PV-modules is given by the unit kWp. The abbreviation kWp stands for "kilowatt peak". This indicates the performance of a PV-system under standardized conditions. This is also called nominal power. In practice, the rated power is higher than the actual power, since the weather and operating conditions usually deviate from the norm. The installed power of a PV-module was calculated as follows (formula 11).

$$P = A * P_p \tag{11}$$

With P Installed capacity [kWp]

A Surface area of module [m²]

P_p Specific peak power of module [kWp]

The specific peak power of a certain module depends on its composition, especially on the efficiency [μ] of its used type of solar cell. Therefore, the efficiency of a silicium cell ranges between 17% (polycrystalline) and 19% (monocrystalline). To preserve the power production of a PV-system, the associated global radiation and efficiency were included (formula 12).

$$E_{PV} = P * G_{G,g,a} \tag{12}$$

With E_{PV} Electricity production of PV – Modul [kW]

$G_{G,g,a}$ Global radiation [kWh/m²]

Efficiency data generally applies to standardized measurement conditions, as the output of a solar cell depends on the spectral light composition, the temperature and the radiation intensity. Standard conditions refer to standard test conditions (STC) with an irradiance of 1000 W/m², a solar cell temperature of 25 °C and a spectral distribution according to the air mass of 1,5 AM. In real life, the module temperature deviates from the test conditions (Raicu, 1992). An increased module temperature leads to a reduction in the performance of the PV-system (Hörstmann-Jungemann, 2005). Using the example of PV–modules (Shell SP140), the conclusion could sound as follows: an increase in the module temperature by 10 °C results in reduction of performance of 5,6 %, whereas an increase of 20 °C leads to a reduction of 10,3 % (Shell Solar, 2006). The module temperature depends on the ambient temperature, the type of mounting and the global radiation (formula 13).

$$T_M = T_A + c * G_{G,g,a} \quad (13)$$

With T_M Module temperature [°C]

T_A Ambient temperature [°C]

c Mounting [-]

The module temperature depends on the type of installation. A distinction is made between open space systems, installations on pitched roofs with a distance of more than 10 cm or less, and roof-integrated systems (Schubert, 2012). Each of these types of mounting has its own temperature coefficient: open space systems (c = 0,02), inclined roof systems (> 10 cm) (c = 0,027), inclined roof systems (< 10 cm) (c = 0,036) and roof integrated systems (c = 0.058) (Drews et al., 2007). Furthermore, the shading of a cell also leads to performance losses, which were neglected in this work.

3.2.2 Wind Power

The solar radiation has not only direct effects but also indirect influences on the air masses in the atmosphere. This is displayed in the fact that 2,5 % of the incident solar radiation is consumed for the movement of the atmosphere, resulting in a theoretical power of $4{,}3 * 10^{15}$ W (Schaefer, 1994). The energy contained in moving air masses, which for example can be converted into mechanical or electrical energy by wind turbines, is thus a secondary form of solar energy. By variations of temperature on surfaces (ocean and terrestrial) differences in air pressure develop, which result in an air movement from areas with high pressures to areas with lower air pressures (Koethe, 1982). In general, it can be distinguished between global air circulation systems and local circulation systems. A global air circulation system is responsible for global air exchange. However, local circulation systems are important for energy use. Such air movements usually occur according to the same principle: ascending air masses are found above areas that warm up rapidly as a result of solar radiation, i.e. have a low heat capacity (e.g. land); descending air masses exist above neighbouring areas with a higher heat capacity (e.g. sea) (Christoffer & Ulbricht-Eissing, 1989). The local circulation systems are suitable for wind power because of their proximity to the earth's surface. However, due to friction, which is dependent on the nature of the earth's surface, changes in air movement occur. This term is often described as the roughness of a medium. Water surfaces have a low roughness, whereas villages are exposed to relatively high roughness. Thus, the roughness of the soil is a measure for the change in wind speed above ground (Kaltschmitt, 2006).

Within the scope of this thesis a power plan was created to determine the energy generation and electricity production of a wind turbine. To understand the created performance plan, the components and factors are considered in more detail below. Therefore, a free, uniform, twist-free and incompressible flow is assumed.

The temporal wind speed distribution is the basis for the design plans of wind turbines. Wind speeds can vary depending on space and time and vary in the course of the day and year. Measurement series regarding wind speed are characterized by their distribution function and can be compared amongst themselves. Wind velocity distributions can be described by the use of Weibull or Rayleigh (Figure 10). In this work, the Weibull distribution is used as the density function (Troen & Petersen, 1989) (figure 10). This kind of distribution is composed of the relative frequency (formula 14), cumulative frequency (formula 15) and the mean wind speed (16).

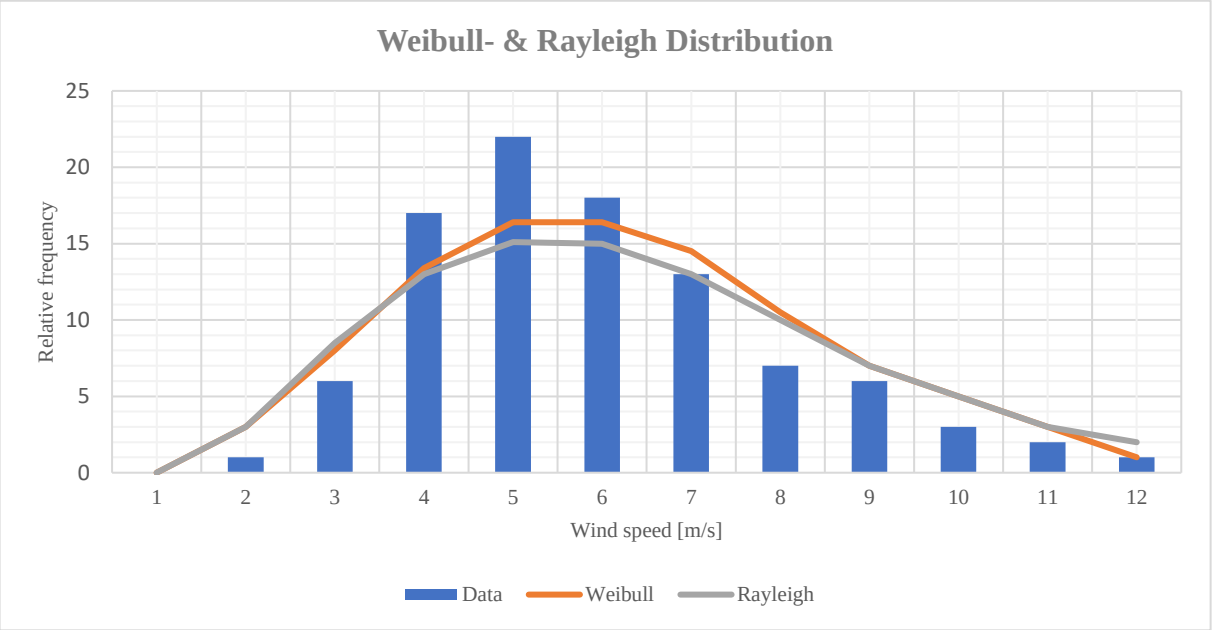

Figure 10 frequency of distribution of time series of wind speed for random locations. Own figure. Source: Own figure based on (Kaltschmitt, 2006)

$$f(v_{Wi}) = \frac{k}{A}\left(\frac{v_{Wi}}{A}\right)^{(k-1)} e^{\left(\frac{v_{Wi}}{A}\right)^{k}}$$

With $f(v_{wi})$ Relative frequency [1/(m/s)] (14)

k Shape parameter [-]

A Scaling factor [-]

v_{Wi} Wind speed at reference height [m/s]

$$F(v_{wi}) = 1 - e^{-\left(\frac{v_{wi}}{A}\right)^{k}}$$

With $F(v_{wi})$ Cumulative frequency [1/(m/s)] (15)

$$v_{mean} = A * \left(0{,}568 + \frac{0{,}434}{k}\right)^{\left(\frac{1}{k}\right)}$$

With v_{mean} Mean wind speed [m/s] (16)

Thereby, the scaling factor A is a measure for the characteristic wind speed of the considered time series and the shape factor k describes the curve shape. It is within the range between 1 and 4, and its value is characteristically for certain wind climates (Pryor & Barthelmie, 2010):

- k ~ 1: Arctic regions (high variation)
- k ~ 2: Regions in Central Europe
- k ~ 3 to 4: Trade wind regions (steady wind)

In addition to the wind speed at a certain reference height, the wind speed at the hub height is also required to drive the rotor blades. For the quantitative description of the vertical wind profile, a semi-empirical power equation is used (Hellmann, 1915) (formula 17).

$$v_H = v_{Wi} * \frac{ln\frac{H}{z_0}}{ln\frac{H_{ref}}{z_0}}$$

With v_H Wind speed at hub height [m/s] (17)

H Hub height [m]

H_{ref} Reference Height [m]

z_o Roughness length [m]

The effect of alternating topography leads to wind speed changes (figure 11), which is called speed-up ratio (formula 18).

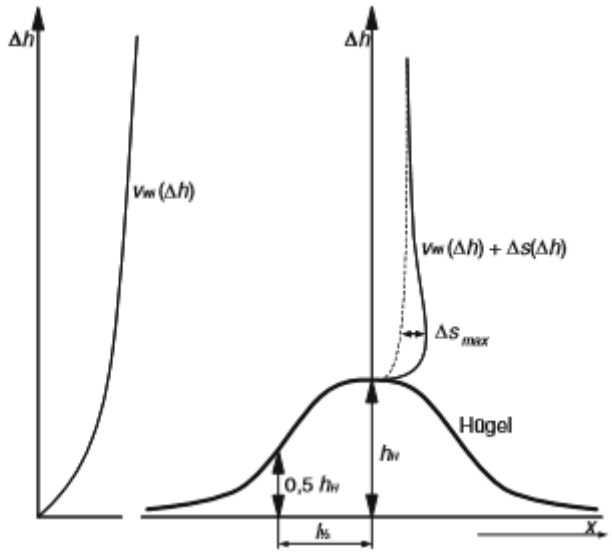

Figure 11 Relationship at an overstreamed hill. Source: (Hoff, 1987)

$$\Delta A = \frac{v_{Wi,x}(\Delta h) - v_{Wi,a}(\Delta h)}{v_{Wi,a}(\Delta h)}$$

With A Stream through cross sectional area [m²] (18)

v_{Wi} Mean wind speed [m/s]

Δh Height over surface [m]

x Cut through the elevation [m]

a Point on the windward side [-]

The relationships described above can be used to describe the kinetic energy of a given wind speed (formula 19).

$$E_{Wi} = 0{,}5\, m_{Wi}\, {v_{Wi}}^2$$

With E_{Wi} Kinetic energy [kW] (19)

m_{wi} Air mass [AM]

v_{wi} Wind speed [m/s]

Out of formula 19 the performance of a given wind speed can be determined (Formula 20) (Quaschning, 2008).

$$P_{Wi} = 0{,}5\, m_{Wi}\, v_{Wi}^2 = 0{,}5\, A\, p_{Wi}\, {v_{Wi}}^3$$

With p_{Wi} Density of air [kg/m³] (20)

Wind turbines use the kinetic energy of flowing air masses. The kinetic power of the wind is determined by the air density, the wind penetration area and the wind speed. The wind turbine extracts parts of the kinetic power of the wind by rotors, which consist mostly of several rotor blades. The extracted wind power is converted into a mechanical power due to the rotational movement of the rotor. This is tapped as a moment at a certain speed and transmitted to a generator. The power withdrawal takes place via an aerodynamic lift principle (Gasch & Twele, 2010). According to Bernoulli, the wind power contained is composed of the kinetic power, the pressure power and the potential power which, however, can be neglected. With the help of the continuity equation, the wind power can be determined at any point, in front of the rotor (S1) and behind the rotor (S2) (formula 21) (Dubbel, 2013).

$$P_{Wi,i} = const. = 0{,}5 m_{Wi} v_{Wi,1}^2 + \frac{m_{Wi} p_{Wi,1}}{p_{Wi}} = 0{,}5 m_{Wi} v_{Wi,2}^2 + \frac{m_{Wi} p_{Wi,2}}{p_{Wi}} + P_{Rot,th}$$

With m_{Wi} Air mass [AM] (21)

v Velocity of wind [m/s]

p Wind pressure [Pa]

$P_{Rot,th}$ Theoretical performance of rotor [kW]

Since the same wind pressure and density must prevail in front of and behind the wind turbine, the theoretical performance of the rotor can be equated with the power P_{Wi} extracted from the wind. The kinetic power contained in the wind is based on a free-flowing rotor surface S_{Rot} and is calculated according to formula 22.

$$P_{Wi} = 0{,}5 m_{Wi,frei} v_{Wi,1}^2 = 0{,}5 p_{Wi} A_{Rot} {v_{Wi,1}}^3$$

With A_{Rot} Rotor surface [m²] (22)

$m_{Wi,frei}$ Free flow of air mass [AM]

The power of the wind depends on the third power of the wind speed. This in turn is crucial for the choice of the location of the wind turbine (Hoff, 1987).

It is noticeable that the force of the wind must correspond to the theoretical rotor power (formula 23).

$$P_{Wi,ent} = P_{Rot,th} = 0{,}5 p_{Wi} (\frac{v_{Wi,1} + v_{Wi,2}}{2}) A_{Rot} (v_{Wi,1}^2 - v_{Wi,2}^2)$$

With $P_{Wi,ent}$ Deprived power of the wind [kW] (23)

The maximum extractable power of the wind is determined by the theoretic power coefficient $c_{p,th}$. This is the ratio between the extractable power $P_{Wi,ent}$ and the maximum wind power P_{Wi} (formula 24).

$$c_{p,th} = \frac{P_{Wi,ent}}{P_{Wi}}$$

With $c_{p,th}$ Performance ratio [-] (24)

The real power coefficient in modern wind turbines, which is equipped with three rotor blades, is determined to 0.47 [-] (Molly, 1990). In addition to the coefficient of performance and wind power, a corresponding efficiency must be considered concerning the calculation of the usable power of a wind turbine (formula 25).

$$P_{WT} = c_p * \mu * P_{Wi}$$

With P_{WT} Performance of a wind turbine [kW] (25)

μ Efficiency of a wind turbine site (electrical and mechanical) [-]

The principle of buoyancy, used in modern turbine constructions, makes use of the deflection of the wind to generate the circumferential force in the rotor. In this case, the buoyancy force depends on the air density p_{Wi}, the flow velocity v_A, the cross-sectional area (l as length and b as profile thickness), the buoyancy coefficient c_a and the drag coefficient c_w (formula 26). The buoyancy coefficient describes the profile shape of a rotor blade, depending on the curvature, the length and the angle of inflow.

$$F_a \; or \; F_W = 0{,}5 p_{Wi} v_A^2 l (c_{A \; or \; W}) b$$

With F_A Buoyanacy force [N] (26)

F_W Drag force [N]

The force that drives the rotor blade is obtained from the buoyancy force and the circumferential force of resistance (formula 27). The power of the rotor can thus be determined with the help of the drive torque (formula 28) (Heier, 2013).

$$F_T = F_A - F_W$$

With F_T Driving force [N] (27)

$$P_{Rot} = 2 \Pi n M = P_{Rot,th} \mu_{Rot}$$

With P_{Rot} Performance of rotor [kW] (28)

n Rotor rotation speed [rpm]

M Drive torque [-]

μ_{Rot} Efficiency of rotor [-]

Beside turbine parameters and corresponding factors, the determination of an energy output depends on the rated capacity, on which a wind turbine was constructed. Other decisive factors, which had to be considered were the rotor diameter, cut–in speed, design speed, cut–out speed and the ratio between rotor power and wind power.

3.2.3 Hydro Power

21 % of the solar energy contributes to the global water cycle. The processes which are directly driven are precipitation, evaporation and runoff. In simplified terms, water evaporates and enters the atmosphere as water vapour. Here the water vapour condenses and falls back onto the land surface or the sea as rain, hail or snow. Thereby, the water constantly transforms into different states of aggregation. For the energy generation by hydropower the fallen precipitation within a catchment area, the discharge and water level of a river had to be considered (Vischer & Huber, 2013). Here, the available water in a given catchment area and over a period of time can be described in the form of a water balance equation (formula 29).

$$N_o = \left(A_{o,O} + A_{u,O}\right) + V_O \pm R_O \tag{29}$$

With N_O Precipitation on surface O of a specific area [l/m²]

$A_{0,O}$ Discharge above ground [m³/s]

$A_{u,O}$ Discharge below ground [m³/s]

V_O Evaporation [l/m²]

R_O Retention [-]

The discharge height describes the value that effectively flows and neither evaporates nor is fed into the groundwater. Depending on the nature of a given area (vegetation, permeability, topography, etc.), the discharge coefficient generally increases with higher precipitation levels. Important here is a clear assignment of the catchment area to the corresponding outflowing water body.

When water descends from a higher level to a lower level hydropower can be generated. The difference between these water surface elevations is stated as a head. A head exists either naturally or can be created artificially by constructing a weir or dam. Generally, with elevation differences gravitational potential energy is stored in the water. The water flow moves the blades of a turbine, converting the potential energy into kinetic energy, whereas this kind of energy is converted into mechanical and lastly into electrical energy by the generator (Figure 12).

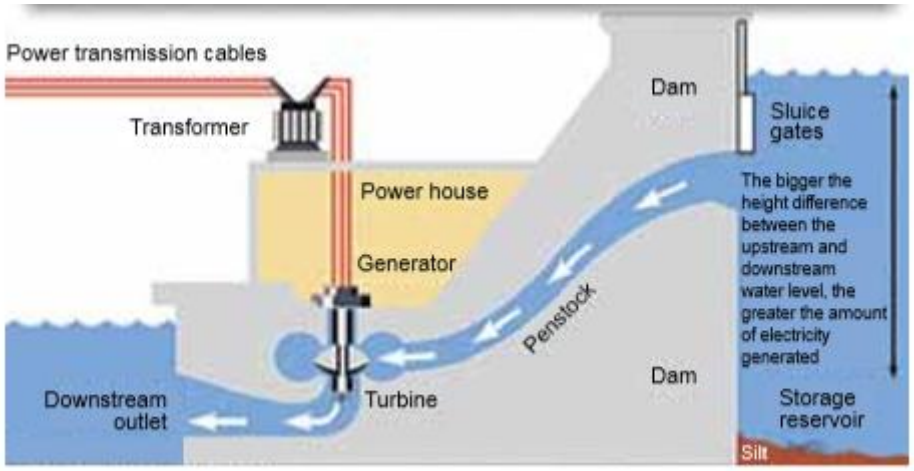

Figure 12 Sketch of a typical hydro power plant. Source: (Environment Canada, 2014)

The water has, depending on location and nature, differences in potential and kinetic energy. Simplified, it is assumed that a stationary and frictionless flow occurs. According to Bernoulli (Kuchling, 1994), the hydrodynamic pressure can be described as follows (formula 30):

$$p + p_{Wa}\, g\, h + 0{,}5\, p_{Wa}\, v_{Wu} = const. \tag{30}$$

With p Hydrostatic pressure [Pa]

p_{Wa} Density of water [kg/m³]

g Gravity [m/s²]

h (Falling) height [m]

v_{Wa} Flow velocity [m/s]

The usable fall height was calculated from the pressure differences, the geodetic height difference and the different flow velocities of the water. Formula 31 follows an idealized view without the losses actually given. Thus, from the usable height, the loss fall height had to be subtracted, which arises due to the friction of water molecules.

$$h_{nutz} = \frac{p_1 - p_2}{p_{Wa}\, g} + (h_1 - h_2) + \frac{{v_{Wa,1}}^2 - {v_{Wa,2}}^2}{2g} \tag{31}$$

With h_{nutz} Net fall height [m]

The maximum energy supply of the water flow is called discharge line potential (Kaltschmitt, 2006). The determination considered the average annual discharge volume of the flow velocity and the existing gradient, at each point i. Flow losses were neglected. The average annual outflow volume resulted from the mean discharge and the number of hours of the year (8760 h). In order to maintain the potential, the head between upstream and downstream water, the gravitational acceleration and the density of the water must be considered. As a rule, the geodetic height difference between two surfaces is equal to the usable fall height. The other

components in formula 30 occur mainly within a hydraulic system of a hydro power plant. In addition to the known parameters, the efficiency of a hydropower plant must be considered. Thus, the performance of a given water supply could be determined (formula 32) (Schröder, Euler, Schneider, & Knauf, 1982).

$$P_{Wa} = p_{Wa}\, g\, q_{Wa}\, h_{nutz}\, \mu \tag{32}$$

With q_{Wa} Discharge [m³/s]

μ Efficiency of a hydro power plant [-]

P_{Wa} Power of a hydro power plant [kW]

The electrical energy performance is as follows (formula 33):

$$E_L = P_{Wa} * 8760 \tag{33}$$

With E_L Energetic performance (Line potential) [Wh]

A distinction is made between run-of-river plants and storage power plants. To convert the potential energy of the water into electricity, the following components are needed for run–of–river power plants. A water inlet upstream, a supply or discharge of the water to and from the turbine, the outlet downstream, and a powerhouse for the conversion of mechanical into electrical energy (Giesecke, Heimerl, & Mosonyi, 2014).

In general, factors change over the year. This poses a difficulty in dimensioning a hydropower plant. Therefore, hydropower plants are constructed based on a performance plan that takes into account seasonal variations (Giesecke et al., 2014). To assess the mean annual performance, the mean exceedance duration curve of the discharge is necessary. If the same procedure is used for the associated duration curves of the headwater level (upstream) and the tailwater level (downstream), the head duration line could be determined from these two characteristic curves. The multiplication of the exceedance duration curve of the discharge and the head duration curve thus provides the power duration curve over one year. Consequently, it is possible to determine the annual work of the hydropower plant from the integration of the power duration curve (figure 13).

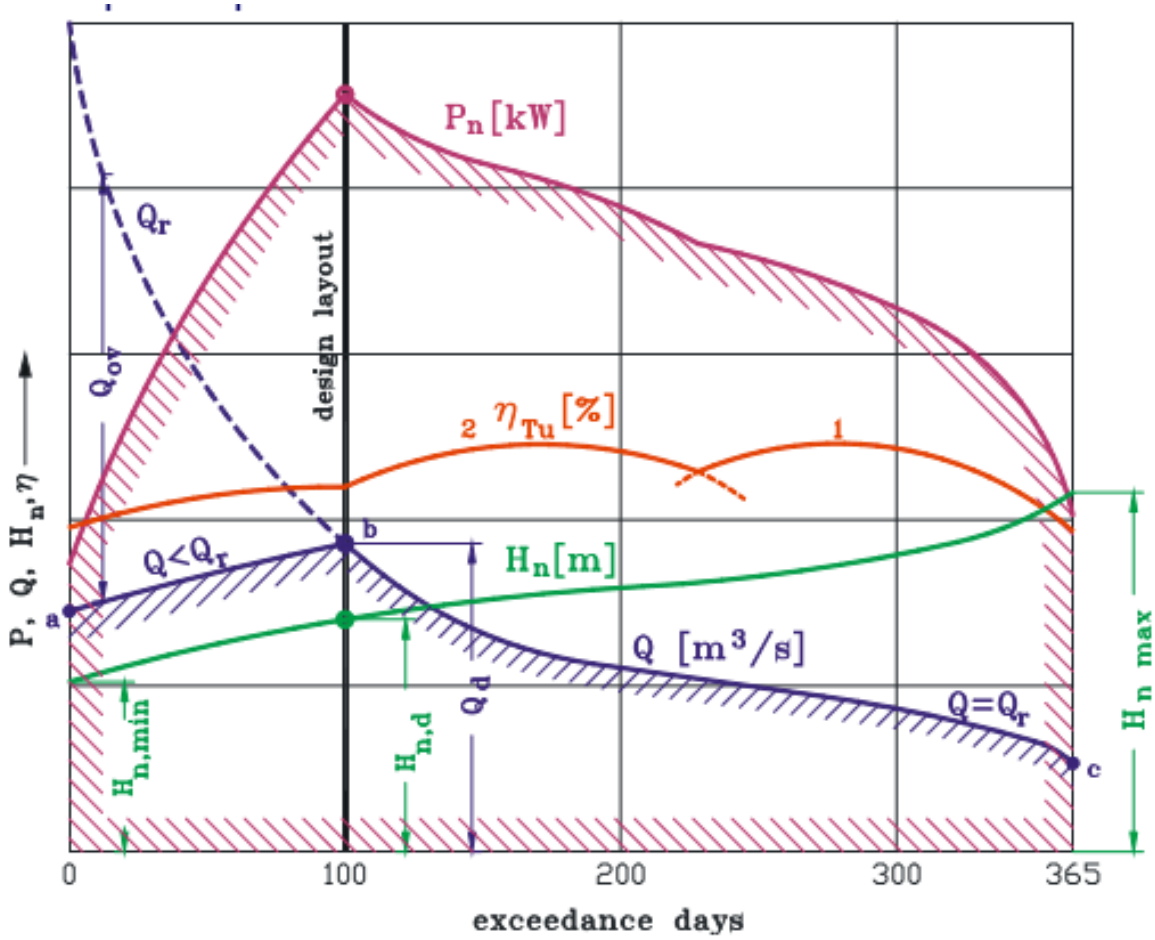

Figure 13 Power plan of hydro power plant with two turbines. Source: (Strobl & Zunic, 2006)

Figure 13 shows an example of a power plan of a hydropower plant. Here, the design layout was determined to 100 exceedance days. This defines the design discharge Q_D (maximum turbine discharge). The gross head line was determined by the head water level (h_{wl} (Q_r)) and the tailwater level (t_{wl} (Q_r)). The net head line resulted by the determination of losses in the trash rack and at the exit which enables the determination of the net design head (at design discharge Q_D). From turbine performances Q(H) one obtains the line a – b (at maximum opening) and thus the flow duration curve of the turbine discharge Q(t) a – b – c. Another parameter, which must be considered is the efficiency as a function of discharge and head. Therefore, the power of the hydro power plant could be calculated the same way as in formula 32 (Strobl & Zunic, 2006).

3.3 Identification of Renewable Energy Sites

Prior to regenerative energy systems as photovoltaic systems, wind turbines and hydropower plants were localized via remote sensing and evaluation in ArcGIS. The location data used is based on the records of the "Energieatlas Bayern" (Bayerische Staatsregierung, 2017). In addition to the location coordinates, other performance-specific data, such as the installed capacity, the full load hours and the type of installation could be determined. Decisive factors for the selection of sampling locations were research results regarding the lateral distance to the study area, the plant type and the size of the specific plant, turbine or module. Based on this methodology, a total of 44.308 sampling locations regarding PV-modules, wind turbines and hydropower plants were identified within the study area and afterwards implemented in ArcGIS via an attribute table with the respective location data and corresponding analysis results (table 4). The study area was divided into catchment areas. Factors that contributed to the classification were the lateral distance to the nearest weather or climate station, and the unanimity in the climate variables (for example, locations with similar values in the global radiation for PV-systems and wind speed for wind turbines). The locations of the renewable energy systems were then assigned to the individual catchment areas. In each individual area, a centre was determined, which was used as a reference, so that the distances to the surrounding weather or climatic stations could be determined by the IDW-method.

Table 4 Distribution of regenerative energy systems within study area. Source: Own table based on (Bayerische Staatsregierung, 2017)

Energy system	***Number (total)***	***Type***	***Number (type)***
Photovoltaic systems	43.777	Open – space systems	215
		Roof – surface systems	43.562
Wind turbines	261	In operation	261
Hydro power plants	270	Run of river plants	266
		Swellable run of river plants	4
		Storage plants	0

3.3.1 PV-Systems

With reference to PV-systems, 43.777 modules have been installed in Lower Franconia, all contributing to the generation of electricity. A distinction was made between open space systems and roof surface systems (no subdivision in the map). Each module contains data about coordinates and installed capacity. The map shows the distribution of the PV-modules within the study area (figure 14).

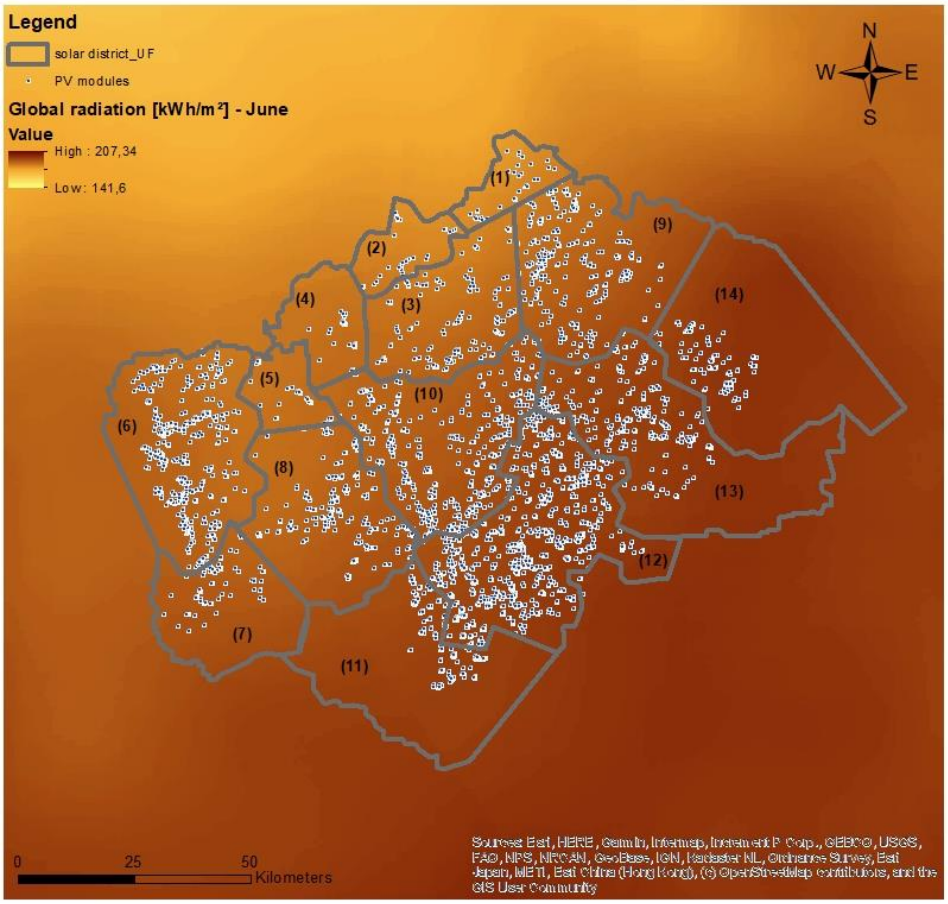

Solar district centres

(1)	Sondheim
(2)	Bad Brückenau
(3)	Oberthulba
(4)	Fellen
(5)	Frammersbach
(6)	Aschaffenburg
(7)	Amorsbach
(8)	Marktheidenfeld
(9)	Bad Neustadt
(10)	Arnstein
(11)	Bütthard
(12)	Kitzingen
(13)	Haßfurt
(14)	Ebern

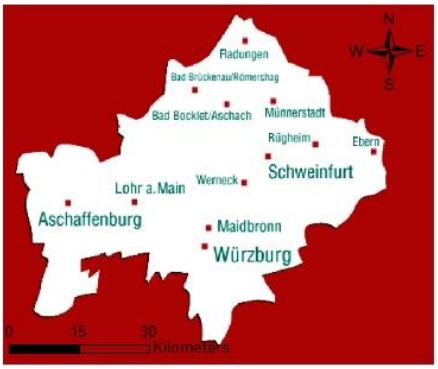

Figure 14 Upper figure: Global radiation including the 14 solar districts and the distribution of the solar modules within the study area in June 2017. Lower figure: Imagery with labels of the Under Franconia (GenWiki commons, 2005). Coordinate system: DHDN_3_Degree_Gauss_Zone_4; Projection: Gauss_Kruger. Source: Own figure, based on Geodata: Esri, DigitalGlobe, GeoEye, Earthstar Geographics, CNES/Airbus DS, USDA, USGS, AeroGRID, IGN, and the GIS User Community (ESRI, 2019).

3.3.2 Wind Turbines

Regarding wind turbines, 261 turbines were installed within the study area. Beside the coordinates, each turbine contains data about installed capacity, full load hours, rotor diameter, height, and the manufacturer which was implemented into the attribute table and mapped in ArcGIS (Figure 15).

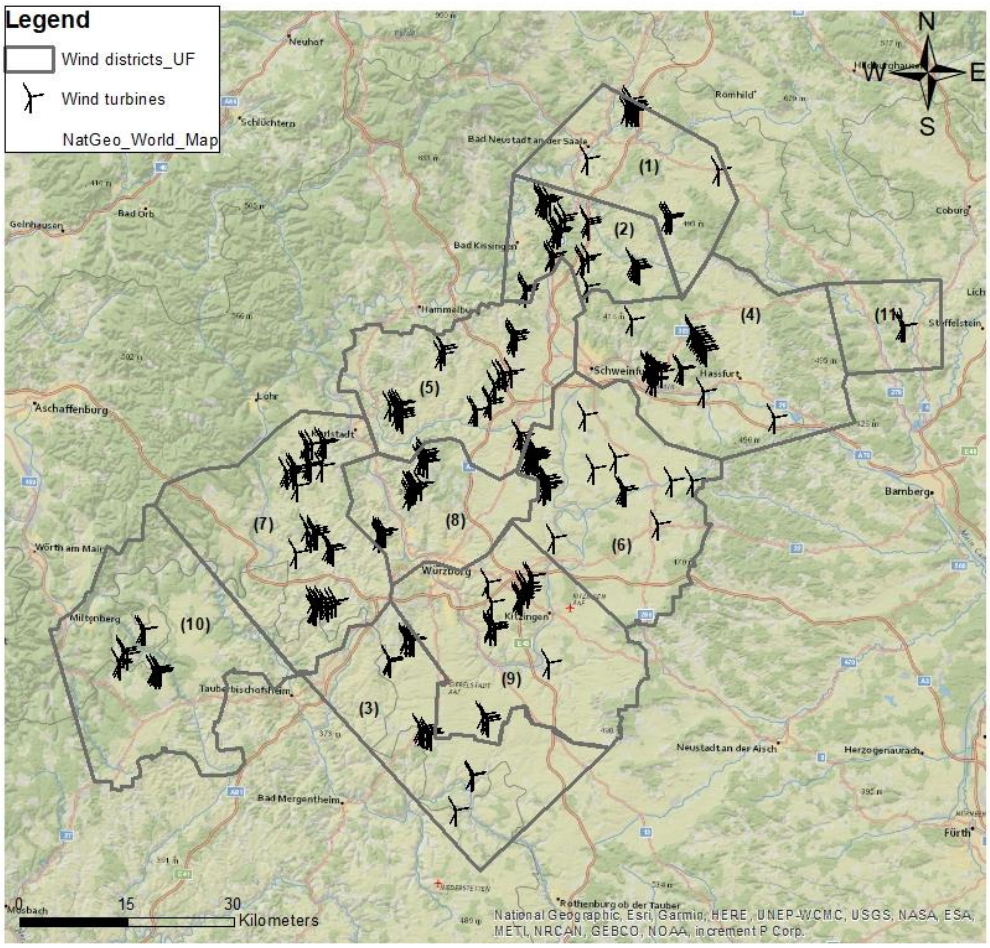

Wind district centres

(1)	Bad Neustadt
(2)	Bad Kissingen
(3)	Bütthard
(4)	Haßfurt
(5)	Arnstein
(6)	Kolitzheim
(7)	Marktheidenfeld
(8)	Retzstadt
(9)	Ochsenfurt
(10)	Eichenbühl
(11)	Ebern

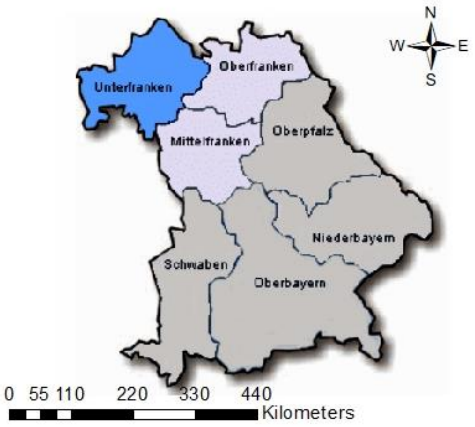

Figure 15 Upper figure: Study area with the location of wind turbines. Region is subdivided into 11 wind districts with accompanying centres. Lower figure: Under Franconia (GenWiki commons, 2005). Coordinate system: DHDN_3_Degree_Gauss_Zone_4; Projection: Gauss_Kruger. Source: Own figure, based on Geodata: National Geographic, Esri Garmin, HERE UNEP-WCMC, USGS, NASA; ESA METL, NRCAN, GEBCO, NOAA increment P Corp (ESRI, 2019).

3.3.3 Hydropower Plants

Concerning hydropower, two main types of plants of a total of 270 hydro power plants were installed within the study area: Run-of-river plants and swellable plants. Therefore, the dominant type is the usual run-of–river plant along the river Main. However, in Lower Franconia no records about any storage plants exist.

Beside the coordinates, the performance class was provided by the '*Energieatlas Bayern'* (Bayerische Staatsregierung, 2017). Plants not on–site of the river were small hydro power plants. Within the frame of this thesis only plants with a performance class of more than 1 MW were of concern. The map shows the distribution of the hydro power plants (without subdivision) within the study area, presented in figure 16.

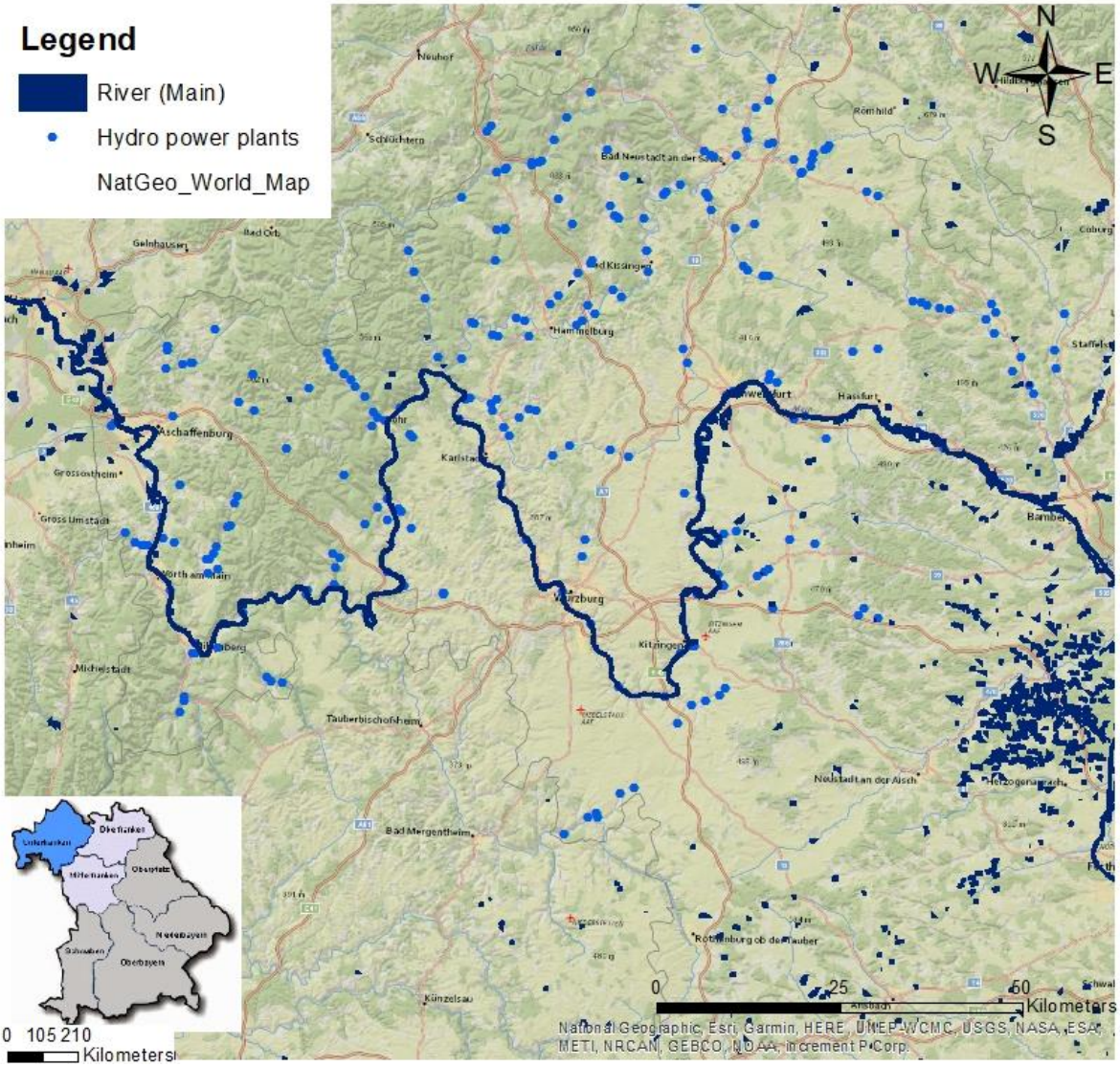

Figure 16 Main figure: Study area with the river 'Main' (dark blue) and the location of all hydro power plants (light blue). Lower left figure: Under Franconia. Source: (GenWiki commons 2005). Coordinate system: DHDN_3_Degree_Gauss_Zone_4; Projection: Gauss_Kruger. Source: Own figure, based on Geodata: National Geographic, Esri Garmin, HERE UNEP-WCMC, USGS, NASA; ESA METL, NRCAN, GEBCO, NOAA increment P Corp (ESRI, 2019).

3.4 Identification of Future Climate Parameters

Regarding to make statements about the future energy generation of the developed renewable energy systems, which map the future, climate parameters were needed.

The climate system must be understood as the basis for this. Essential single systems in the entire climate system were the stratosphere, troposphere, atmosphere, biosphere, hydrosphere, cryosphere and lithosphere (Miller & Yates, 2005). Furthermore, every single system contains different components and influencing factors, which lead to a climate cycle and thus had an impact on the climate. The earth's climate is a complex system characterized by the absorption of energy (solar radiation), redistribution of energy caused by the individual systems (atmosphere, hydrosphere, etc.) and energy output (emitted radiation of the earth). Industrialization and the associated increased emission of carbon dioxide and along with other greenhouse gases, mixed through the energy balance.

The use of a ‘GCM’ which tries to model future climate scenarios started in the 1970s. Climate models are computer programs that subdivide the atmosphere, oceans and soil into pixels (the side length of these pixel is about 200 km) and in each of these pixels calculating the physical condition as well as the mass and energy exchange with the adjacent pixels using physical equations (in the atmosphere it is a simplified form of the Navier-Stokes equations). The dynamic nature of these equations allowed us to calculate not only the state of the climate system at a given time, but also its evolution over time. In addition, climate processes which cannot be described by the above-mentioned physical equations or which take place on too small spatial scales to be represented by the coarse model lattice, were integrated into climate models through parameterizations (semi-empirical simplified descriptions of the processes). These included turbulent processes in the atmospheric boundary layer, convective precipitation ("summer storms") and radiation transfer.

The functioning of GCMs is very similar to weather models used to predict the weather over a few days. In contrast to weather models, however, climate models calculate the state of the climate system over many decades, which leads to important limitations in the interpretation of their results. It is known that weather forecasts only make sense to predict a few days, and that weather models quickly move away from the current state of the atmosphere after this predictable time span. The reason for this behaviour are chaotic components of the weather and the climate system, which take over the determiners after a short time. The informative value of climate models becomes limited to the non-chaotic parts of the climate system on the time scale of decades. They describe statistical parameters of the weather which refer to several decades, such as mean temperatures or precipitation. Apart from this restriction, climate models can also be faulty in the description of statistical climate parameters and any climate simulation is subject to uncertainties.

The presented climate models could be divided into three levels of complexity: conceptual climate models for simplified assumptions. Complex climate models, also called General circulation model and models of medium complexity.

To obtain a smaller scale for climate modelling, as required in this work, the GCMs were scaled down to Regional Models (RCMs). There are two ways to differentiate: Dynamic downscaling, which, like the GCMs, calculates climate changes in a three-dimensional section of the atmosphere (with higher spatial resolution), and statistical downscaling. Thus, the relationships between global circulation patterns and local climate data were examined (Brasseur, Jacob, & Schuck-Zöller, 2017).

On this basis, reference was made to the ClimEx Project, which examined the effects of climate change on meteorological and hydrological extreme events and the consequences for the water balance. Extreme events were investigated based on an RCP 8,5. The RCP is defined as the representative concentration pathway, a greenhouse gas concentration trajectory adopted by the IPCC (AR5). An RCP 8,5 is equivalent to 8,5 W / m² net irradiation. This emission scenario was estimated to be a worst case as it assumed that the world population will continue to grow, with little technical development, unchanged ideas and a world without climate change prevention (Riahi et al., 2011).

The GCM, CanESM2, developed by the '*Candian Center of Climate Modelling and Analysis at Environment and Climate Change Canada*', was used as a climate model. The simulations with a 1000-year equilibrium state of the atmosphere under pre-industrial conditions of 284.7 ppm CO_2 concentration began in 1850. Between 1850 and 1950 five historical runs were created, from which ten more runs were made from 1950 onwards, differ in random disturbances of the atmosphere as an initial condition. Up to 2005, observed emission values, volcanic eruptions and drives from solar cycles were considered. From 2006, the simulations run under the RCP 8.5, independently of volcanic eruptions (Leduc et al., 2019).

The model CanESM2 consists of 50 members. This allows a natural variability of the climate differ in their initial conditions. Since the resolution of ~ 310 km of the CanESM2-LE model is too inaccurate, a dynamic downscaling was performed with the help of the regional climate model *'Canadian Regional Climate Model'* (CRCM5-LE) (Fyfe et al., 2017). With a resolution of ~ 12 km the study area could be analysed more precisely (Leduc et al., 2016). Figure 17 shows the connections of the different models:

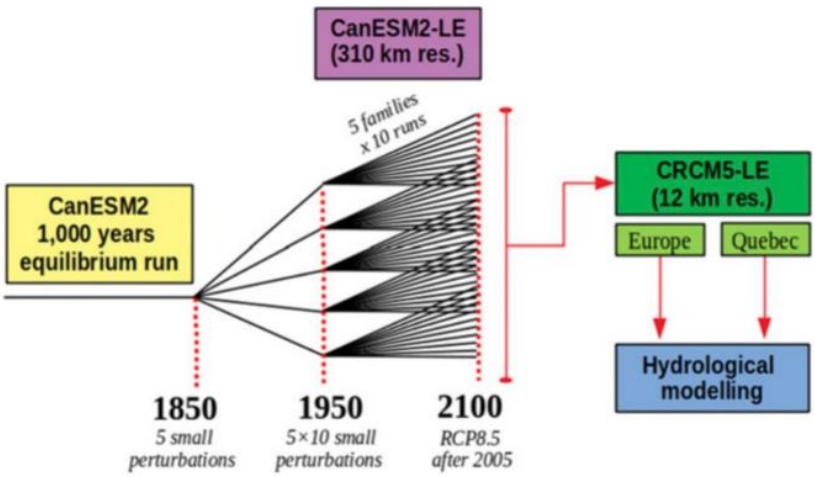

Figure 17 ClimEx model chain. Source: (Leduc, et al., 2016)

3.4.1 Water Balance Model

In order to determine the future water levels and outflows of the river Main a water balance model (WaSIM), based on the model CRCM5-LE, was used. Considering various factors (such as relief, soil type, precipitation and temperature), this model calculated the water discharge at selected levels. The WaSIM model is based on physical quantities and took several input quantities into account (Gebhardt, Glaser, Radtke, & Reuber, 2007). For a quick model process, a certain area was covered with a regular grid. Input was based on geographic (e.g., land use and topography), metrological (based on CRCM5 LE, e.g., precipitation, temperature, global radiation, wind speed and relative humidity) and hydrological data (e.g. levels of discharge) (Schulla, 1997). All these components were used to calibrate this model. The resolution for Bavaria was ~ 500 m.

3.4.2 Modelling of climate parameters for the study area

In the context of this thesis, climate parameters with statements about global radiation, wind force, temperature and runoff were essential. The data had a resolution of three hours aggregated to daily values. Overall, the climate model included 50 members, which figured out the natural variability of the climate. Each member had the same probability, although the simulation did not reflect the forecast, but a trend for the climate in the future, under a given emission scenario (Leduc et al., 2019). From these 50 members, a choice of five was made: A reference member, two extremes as a maximum and minimum in radiation and a dry and a wet scenario.

For selection, the modelled values of the years 1991-2010 and 2071-2090 were chosen. These were aggregated within the period from 1991 to 2010 to monthly values for each individual year. The reference value used was the arithmetic mean from global radiation, since global radiation is seen as the driving force behind the climate. In order to yield the other four members, the deviation of each run was determined to this reference value. On the one hand, members were selected with a maximum and a minimum of global radiation and on the other hand with a dry and a wet scenario, based on the future state.

As mentioned, this work dealt with the climate parameters global radiation, temperature, wind force and runoff, in order to explain the future energy production of electricity using regenerative energies. The climate model used divided the area of eastern Switzerland, parts of Baden Württemberg and all of Bavaria into a total of 114 catchment areas, each catchment area provided information in three hours on the parameters to be determined. The parameters were determined within a reference period (1991–2010) and within a future period 2071–2090). Of the 114 catchment areas, 14 were relevant to the study area. These 14 areas cover the western part of Upper Franconia, Lower Franconia, the eastern part of Hesse, the ‘Frankfurt – Osthafen’ and ‘Nordbaden’ (Figure 18). Based on this, the climate parameters of the individual catchment area could be determined.

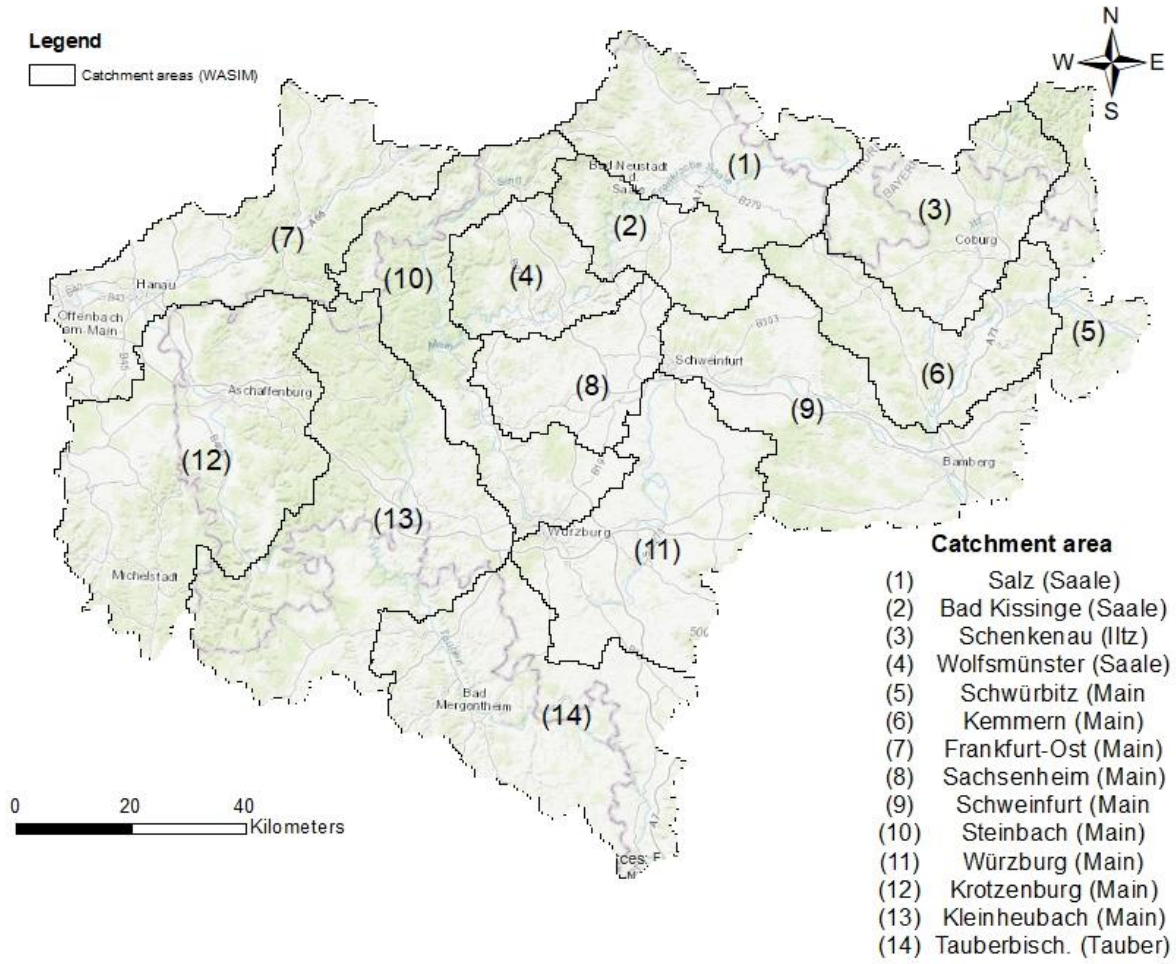

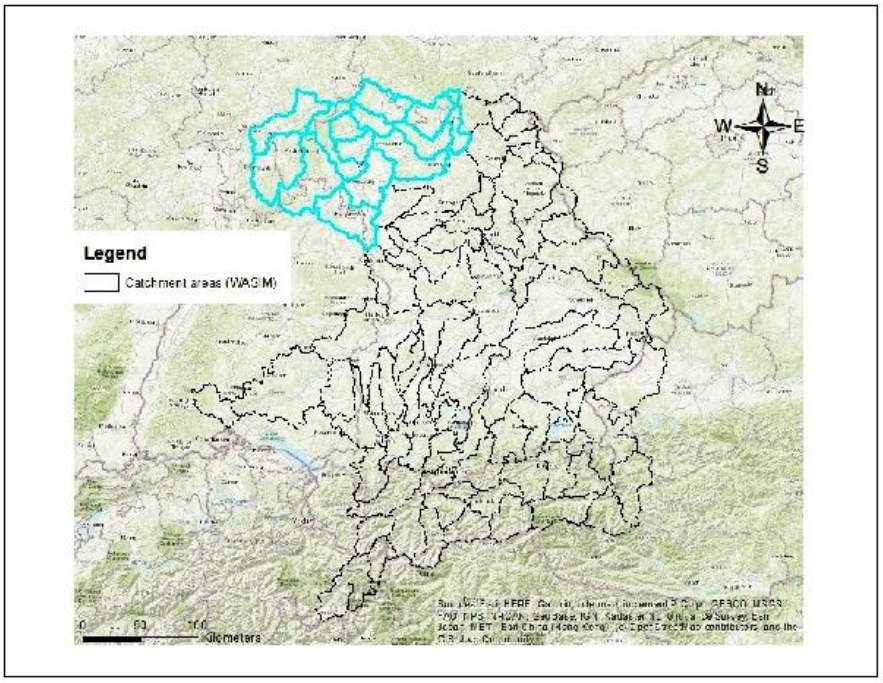

Figure 18 Upper picture illustrates the study area including 14 climate catchment areas. Lower picture shows the created catchment areas for the entire area, which was of concern for the appliance of the climate model CanESM2 Leduc, et al., 2019); Coordinate system: DHDN_3_Degree_Gauss_Zone_4; Projection: Gauss_Kruger. Source: Own figure based on Geodata: National Geographic, Esri Garmin, HERE UNEP-WCMC, USGS, NASA; ESA METL, NRCAN, GEBCO, NOAA increment P Corp (ESRI, 2019).

With regard to the runoff, the technical data is linked to a route (routing). In the case of waterways, the water locality, from source to mouth, is stored allowing events such as runoff to be positioned along that route. In order to maintain the future runoff at selected locations on the river Main, the outflows in each of the 14 catchment areas are compared both during the period (1991-2010 & 2071-2090) monthly and annually.

For the climate parameters global radiation, temperature and wind strength, the approach for calculating the variables is different, since the values do not have to be derived from a routing of the water structure, but an area-weighted average has to be determined on the basis of the respective catchment areas. In turn, a catchment area from the total of 14 areas is composed of several smaller catchment areas. Based on this, the climate parameters have to be offset with the area-weighted means in order to obtain a clear statement about future climate parameters in a catchment (formula 34).

$$M = \frac{\sum_i^n x_i * g_i}{\sum_i^n g_i} \quad (34)$$

With M Weighted average [depends on parameter]

x_i Value of parameter i [depends on parameter]

g_i Weighting factor [-]

As an example, the catchment area Schweinfurt (ID 20006) consists of 17 individual smaller catchment areas in which each individual area has a specific size. Likewise, each individual surface is characterized by the parameters to be determined. Thus, for each individual area, an area-weighted average must be calculated in order to obtain weighted values in the form of climate parameters within a catchment area (Figure 19).

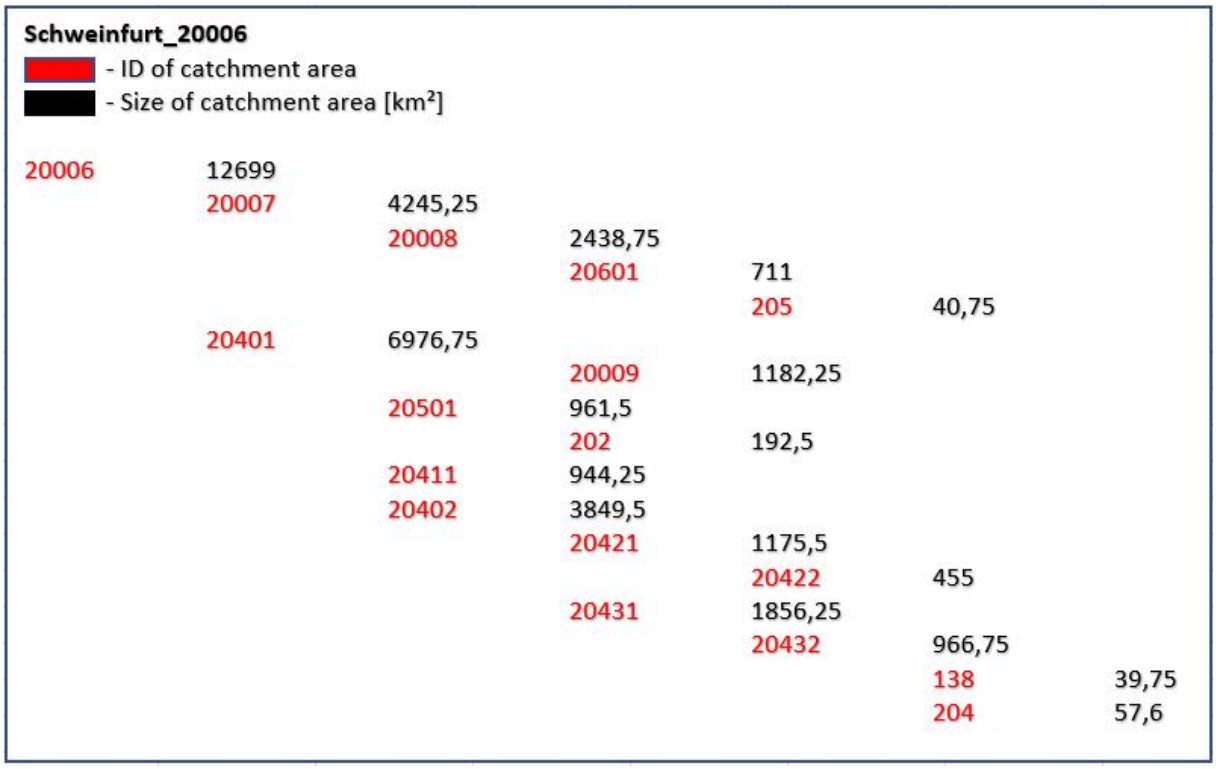

Figure 19 Composition of a catchment area (Schweinfurt) including its according subcatchment areas. ID of catchments in red. Size of catchment area in black. Source: Own figure based on (Leduc, et al., 2019)

3.4.3 Relation between Present and Future Climate

In order to establish a link between the climatic regions, on which the locations of regenerative energy systems and the climate parameters for the time period 2000-2019 are based on and the catchment areas of the climate model CanESM2, the individual areas must be linked together. The catchment areas were area-average weighted based on solar and wind districts (formula 33). Table 5 shows the proportion of the respective districts in the specific catchment areas of the climate model. If a row shows the symbol [/], there is no specific regenerative energy system in the catchment area of the climate model.

Table 5 Alignment of climate districts from the present state to the catchment areas according to CanESM2. Source: Own table

ID_Catchment area (CanESM2)	***ID_Solar district***	***ID_Wind district***
1_Salz	25% x 1_Sondheim 70% x 9_Bad Neustadt 5% x 3_Oberthulba	1_Bad Neustadt
2_Bad Kissingen	45% x 3_Oberthulba 55% x 9_Bad Neustadt	80% x 2_Bad Kissingen 20% x 1_Bad Neustadt
3_Schenkenau	14_Ebern	/
4_Wolfsmünster	3_Oberthulba	2_Bad Kissingen
5_Schwürbitz	14_Ebern	/
6_Kemmern	95% x 14_Ebern 5% x 9_Bad Neustadt	80% x 11_Ebern 20% x 4_Haßfurt
7_Frankfurt Ost	/	/
8_Sachsenheim	10_Arnstein	5_Arnstein
9_Schweinfurt	13_Haßfurt	4_Haßfurt
10_Steinbach	25% x 2_Bad Brückenau 35% x 4_Fellen 40% x 10_Arnstein	80% x 8_Retzstadt 20% x 7_Marktheidenfeld
11_Würzburg	12_Kitzingen	50% x 6_Kolitzheim 50% x 9_Ochsenfurt
12_Krotzenburg	6_Aschaffenburg	
13_Kleinheubach	35% x 7_Amorsbach 20% x 5_Frammersbach 45% x 8_Marktheidenfeld	50% x 7_Marktheidenfeld 50% x 10_Eichenbühl
14_Tauberbischofsheim	11_Bütthard	3_Bütthard

Beside the connection between the catchment area, a connection between the climate parameters of the present state (2000–2019) and the future state (2071–2090) needed to be established. Therefore, the following method was applied: Adding the delta between historical (reference) and future values, based on the climate model, up to the determined values of the present climate (formula 35).

$$x_{f(real)} = \left(x_{f(i)} - x_{ref(i)}\right) + x_{p(i)} \quad (35)$$

With $x_{f(real)}$ Real climate value in the future

$x_{f(i)}$ Climate value from future state (CanESM2)

$x_{ref(i9)}$ Climate value from historical state (reference) (CanESM2)

$x_{p(i)}$ Determined climate value from present state

4 Results and Discussion

Within this chapter a first picture was drawn regarding the present climate and renewable energy situation in the study area, based on the graphical as well as statistical data analysis and mapping of the corresponding climate districts and energy systems. In addition, it was intended to show the relationship of present climate parameters and the energy generation of regenerative energy systems which were already installed. Afterwards, the results of the climate model CanESM2 for future climate parameters were pointed out. These were discussed and mapped based on a graphical and statistical analysis. Therefore, the climate districts were related to corresponding catchment areas based on the climate model (Chapter '*Relation between Present and Future Climate'*). Hence, data and analysis of both approaches could be compared and transferred among themselves. The climate parameters modelled for future scenarios were applied to the different regenerative energy systems by using the created performance plans determining the future electrical energy production in the years 2071 – 2090. As a result, comparisons between present and future power generation were demonstrated.

4.1 Climate Parameters (Present Period)

Within this subsection the following climate parameters of the present time period (2000 – 2019) were going to be discussed and afterwards applied to the renewable energy systems within the related districts in which the study area was subdivided:

- Global radiation -> 14 Solar districts -> PV-systems
- Temperature -> 14 Solar districts -> PV-systems
- Wind speed -> 11 wind districts -> Wind turbines
- Water level and discharge -> Routing–gauges at 6 locations ->RoR-plants

The values of the parameters global radiation, wind speed, temperature, water level and discharge were calculated on a monthly average basis, according to the arithmetic mean determination (formula 36).

$$x_{mean} = \frac{1}{n} \sum_{i=1}^{n} x_i \tag{36}$$

With x_{mean} Averaged value of parameter [depends on parameter]

n Number of parameters [-]

x_i Value of specific parameter [depends on parameter]

4.1.1 Present Global Radiation

Figure 20 shows the transformation of the climate data of the study area into a diagram displaying monthly mean values in global radiation in the specific solar districts, labeled by numbers (formula 34) (Chapter '*Global Radiation'*). Throughout the year the global radiation showed a typical quadratic function in form of a negative parabola. A significant trend could be determined displayed on a polynomic function of second order. The global radiation had its minimum in the winter months, whereas it reached its peak in the summer months. Hence, the range was between 13,3 kWh/m² in December (District 4) and 193,6 kWh/m² in June (District 14).

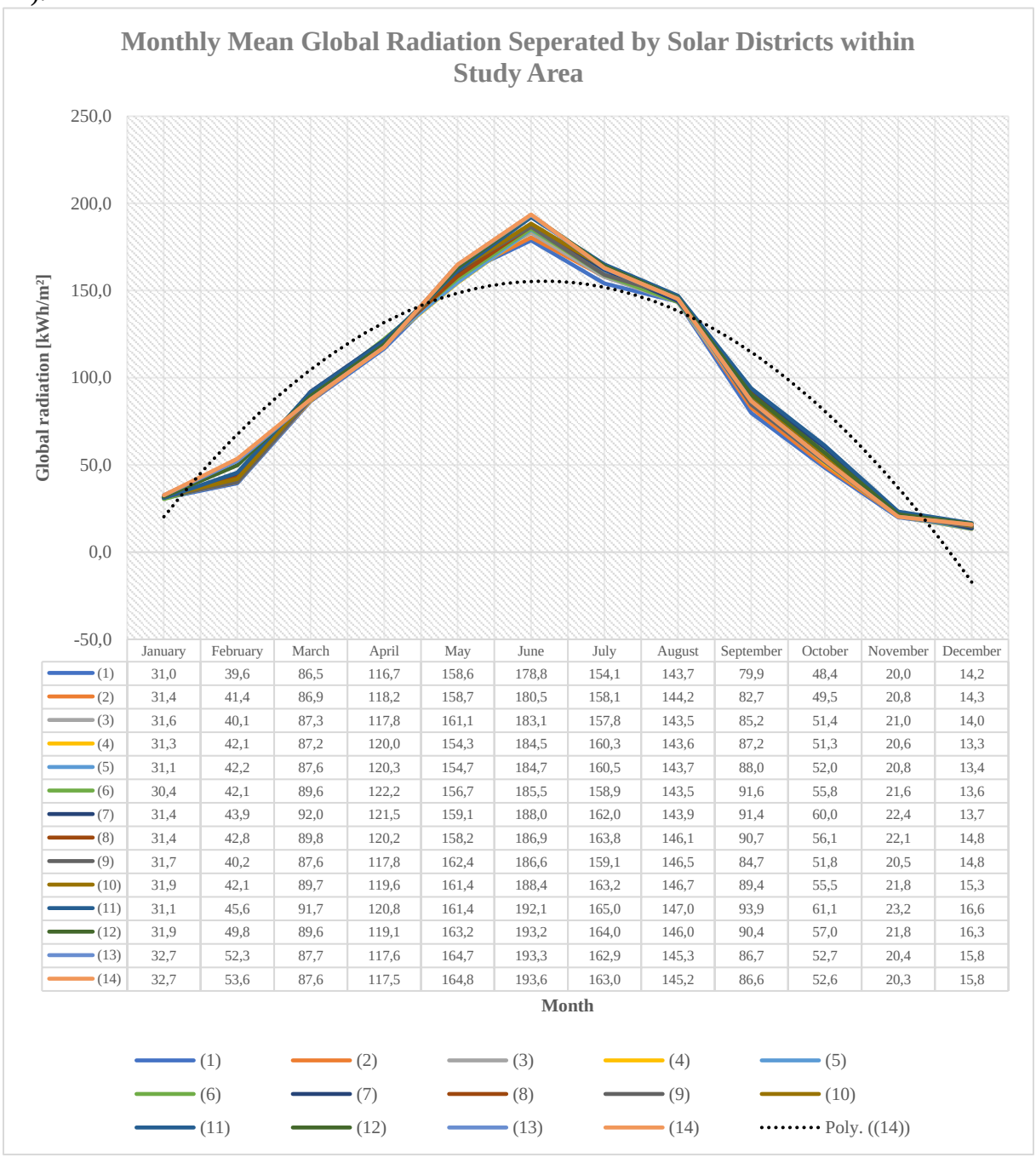

	January	February	March	April	May	June	July	August	September	October	November	December
(1)	31,0	39,6	86,5	116,7	158,6	178,8	154,1	143,7	79,9	48,4	20,0	14,2
(2)	31,4	41,4	86,9	118,2	158,7	180,5	158,1	144,2	82,7	49,5	20,8	14,3
(3)	31,6	40,1	87,3	117,8	161,1	183,1	157,8	143,5	85,2	51,4	21,0	14,0
(4)	31,3	42,1	87,2	120,0	154,3	184,5	160,3	143,6	87,2	51,3	20,6	13,3
(5)	31,1	42,2	87,6	120,3	154,7	184,7	160,5	143,7	88,0	52,0	20,8	13,4
(6)	30,4	42,1	89,6	122,2	156,7	185,5	158,9	143,5	91,6	55,8	21,6	13,6
(7)	31,4	43,9	92,0	121,5	159,1	188,0	162,0	143,9	91,4	60,0	22,4	13,7
(8)	31,4	42,8	89,8	120,2	158,2	186,9	163,8	146,1	90,7	56,1	22,1	14,8
(9)	31,7	40,2	87,6	117,8	162,4	186,6	159,1	146,5	84,7	51,8	20,5	14,8
(10)	31,9	42,1	89,7	119,6	161,4	188,4	163,2	146,7	89,4	55,5	21,8	15,3
(11)	31,1	45,6	91,7	120,8	161,4	192,1	165,0	147,0	93,9	61,1	23,2	16,6
(12)	31,9	49,8	89,6	119,1	163,2	193,2	164,0	146,0	90,4	57,0	21,8	16,3
(13)	32,7	52,3	87,7	117,6	164,7	193,3	162,9	145,3	86,7	52,7	20,4	15,8
(14)	32,7	53,6	87,6	117,5	164,8	193,6	163,0	145,2	86,6	52,6	20,3	15,8

Figure 20 Mean monthly global radiation of the 14 solar districts displayed in figure 11 in the present period (2000 – 2019). All values were determined in the unit kWh/m². A polynomic trendline shows the trend throughout the year. Source: Own figure based on DWD (DWD Climate Data Center (CDC), 2019).

4.1.2 Present Wind Force

Figure 21 shows the transformation of the data of the study area into a chart displaying monthly mean values of wind force in the specific wind districts (formula 34). Hereby, a fluctuating function of third order could be evaluated, whereas a meaningful trend was not recognizable. From January to March wind force was strengthen up, then the power decreased until May, whereas the function increased again until June. Afterwards the wind force fell until August and was about to reinforce until the end of the year in December. Hence, several maximums (March and June) and minimums (May and August) occurred during the year, whereas the wind force ranged between 1,95 m/s in August (District 1) and 4,43 m/s in June (District 7). The variance of all districts was determined to $\sigma = 0{,}22$.

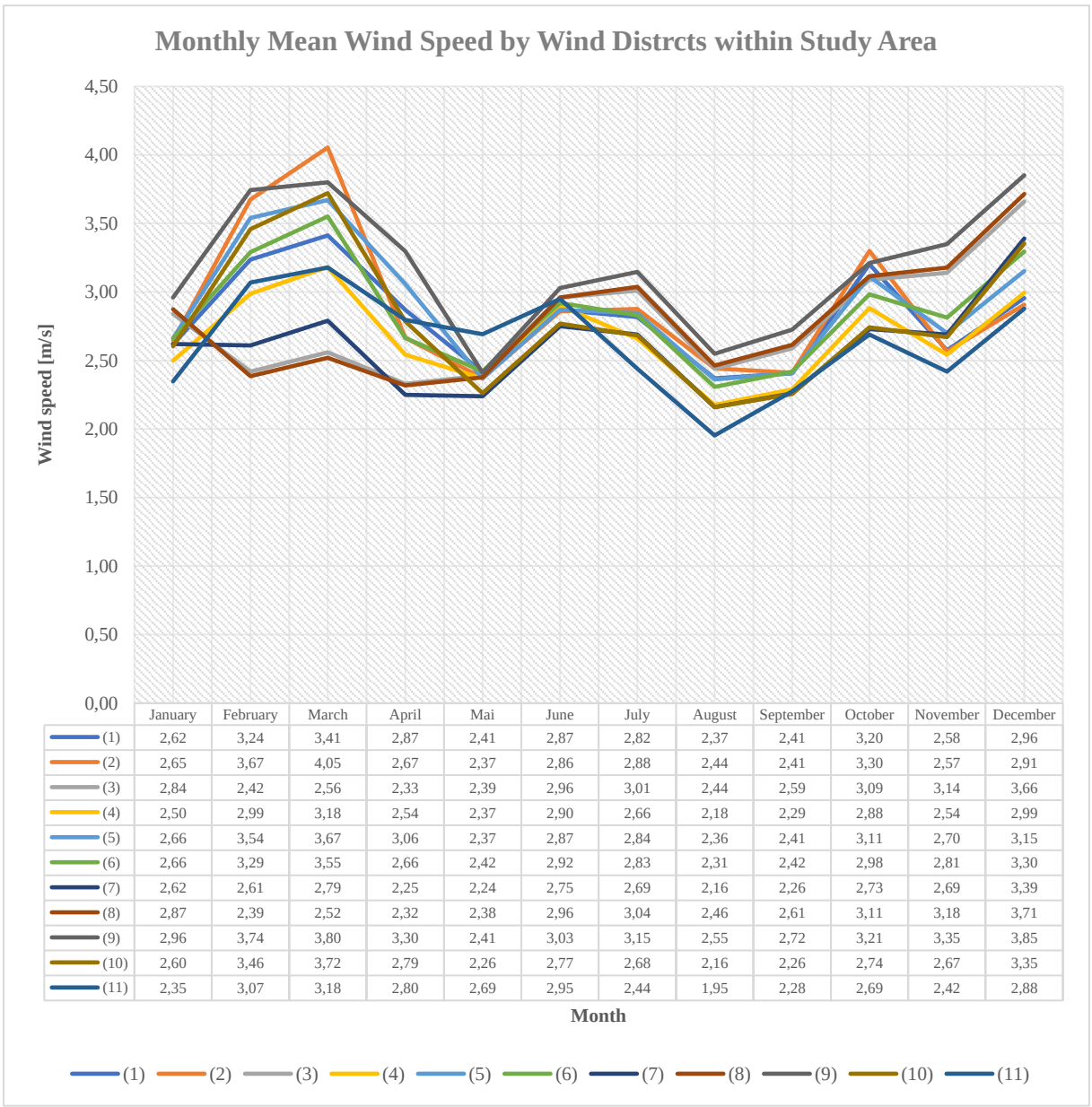

	January	February	March	April	Mai	June	July	August	September	October	November	December
(1)	2,62	3,24	3,41	2,87	2,41	2,87	2,82	2,37	2,41	3,20	2,58	2,96
(2)	2,65	3,67	4,05	2,67	2,37	2,86	2,88	2,44	2,41	3,30	2,57	2,91
(3)	2,84	2,42	2,56	2,33	2,39	2,96	3,01	2,44	2,59	3,09	3,14	3,66
(4)	2,50	2,99	3,18	2,54	2,37	2,90	2,66	2,18	2,29	2,88	2,54	2,99
(5)	2,66	3,54	3,67	3,06	2,37	2,87	2,84	2,36	2,41	3,11	2,70	3,15
(6)	2,66	3,29	3,55	2,66	2,42	2,92	2,83	2,31	2,42	2,98	2,81	3,30
(7)	2,62	2,61	2,79	2,25	2,24	2,75	2,69	2,16	2,26	2,73	2,69	3,39
(8)	2,87	2,39	2,52	2,32	2,38	2,96	3,04	2,46	2,61	3,11	3,18	3,71
(9)	2,96	3,74	3,80	3,30	2,41	3,03	3,15	2,55	2,72	3,21	3,35	3,85
(10)	2,60	3,46	3,72	2,79	2,26	2,77	2,68	2,16	2,26	2,74	2,67	3,35
(11)	2,35	3,07	3,18	2,80	2,69	2,95	2,44	1,95	2,28	2,69	2,42	2,88

Figure 21 Mean monthly wind speed of the eleven wind districts displayed in figure 6 in the period 2000-2019. All values in wind speed were determined in the unit [m/s]. Source: Own figure based on DWD (CDC, 2019).

4.1.3 Present Temperature

The temperature plays a significant role in the power generation output of PV-modules. When a module overheats (> 25°C), a substantial power reduction takes place. The weather stations regarding temperature observation were related to the solar districts. Figure 22 pointed out the distribution of the temperature displaying monthly mean values within the solar districts (formula 34). Throughout the year, the temperature occurred in a quadratic function (parabola), whereas a trend could be determined displayed in a polynomic function of second order as for global radiation. The study area showed a typical minimum in winter and a maximum in the summer months. The range was between - 4,8 °C in January (District 1) and 20,1 °C in July (District 12).

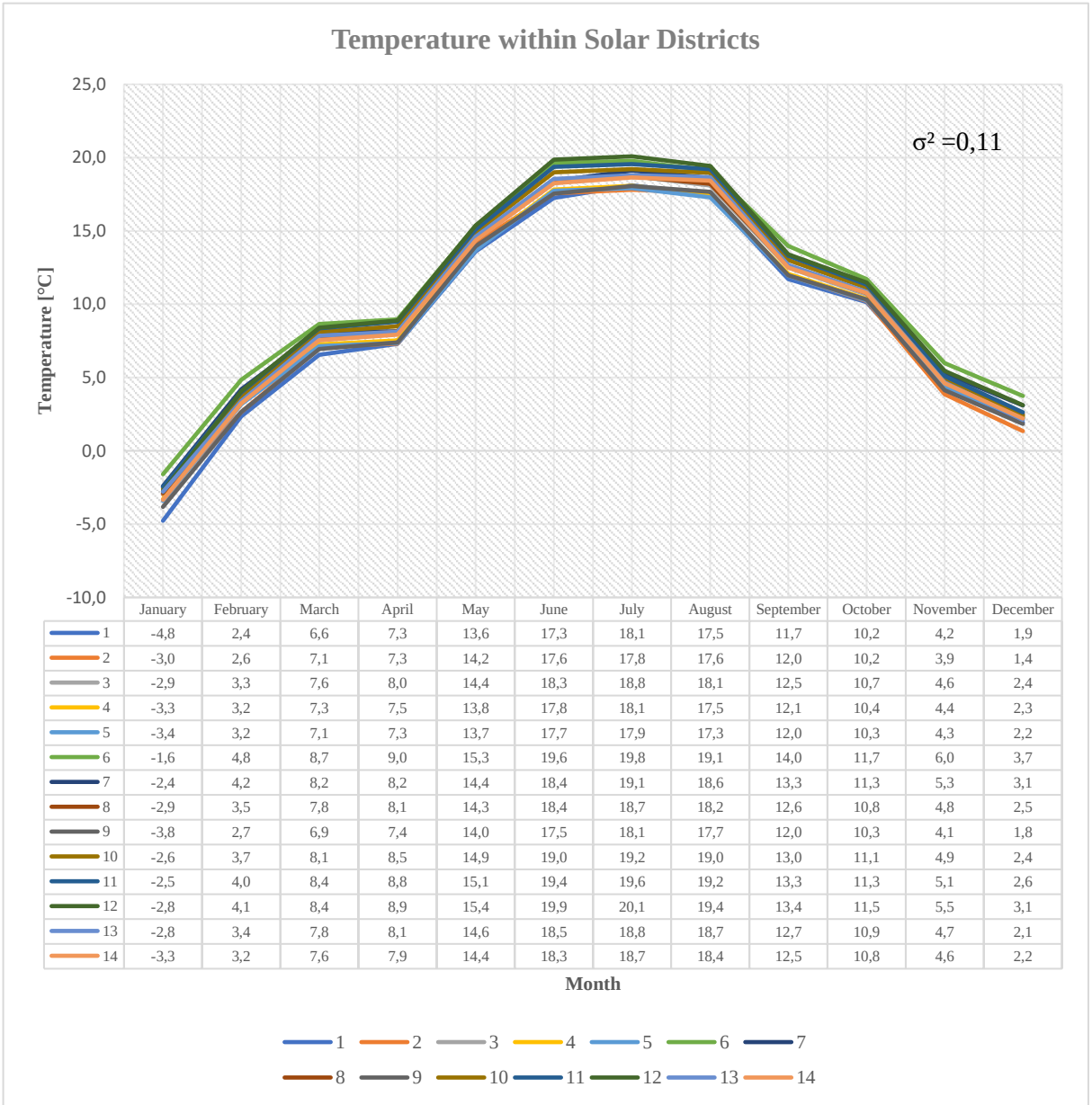

	January	February	March	April	May	June	July	August	September	October	November	December
1	-4,8	2,4	6,6	7,3	13,6	17,3	18,1	17,5	11,7	10,2	4,2	1,9
2	-3,0	2,6	7,1	7,3	14,2	17,6	17,8	17,6	12,0	10,2	3,9	1,4
3	-2,9	3,3	7,6	8,0	14,4	18,3	18,8	18,1	12,5	10,7	4,6	2,4
4	-3,3	3,2	7,3	7,5	13,8	17,8	18,1	17,5	12,1	10,4	4,4	2,3
5	-3,4	3,2	7,1	7,3	13,7	17,7	17,9	17,3	12,0	10,3	4,3	2,2
6	-1,6	4,8	8,7	9,0	15,3	19,6	19,8	19,1	14,0	11,7	6,0	3,7
7	-2,4	4,2	8,2	8,2	14,4	18,4	19,1	18,6	13,3	11,3	5,3	3,1
8	-2,9	3,5	7,8	8,1	14,3	18,4	18,7	18,2	12,6	10,8	4,8	2,5
9	-3,8	2,7	6,9	7,4	14,0	17,5	18,1	17,7	12,0	10,3	4,1	1,8
10	-2,6	3,7	8,1	8,5	14,9	19,0	19,2	19,0	13,0	11,1	4,9	2,4
11	-2,5	4,0	8,4	8,8	15,1	19,4	19,6	19,2	13,3	11,3	5,1	2,6
12	-2,8	4,1	8,4	8,9	15,4	19,9	20,1	19,4	13,4	11,5	5,5	3,1
13	-2,8	3,4	7,8	8,1	14,6	18,5	18,8	18,7	12,7	10,9	4,7	2,1
14	-3,3	3,2	7,6	7,9	14,4	18,3	18,7	18,4	12,5	10,8	4,6	2,2

Figure 22 Monthly mean temperature of weather stations within study area (2000 - 2019). Source: Own figure based on DWD (DWD Climate Data Center (CDC) 2019)

4.1.4 Present Water Level and Discharge

Regarding hydropower at the river Main, the decisive parameters water level and discharge needed to be determined. Therefore, six gauging stations from west to east were mapped and statistically analysed. For each gauging station, the values of both parameters were averaged, based on the arithmetic mean over the month in the period from 2000 to 2019 (formula 34). Within figure 23, the bars showed the water level, whereas the discharge was symbolized by lines. Furthermore, two polynomic trendlines were inserted into the diagram, displaying the trend of the water level and discharge of gauging station Schweinfurt. Therefore, a significant trend could be determined, with a maximum in water level and discharge in the winter months and a minimum of both in late summer and autumn. Regarding the gauging station Schweinfurt, the range of the water level was between 200 cm in October and 247 cm in January. The range of the discharge was between 76 m³/s in August and 200 m³/s in January.

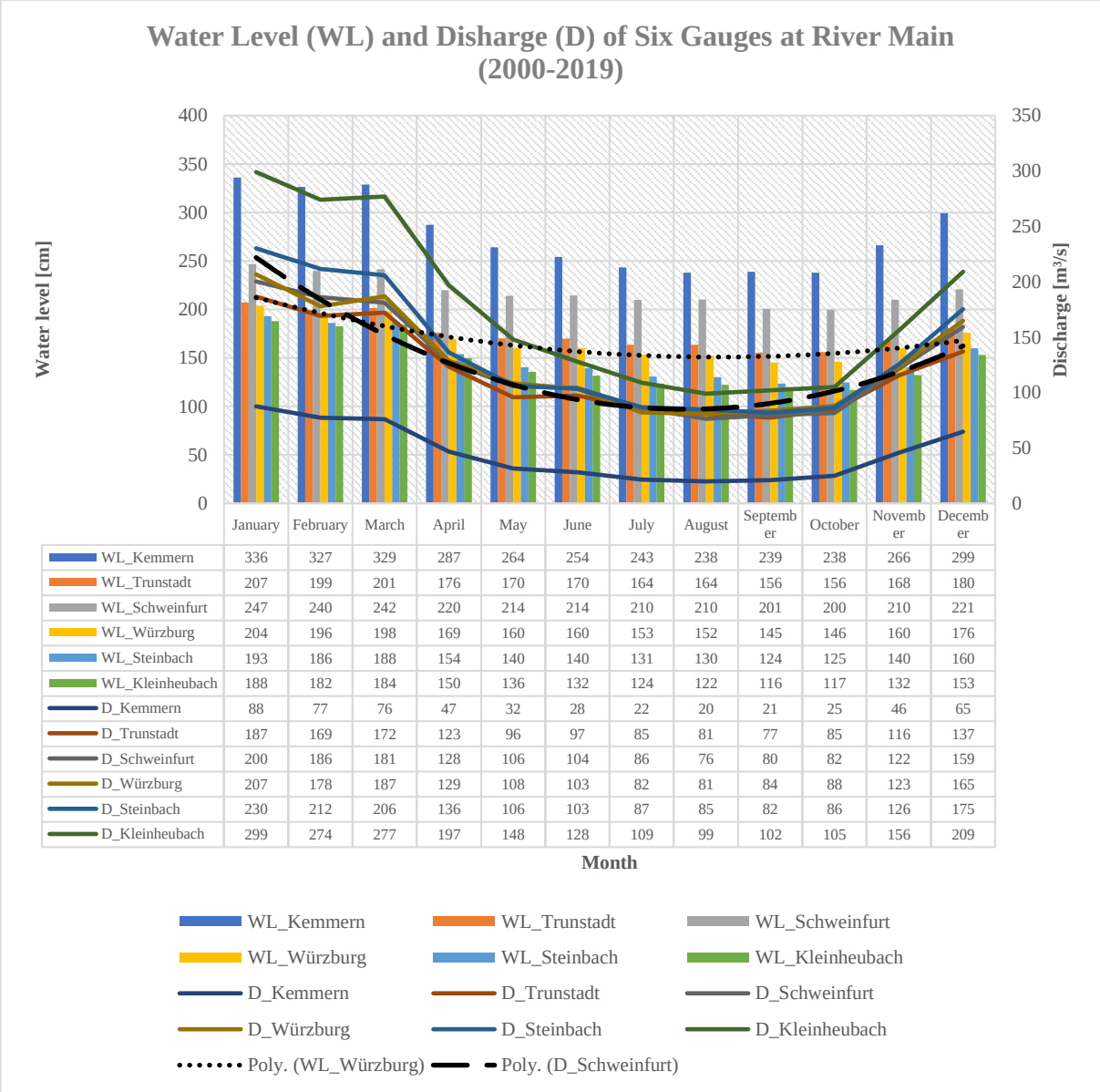

	January	February	March	April	May	June	July	August	September	October	November	December
WL_Kemmern	336	327	329	287	264	254	243	238	239	238	266	299
WL_Trunstadt	207	199	201	176	170	170	164	164	156	156	168	180
WL_Schweinfurt	247	240	242	220	214	214	210	210	201	200	210	221
WL_Würzburg	204	196	198	169	160	160	153	152	145	146	160	176
WL_Steinbach	193	186	188	154	140	140	131	130	124	125	140	160
WL_Kleinheubach	188	182	184	150	136	132	124	122	116	117	132	153
D_Kemmern	88	77	76	47	32	28	22	20	21	25	46	65
D_Trunstadt	187	169	172	123	96	97	85	81	77	85	116	137
D_Schweinfurt	200	186	181	128	106	104	86	76	80	82	122	159
D_Würzburg	207	178	187	129	108	103	82	81	84	88	123	165
D_Steinbach	230	212	206	136	106	103	87	85	82	86	126	175
D_Kleinheubach	299	274	277	197	148	128	109	99	102	105	156	209

Figure 23 Monthly averaged values in water level and discharge within the study area (2000 - 2019). Source: Own figure based on HND Bayern (Hochwassernachrichtendienst Bayern (Hnd Bayern), 2019).

4.1.5 Statements Regarding Present Climate Parameters

Looking more closely at the climate parameters global radiation, temperature, wind speed, water level and runoff mentioned above, the following points were noticeable:

1. There was a correlation between global radiation of temperature. Both parameters showed a minimum in the winter months and a maximum in the summer months. This was due to the processes in the long-wave range which occurred because of the difference of radiation and atmospheric radiation (effective radiation). This resulted in the cooling or warming of the earth's surface and also affected the air layers above it. In addition to this element, advective and convective air masses also contributed to the variability of climate elements (Hasenfratz, 2006). Figure 24 plotted the values, based on a Pearson correlation, on global radiation and temperature in the solar district 1_Sondheim. The Pearson correlation coefficient r was determined to 0,85, based on formula 37.

$$r = \frac{\sum_{i=1}^{n}(x_i - x_{mean})(y_i - y_{mean})}{\sqrt{\sum_{i=1}^{n}(x_i^2 - n x_{mean}^2)} * \sqrt{\sum_{i=1}^{n}(y_i^2 - n {y_{mean}}^2)}} \quad (37)$$

With r Pearson correlation coefficient [-]

x_i Value of parameter x at point I [-]

x_{mean} Mean value of all parameter of x [-]

y_i Value of parameter y at point I [-]

y_{mean} Mean value of all parameter of y [-]

n Number of parameters [-]

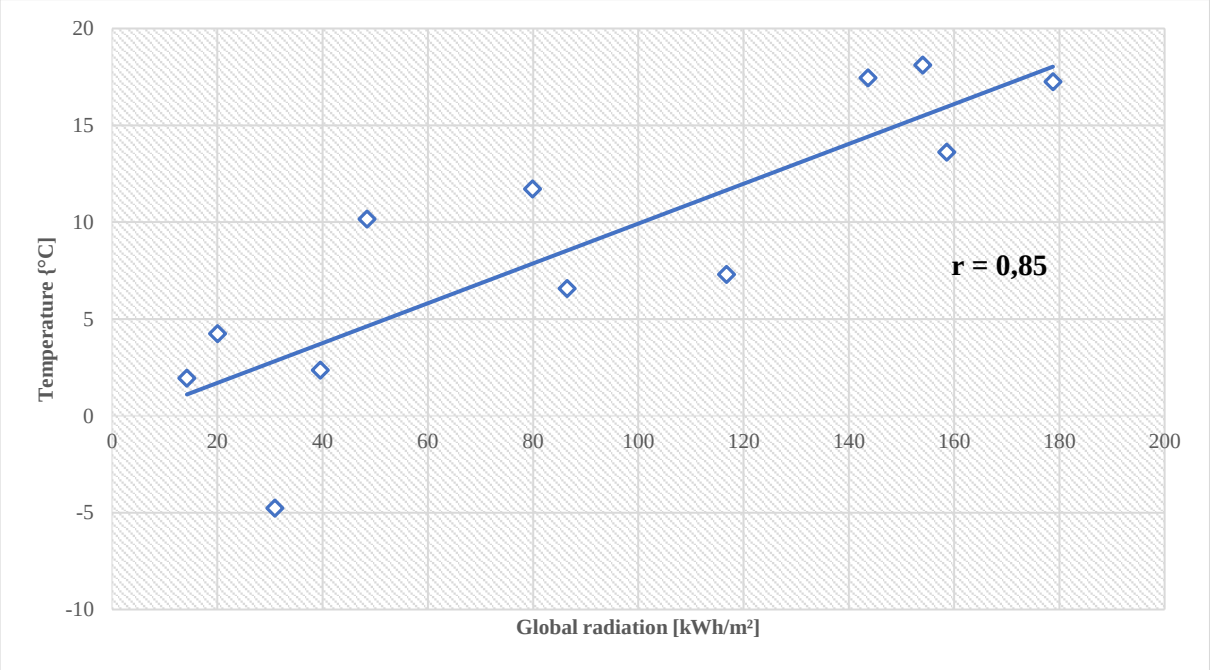

Figure 24 Pearson correlation between global radiation and temperature within present time period (2000 - 2019). Source: Own figure

1. Monthly totals were only of limited validity for wind speeds. The wind speed was periodic within one year and had its maxima in the winter months, while the wind speed decreased towards the summer.
2. The runoff or water level ran inversely to the global radiation and temperature. The water balance played a role, which was controlled by the interaction of precipitation, temperature, relative humidity and sunshine duration. As the average air temperature increased, the rate of evaporation generally increased, and less water remained for the runoff and water level in rivers and groundwater. However, it should be noted that higher air temperatures resulted in higher evaporation associated with higher water content in the atmosphere. This could cause rainfall and higher drains (Bayerisches Landesamt für Umwelt, 2018a).

4.2 Energy Generation by Regenerative Energy Systems (Present Period)

In this chapter, the energetic power generation of existing regenerative energy systems was graphically and analytically analysed based on climate observed by the DWD in the period between 2000-2017. The climate parameters were monthly and yearly averaged providing a reliable statement within the 20-year period. As mentioned in the chapter '*Technical Potentials of the Regenerative Energy Systems'*, performance plans had been drawn up for the individual renewable energy systems. From the designed power plans, the theoretical potential, based on existing technology, could be determined and compared with the real potential of power generation.

4.2.1 PV-Systems (Present Period)

Regarding photovoltaic systems, this work exclusively dealt with open-space systems, as they had a much higher distribution and installed capacity as roof systems. Apart from the systems, it was also important to distinguish between the different modules. PV–modules could be differentiated between silicon cells, III-V semiconductor cells, II-VI semiconductor cells, I-III-VI-I semiconductor cells, organic solar cells (OPV), dye cells and semiconductor electrolyte cells. Due to technical and economic potential advantages, PV-modules with silicon cells were the most widely used and analysed within the scope of this thesis. Silicon cells could again be distinguished between monocrystalline and polycrystalline cells. Likewise, these two types of modular cells needed to be differentiated (Table 6) (Quaschning, 2015b).

Table 6 Distinction between silicon cells including their specific efficiency and module area. Source: Own figure based on (Quaschning, 2015b).

Type of silicium cell	***Efficiency [%]***	***Area of module [m²] for 1 kWp***
Monocrystalline cell	19	5,3
Polycrystalline cell	17	5,9

According to the '*Energieatlas Bayern'* (Bayerische Staatsregierung, 2017), a total of 216 open–space systems were installed in the Lower Franconia area with a total installed capacity of ~ 432,5 MWp and a mean of ~ 2 MWp. The full load hours of these plants averaged ~ 979 h per year, with a total electrical energy generation of ~ 446,9 GWh/a and an average of ~ 2,1 GWh/a.

On the basis of formula 11 and the assumption, that it requires a module area of 5,6 m² for 1 kWp (arithmetic mean of mono- and polycrystalline cell) (Quaschning, 2015a), a total of ~ 2,4 km² of open–space PV–modules were installed in the study area. Based on the calculated global radiations within the different solar district, the total theoretic electricity generation was ~ 489,3 GWh/a, the average amounted to ~ 2,3 GWh/a (formula 12). The performance ratio of real and theoretic generation amounted to 8 7% on average.

In the case of theoretical regenerative power generation by PV-systems, factors such as the module temperature had to be considered. The monthly averaged module temperature was calculated according to formula 13 and based on measured air temperature at 2 m altitude, observed by 11 selected weather stations. Figure 25 shows the module temperature of the solar district 12_Kitzingen which had been calculated as the highest. It was found that the module temperatures of the PV ground-mounted systems in the district 11_Kitzingen (~ 23,7 °C in June) were below the 25 °C limit on which the PV modules were designed under STC conditions.

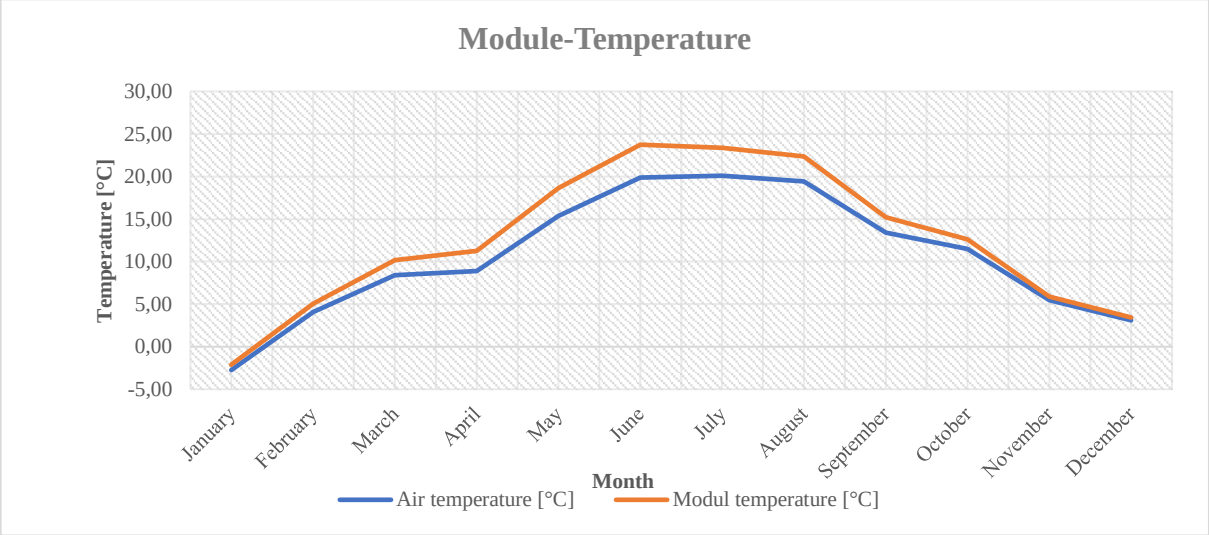

Figure 25 Chance of overheating regarding the solar district 12_Kitzingen, which shows the highest monthly averaged air temperatures within present time period (2000 - 2019). Source: Own figure

Beside the general energy generation of all open–space systems within the study area, a more precise look was given to a single system located in Aschaffenburg (40° 56' 38,9'' N – 9° 6' 16,6'' E). The system lies within the eponymous solar district and was erected with an installed capacity of 321,3 kWp. Based on an area utilization of 5,6 m² for 1 kWp, the system has a module area of ~ 57,4 m². Figure 26 shows the selected system including global radiation and electricity production on a monthly basis (formula 12). Corresponding to the global radiation, the electricity production generates a maximum in summer, especially in June. The total production was determined to ~ 357,2 MWh per month. Considering the chance of module overheating, a maximal module temperature of 23 °C occurs in June, whereas this factor could be neglected.

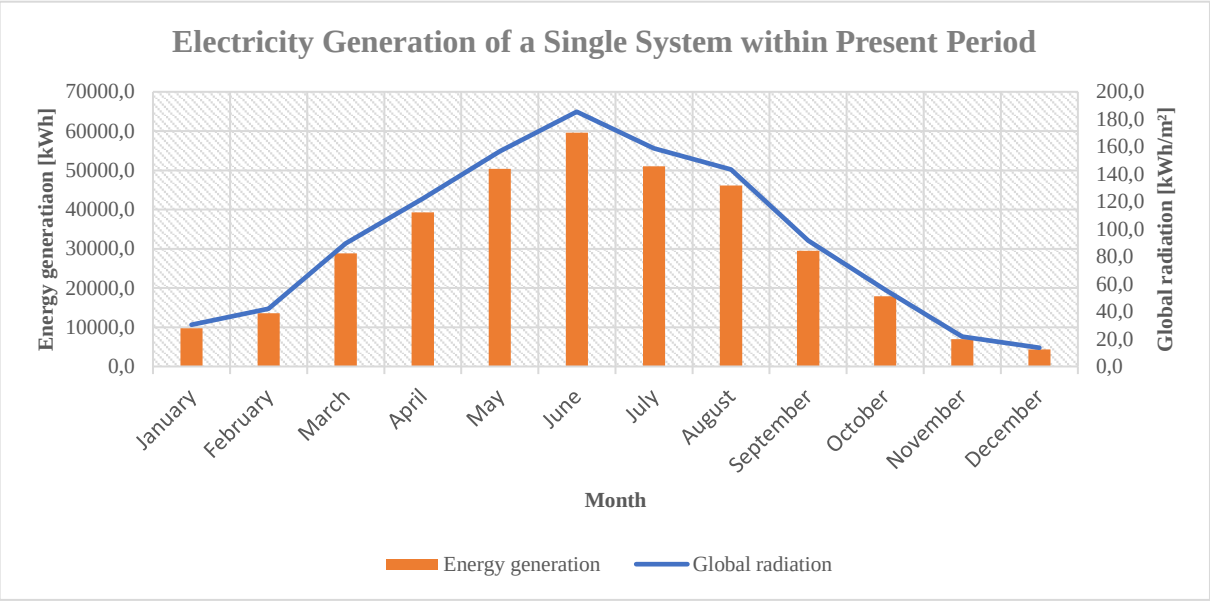

Figure 26 Electricity generation and global radiation of a single system located in Aschaffenburg with an installed capacity of 132,3 kWp. Source: Own figure

4.2.2 Wind Turbines (Present Period)

In the Lower Franconia area, a total of 261 wind turbines were installed in wind parks with several turbines or as a single unit. The individual wind turbines were assigned to the created wind districts with an average monthly wind speed. In order to determine the accumulated energy generation of a turbine per year, a wind power plan was drawn up. To illustrate the wind turbine performance plan and the resulting expected annual energy production, the following components and calculations were explained in more detail, step by step:

1. Places in the same region might have different average wind speeds, but usually they would have a rather similar wind speed distribution. This fact also contributed to the separation of the study area into wind districts. The measured wind speed distributions could be approximated by a mathematical description, the Weibull distribution function (formula 14 & 15), which included the flexible parameters k and A.
    a. Lower Franconia is located in central Europe, which led to a shape factor of k = 2.
    b. The scale factor A depends on the average wind speed.
    c. Calculation of the approximate mean wind speed (formula 16).
2. Creation of a range of wind speeds from 0,5 – 29,5 m/s, which represented the average wind speed of 30 speed classes, each 0,5 m/s wide.
3. Addition of input regarding reference height, hub height and roughness length.
    a. Reference height was defined as the height at which wind speed observations were made. Reference height = 10.
    b. The hub height of the wind turbine depends on the type of the installed wind turbine. Within the study area, the hub height ranges between 65 m at Neubrunn (district 7) and 149 m at Schwanfeld (district 6).
    c. The roughness was defined by roughness classes and a roughness length (z_0), on which the decrease of the wind speed near the ground mainly depends (Table 7).

Table 7 Roughness classes. Source: Own figure based on (Ragheb, 2012)

Surface	***Class***	***Length (z_0)***
Sea	0	0,0002
Flat terrain	0,5	0,0024
Fields, no fences	1	0,03
Fields with hedges etc.	2	0,1
Villages, forests	3	0,4
Large cities	4	1,6

d. Determination of the wind speed at hub height (formula 17).
e. Determination of the relative and cumulative frequency as a function of the speed at hub height.
f. Calculation of the wind power in the rotor plane, by inserting the air density and rotor diameter (formula 22). Within this power plan, the air density is defined as p_{Wi} = 1,2 kg/m³, whereas the rotor diameter depends on the type of the wind turbine within the study area. It ranged between 44 m in Neubrunn (district 7) and 122 m in Unsleben (district 1).
g. Calculation of the extracted power by the rotor, which is equal to the produced electrical power ($P_{ent,Wind} = P_{el}$) (formula 23). Therefore, information about cut–in speed, design speed and cut–out speed was needed. The turbine needs a certain torque to start the turbine, which was defined as the cut–in speed. The power train (gearbox, generator, etc.) is only capable of transmitting at a certain design power. Hence, the rotor must be safely limited to avoid overloading of the power train. When the wind speed is too high, safe operation would be no longer possible, which was defined as the cut–out speed. Therefore, 4 phases of operation could occur:
    - Below cut–in speed: Standstill
    - Up to rated wind speed: Maximal power extraction
    - Above rated wind speed: Power limited to design power
    - Above cut–out wind speed: Operation suspended

    Within the scope of this thesis, following assumptions were made: The cut–in speed was determined to 4 m/s, the design speed to 15 m/s and the cut–out speed to 25 m/s (Wind power program, 2019).

h. Determination of the maximal power coefficient (formula 24). Thereby, the mechanical power and the wind power were set in ratio. This coefficient considered generator losses, exit swirl losses and the profile drag resistance.
i. As the next step, the time in each velocity class was added, which was defined as the relative frequency times the hours per year. On this basis, the energy produced in this time could be calculated as followed (formula 38):

$$E = P_{el} * t \quad (38)$$

With E Electrical energy [kWh]
P Electrical power [kW]
t Time of velocity class [h]

j. Hence, the accumulated energy as the expected annual output could be determined.
k. Together with the rated capacity, the load factor as a measure of the economic efficiency of the chosen setup could be computed (formula 39).

$$LF = \frac{E_{acc}}{t * C} \tag{39}$$

With LF Load factor [-]
$E_{acc.}$ Expected annual output [kWh]
C Rated capacity [kW]

Case Study for a Single Wind Turbine

Within the scope of this thesis, a case study was executed for a wind turbine near Maßbach (50° 10’ 25,1’’ N and 10° 18’ 45,6’’ E) located in the wind district Bad Kissingen. The selected wind turbine was constructed by the company Nordex, which erected five more wind turbines with the same parameters around the area of Maßbach.

The entire created power plan was based on the monthly averaged wind behaviour within the present time period between 2000 – 2019, with a yearly averaged wind speed of 2,9 m/s. Decisive turbine characteristics as hub height (141 m), rotor diameter (117 m) and rated capacity (2.400 kW) were given by Nordex (Nordex, 2019). Within this case study different graphical and statistical figure illustrate main functions of the wind turbine and its annual energy output. The method was applied after formulas of wind power and process steps after the chapter ‘*Wind Turbines’*. Hence, the annual production could be predicted very accurate for a selected wind turbine installation.

The wind speed distribution at chosen site was extrapolated from measured data of the reference height and hub height at a given roughness length (formula 17). The sum of the relative frequency must be 1. The relative frequency increased until a hub height speed of 3,9 m/s with its peak at 0,26 and had an exponential decrease until 13,4 m/s, which gave a statement about the peak of the cumulative frequency (figure 27).

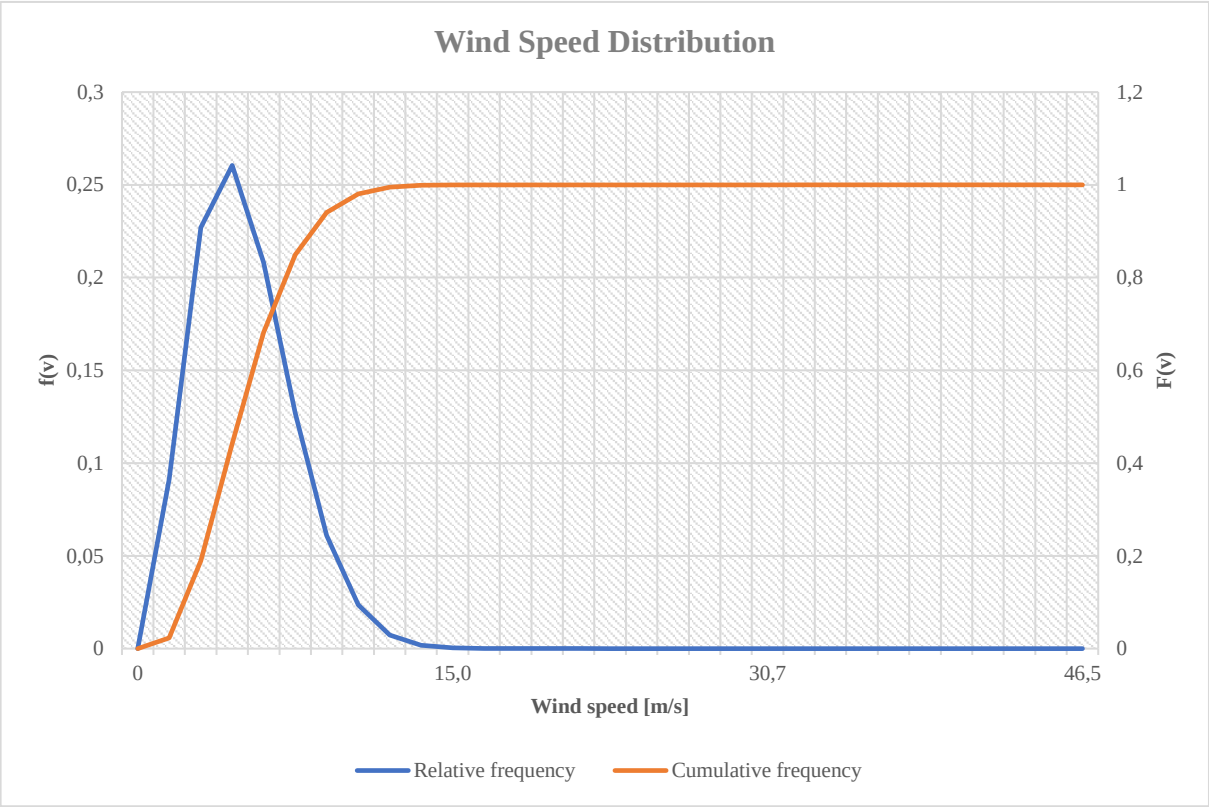

Figure 27 Wind speed distribution after Weibull of the selected wind turbine in Maßbach. Source: Own figure

In Figure 28, the relative wind speed frequency at hub height, wind power within rotor area and power curve of the wind turbine were displayed. The function of electrical power versus wind speed assumed following:

- $P_{el} = 0$ for v < cut – in wind speed
- $P_{el} = P_{Wind} * cp_{real}$ for v < design wind speed
- $P_{el} = P_{Max}$ for v < cut – out wind speed
- $P_{el} = 0$ for v > cut – out wind speed

The wind power in the rotor blade had an exponential increase with rising wind speed at hub height. The output power, which was extracted from the wind by the rotor blades, reached its peak at a wind speed (hub height) of 15 m/s and was determined to 9069 kW. After reaching the top it decreased drastically and the wind turbine kept producing the same output (2.400 kW) until a hub wind speed of 24,4 m/s. This is owed to the fact, that the rated capacity installed by the wind turbine company was set to 2.400 kW. As mentioned before in point (g.), the design speed was set to 15 m/s. This is the reason why at this wind speed the highest electrical power output was generated and no further increase would occur afterwards. Hence, the power is limited to design speed.

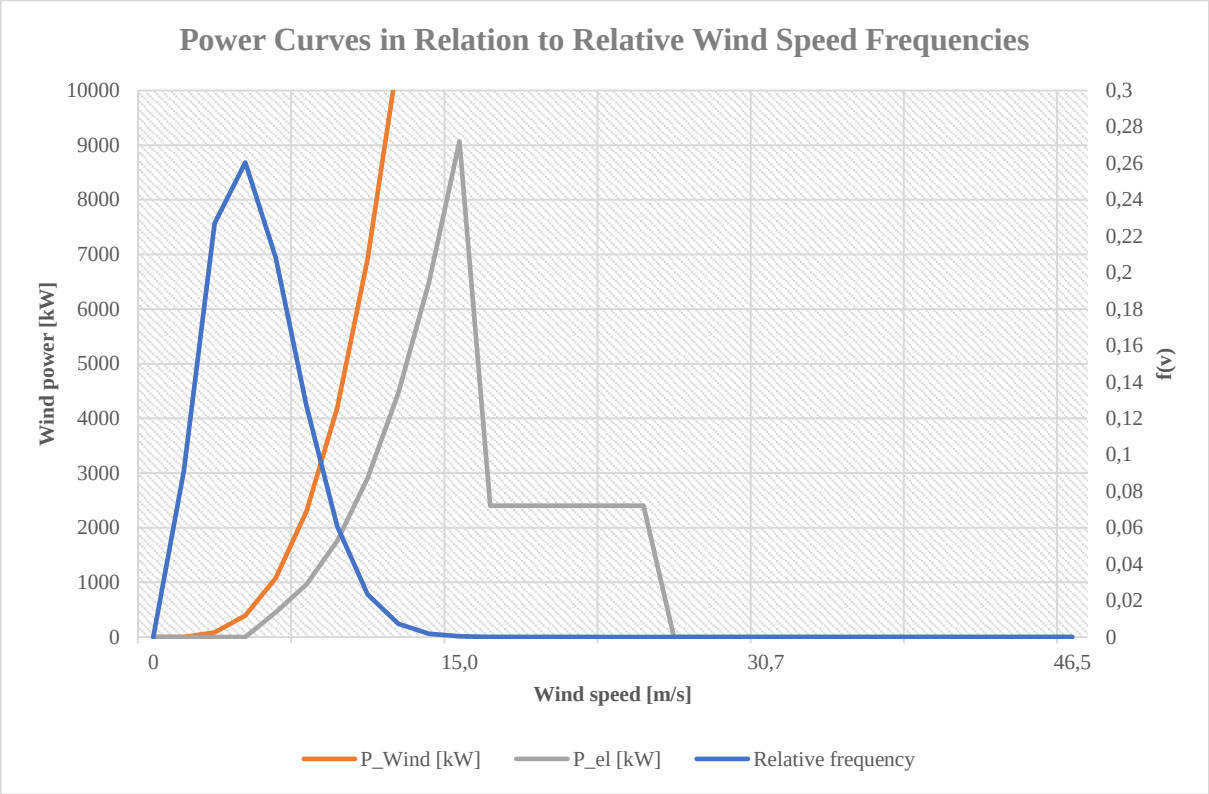

Figure 28 Power curve of selected wind turbines including relative frequency, extracted power of wind and power curve of wind turbine. Source: Own figure

Figure 29 represents the power distribution over the accumulated operating hours. Thereby, the accumulated energy was integrated (annual production) and showed the expected annual output. The accumulated energy rose exponentially and had its maximum by the end of the year (8.760 h). The annual output was determined to 3.860 MWh/a. The load factor was amounted to 0,18. Due to the fact that the load factor depends on the wind yield, which is fluctuating throughout the year, this parameter is always smaller than 1.

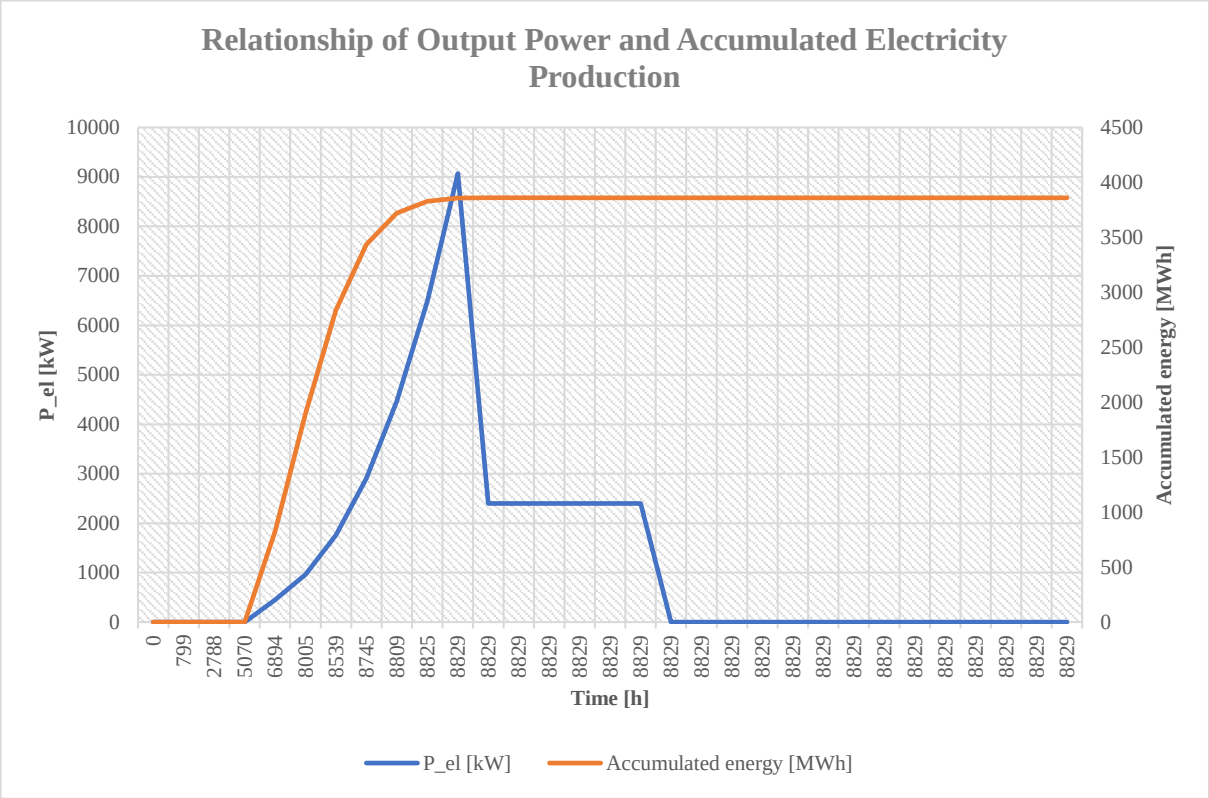

Figure 29 Relation between power curve of wind turbine and accumulated electricity production in the course of a year. Source: Own figure

The procedure of the mentioned power plan was executed and applied to all wind turbines within the study area, considering their specific turbine characteristics and with respect to the monthly averaged wind speeds in the different wind districts. Hence, a total power generation of 645,2 GW/a was determined.

Wind resource at location			**Wind resource at hub height**			**Wind turbine data**			**Power generation**	
v(mean) [m/s]	2,9		ref.Height) [m]	10		rotor dia [m]	117		rated capacity [kW]	2400
k	2		hub height [m]	141		cut-in speed [m/s]	4		production [MWh/a]	3860
A	3		roughness length [m]	0,1		design speed [m/s]	15		load factor [-]	0,183589283
			air density [kg/m³]	1,2		cut-out speed [m/s]	25			
						cp real	0,42			

speed at ref. Height	relative frequency	cumulative frequency	speed at hub height	P_wind [kW]	P_el [kW]	cp	time [h]	energy [MWh]	accumulated time [h]	accumulated energy [MWh]
0	0	0	0	0	0	0	0	0	0	0
0,5	0,09	0,02	0,8	3	0	0,00	799,2	0	799	0
1,5	0,23	0,19	2,4	85	0	0,00	1989,1	0	2788	0
2,5	0,26	0,44	3,9	394	0	0,00	2281,8	0	5070	0
3,5	0,21	0,68	5,5	1080	454	0,42	1824,1	827	6894	827
4,5	0,13	0,85	7,1	2295	964	0,42	1111,1	1071	8005	1898
5,5	0,06	0,94	8,7	4190	1760	0,42	533,7	939	8539	2837
6,5	0,02	0,98	10,2	6916	2905	0,42	205,7	597	8745	3435
7,5	0,01	0,99	11,8	10625	4462	0,42	64,2	286	8809	3721
8,5	0,00	1,00	13,4	15466	6496	0,42	16,3	106	8825	3827
9,5	0,00	1,00	15,0	21592	9069	0,42	3,4	31	8829	3858
10,5	0,00	1,00	16,5	29154	2400	0,08	0,6	1	8829	3860
11,5	0,00	1,00	18,1	38302	2400	0,06	0,1	0	8829	3860
12,5	0,00	1,00	19,7	49188	2400	0,05	0,0	0	8829	3860
13,5	0,00	1,00	21,3	61963	2400	0,04	0,0	0	8829	3860
14,5	0,00	1,00	22,8	76778	2400	0,03	0,0	0	8829	3860
15,5	0,00	1,00	24,4	93784	2400	0,03	0,0	0	8829	3860
16,5	0,00	1,00	26,0	113131	0	0,00	0,0	0	8829	3860
17,5	0,00	1,00	27,6	134973	0	0,00	0,0	0	8829	3860
18,5	0,00	1,00	29,1	159458	0	0,00	0,0	0	8829	3860
19,5	0,00	1,00	30,7	186739	0	0,00	0,0	0	8829	3860
20,5	0,00	1,00	32,3	216967	0	0,00	0,0	0	8829	3860
21,5	0,00	1,00	33,9	250292	0	0,00	0,0	0	8829	3860
22,5	0,00	1,00	35,4	286866	0	0,00	0,0	0	8829	3860
23,5	0,00	1,00	37,0	326840	0	0,00	0,0	0	8829	3860
24,5	0,00	1,00	38,6	370365	0	0,00	0,0	0	8829	3860
25,5	0,00	1,00	40,2	417592	0	0,00	0,0	0	8829	3860
26,5	0,00	1,00	41,7	468672	0	0,00	0,0	0	8829	3860
27,5	0,00	1,00	43,3	523757	0	0,00	0,0	0	8829	3860
28,5	0,00	1,00	44,9	582997	0	0,00	0,0	0	8829	3860
29,5	0,00	1,00	46,5	646543	0	0,00	0,0	0	8829	3860

Figure 30 Power plan of a single wind turbine (Maßbach) in the course of a year. Source: Own figure

4.2.3 Run-of-River Plants (Present Period)

A total of 270 hydro power plants were installed within in the study area. Regarding to the fact that all of the installed plants have a head of less than 1 m, these power plants were characterized as low head hydro power plants, However, in this work only run–of–river plants with a performance class of > 1 MW were investigated. Along the river 'Main', from east to west, a total of 28 of these types of plants were installed. Providing a statement about the energy production, decisive parameters were needed. As a basis, discharge and water level upstream and downstream of the selected hydro power plants were required, which were provided by selected gauging stations (Hnd Bayern, 2019).

Within the scope of this thesis, three different approaches were undertaken:

1. General power generation per year of the 28 run-of-river plants (present period).
2. Power generation per year of five selected run–of–river plants (present period).
3. Power plan of the run–of–river plant Limbach in the course of a year (present period).

1. General power generation

The 28 hydro power plants were well separated along the river Main. In order to determine the power generation of a hydroelectric power station, the parameters runoff, effective head, gravity, efficiency, and water density were required (formula 32). Regarding discharge and water level, only five water gauges (Trunstadt, Schweinfurt, Würzburg, Steinbach and Kleinheubach) delivered reliable data, due to its vicinity to the run–of–river plants (Chapter '*Water Level and Discharge'*). The archives of the 'Wasser- und Schiffsfahrtsverwaltung' (Wasser- und Schifffahrtsverwaltung des Bundes, 2003) delivered information regarding parameters in terms of river kilometers, length of retention, normal backwater in the upper water, hydrostatic head, design performance and design discharge for all the 28 hydro power plants. Furthermore, the discharge of the remaining hydro power plants and the efficiency needed to be determined.

The procedure of the determination was designed as follows:

1. Regarding the discharge of the remaining run–of–river plants, the discharge at the five selected water gauges and the design discharge of the adjacent hydro power plant downstream was set into ratio providing a coefficient to determine the discharges upstream of the remaining hydro power plants. Therefore, the mean ratio was calculated to 1,22 (formula 40).

$$R_{Discharge} = \frac{MQ_{Gauge}}{Q_{Design}}$$

With $R_{Discharge}$ Ratio between observation discharge and design discharge [-] (40)
MQ_{Gauge} Observed discharge at selected gauging station
Q_{Design} Design discharge

2. Identifying the efficiency of the run–of-river plant, formula 32 was used and dissolved after the efficiency parameter. Thereby, the mean efficiency of all 28 plants was determined to 66 %. However, the typical efficiency of such a plant evens out between 80 – 90 % (Basso & Botter, 2012). Owed by this fact, both values (66 % and 85 %) in efficiency were used in the calculation of the power generation.

Run-of-river plant	Head [m]	Design performance [kW]	Energetic performance [GWh]	Design discharge [m³/s]	load hours [h]	Efficiency (present state)	MQ (Gauges)	Ratio	P (μ=66%) [kW]	E (μ=66%) [GWh]	P (μ=0,85) [kW]	E (μ=0,85) [GWh]	Performance (Design/Theo.)
Viereth	6	6200	32,8	159	5290	66%	194	1,22	7564	40,0	9705	51,3	82%
Limbach	5,36	3700	24,9	104	6730	68%	119	1,14	4234	28,5	5319	35,8	87%
Knetzgau	4,24	2900	18,9	112	6517	62%	137	1,22	3538	23,1	4831	31,5	82%
Ottendorf	7,59	6300	39,7	130	6302	65%	159	1,22	7686	48,4	10038	63,3	82%
Schweinfurt	4,67	3800	23,4	125	6158	66%	153	1,22	4636	28,5	5938	36,6	82%
Garstadt	4,69	3900	23	120	5897	71%	126	1,05	4095	24,2	4928	29,1	95%
Wipfeld	4,31	2900	19,6	110	6759	62%	134	1,22	3538	23,9	4823	32,6	82%
Gerlachshausen	6,3	1500	10,8	50	5542	78%	61	1,22	2928	16,2	3204	17,8	67%
Dettelbach	5,5	4200	27,2	120	6476	65%	146	1,22	5124	33,2	6714	43,5	82%
Kitzingen	3,66	3000	18,9	130	6300	64%	159	1,22	3660	23,1	4840	30,5	82%
Marktbreit	3,31	2100	15,1	110	7190	59%	134	1,22	2562	18,4	3704	26,6	82%
Goßmannsdorf	3,4	2000	14,1	100	7050	60%	122	1,22	2440	17,2	3459	24,4	82%
Randersacker	3,3	2000	14	100	7000	62%	122	1,22	2440	17,1	3357	23,5	82%
Würzburg	2,75	900	7,5	50	8333	67%	61	1,22	1098	9,2	1399	11,7	82%
Erlabrunn	4,15	2700	19,7	92	7296	72%	128	1,39	3757	27,4	4429	32,3	72%
Himmelstadt	4,3	2500	17,8	87,5	7120	68%	107	1,22	3050	21,7	3828	27,3	82%
Harrbach	4,9	3000	24	90	8000	69%	110	1,22	3660	29,3	4486	35,9	82%
Steinbach	5,14	4200	30,7	115	7310	72%	140	1,22	5124	37,5	6013	44,0	82%
Rothenfels	5,26	4200	30,3	115	7214	71%	136	1,18	4967	35,8	5965	43,0	85%
Lengfurt	3,99	2600	19,1	109	7346	61%	133	1,22	3172	23,3	4424	32,5	82%
Eichel	4,5	3100	23,4	115	7548	61%	140	1,22	3782	28,5	5265	39,7	82%
Faulbach	4,51	4100	29	145	7073	64%	177	1,22	5002	35,4	6653	47,1	82%
Freudenberg	4,51	4300	29,7	145	6907	67%	177	1,22	5246	36,2	6653	45,9	82%
Heubach	4	3400	25,1	133	7382	65%	162	1,22	4148	30,6	5412	40,0	82%
Klingenberg	4	3000	21,9	130	7300	59%	175	1,35	4038	29,5	5837	42,6	74%
Wallstadt	4	3400	25,7	135	7559	64%	165	1,22	4148	31,4	5493	41,5	82%
Obernau	4,01	3200	25	133	7813	61%	162	1,22	3904	30,5	5426	42,4	82%
Kleinostheim	6,8	9700	59,8	204	6165	71%	249	1,22	11834	73,0	14112	87,0	82%
Mean				***116,7***	***6913***	***66%***	***142***	***1,22***					***82%***
Total		***98800***	***671,1***						***121375***	***821,0***	***156254***	***1059,2***	

Figure 31 Power and electricity generation of the 28 run - of - river plants within the study area. Yellow marked values are measured values from which the MQ of the other plants was calculated by the mean factor of 1,22. Source: Own figure

Using formula 32, a total power of 121,4 MW/a and a total electricity generation of 821 GWh/a was determined regarding an efficiency coefficient of 66 %. Concerning an efficiency of 85 %, the generated power was calculated to 156,3 MW/a with an electricity production of 1059,2 GWh/a (Figure 31).

With an average performance ratio of 82 % between design and theoretic performance, there is no clear match between design performance and theoretic performance. This is since the design discharge does not display the real discharge of a river.

2. Power generation of selected run–of–river plants

Within this subchapter, a closer look was taken at the run-of-river power plants located downstream in the immediate vicinity of the gauging stations. The performances of the plants were listed monthly in order to obtain a statement about the energy generation over the course of a year. In addition to the formulas in chapter '*Hydropower Plants'* and the calculated parameters in the chapter '*Water Level and Discharge'*, the same methodology was used as in the previous subchapter '*General Power Generation'*. The illustrated run-of-river power plants with their respective efficiencies and design parameters after (Wasser- und Schifffahrtsverwaltung des Bundes, 2003) were displayed in figure 33.

The performance ratio between design performance and theoretic performance was determined to a mean of 66 %. This relatively low accordance could be ascribed due to the same fact as described in subchapter '*General Power Generation'*.

Figure 32 shows the power output of selected run-of-river power plants during the year. An efficiency of 85 % was assumed.

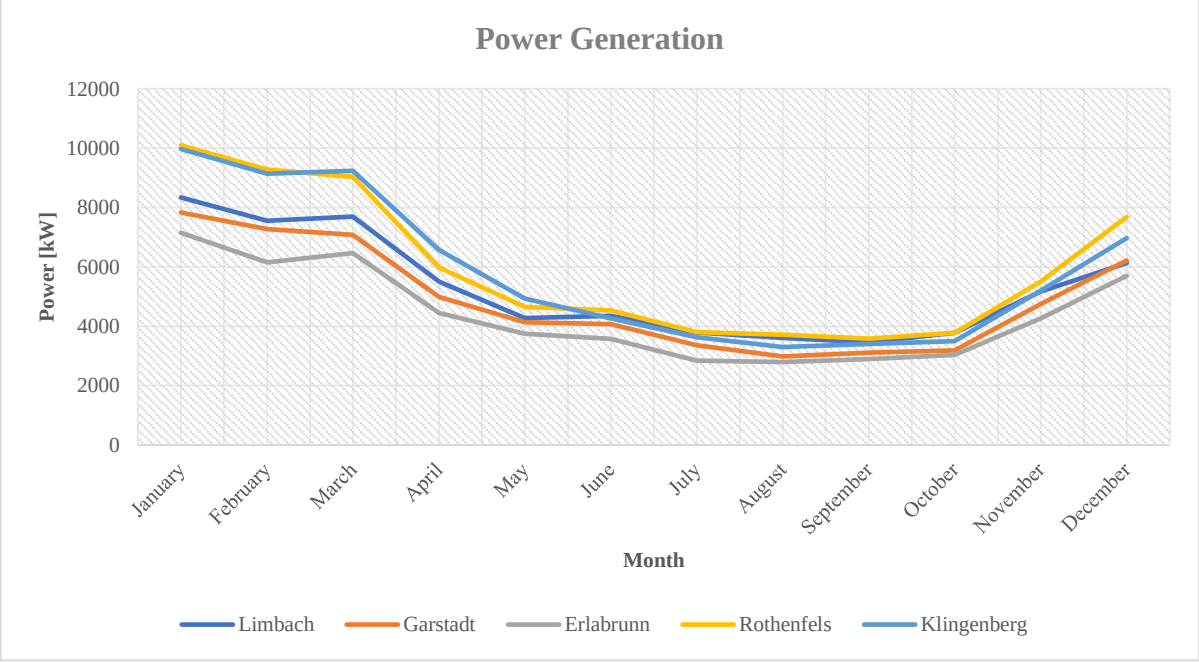

Figure 32 Power generation of the five selected run - of - river plants in the course of a year. Source: Own figure

Therefore, the maxima were achieved in the winter months, whereas the curve is flattening in summer, due to increased temperatures and the associated increase of evaporation. Even a lack of rainfall could provide a reason for reduced performance during the summer months. The Rothenfels run-of-river power plant is the most powerful power plant with a maximum output of 10,1 MW in January and a minimum of 3,6 MW in September.

Run of river plant	Gauging station	Head [m]	Design performance [kW]	Energetic performance [GWh]	Design discharge [m³/s]	load hours [h]	Efficiency (present state)
Limbach	Trunstadt	5,36	3700	24,9	104	6730	68%
Garstadt	Schweinfurt	4,69	3900	23	120	5897	71%
Erlabrunn	Würzburg	4,15	2700	19,7	92	7296	72%
Rothenfels	Steinbach	5,26	4200	30,3	115	7214	71%
Klingenberg	Kleinheubach	4	3000	21,9	130	7300	59%
Mean					***112,2***	***6888***	***68%***
Total			***17500***	***119,8***			

Run of river plant	P (μ = p.s.) [kW]	P (μ=0,85) [kW]	E (μ=p.s.) [GWh]	E (μ=0,85.) [GWh]	Performance (Design/Theo.)
Limbach	3933	5306	26,5	35,7	0,70
Garstadt	3495	4919	20,6	29,0	0,79
Erlabrunn	3723	4425	27,2	32,3	0,61
Rothenfels	5239	5972	37,8	43,1	0,70
Klingenberg	3820	5845	27,9	42,7	0,51
Mean					***66%***
Total	***20210***	***26468***	***139,9***	***182,8***	

Figure 33 Power and electricity generation for the five selected run - of - river plants.
Source: Own figure

3. Case study - Power plan of the run–of–river plant Limbach

By creating an individual power plan, a more detailed look was given to the run–of–river plant Limbach (Figure 34). The base of the power plan was the gauging station Trunstadt with its observed values in discharge and water level, which were daily averaged within the present time period (2000–2019). Such a performance plan shows the duration lines as exceedance lines. Further decisive parameters needed for calculations were named in the following procedure of creating the power plan:

- Identification of the length of retention [m] between the hydro power plants Viereth and Limbach (Google Maps, 2019).
- Determination of the mean water level and mean discharge in the course of a year within the time period (2000–2019) (Hnd Bayern, 2019). These parameters had to be sorted in descending order.
- Identification of head water level upstream (224,9 m) and tailwater level downstream (219,5 m) (Wasser- und Schifffahrtsverwaltung des Bundes, 2003).
- Identification of hydrostatic design head (H_{Nutz} = 5,36 m), design performance (P = 3.700 kW), energetic design performance (E = 24,9 GWh) and design discharge (Q_{Design} = 104 m³/s) (Wasser- und Schifffahrtsverwaltung des Bundes, 2003).
- Determination of width of the river Main downstream of hydro power plant Limbach (Google, 2019).
- Setting of efficiency of hydro power plant (μ = 85 %).
- Calculation of the slope by the quotient of difference in height and length of retention
- Calculation of the head water bed (upstream), tailwater bed (downstream) and tailwater level by applying the Manning–Strickler equation (Jirka, 2007) (formula 41). The equation was used as a function of the known upstream and downstream water level.

$$v_m = k_{st} * R^{\frac{2}{3}} * I^{\frac{1}{2}} \quad (41)$$

With v_{mean} Mean flow velocity [m³/s]
k_{st} Strickler coefficient of channel roughness [-]
R Hydraulic radius [m]
I Slope [‰]

- For the river Main an earth channel with medium gravel (40 – 60 mm) was assumed. Therefore, the Strickler coefficient was determined to 40 (Jirka, 2007).
- Determination of the degree of expansion.
- Calculation of the generated power by using formula 32. The power duration curve changed in the course of the year depending on MQ and head duration line.

Regarding the run–of–river plant Limbach, the range of discharge was determined between 212,9 – 69,8 m, whereas the water level ranges between 222 – 159 cm. The length of retention between both hydro power plants was identified to 13.096 m, with a height difference of 35,6 m. Hence, the slope could be determined to 2,7 ‰. The width needed for further calculations was determined ~ 184 m. By the use of the identified parameters and the application of the Manning–Strickler formula, the head water-bed upstream was ascertained to 224,69 m, whereas the tailwater bed downstream had a height of 219,3 m. Thus, the alternating tailwater level could be determined, with a range between 27 – 14 cm. Hence, in the course of a year within the selected time period, the performance duration curve ranges between 4.647 and 3.141 kW.

The multiplication of the sorted mean discharge exceedance duration line and the head duration line thus provided the power duration line over one year. The annual work of the hydropower plant could be determined by the integration of the performance duration curve. Since the maximum discharge of a hydroelectric plant is limited, the water must be diverted unused with high water flow. About this maximum discharge, which is also called design discharge of a plant, the degree of expansion could be determined. This corresponds to the number of days in the year in which the water supply of the river was above the design discharge (Bundesministerium für Umwelt, Naturschutz und Reaktorsicherheit, 2010). Modern hydro power plants usually set the degree of expansion between 30 – 60 days.

In the example of the run-of-river power plant Limbach, it is noticeable that the design discharge is exceeded 174 days a year. If this day is reached, however, the power plant generates a maximum power output of 4.647 kW with an effective head of 5,36 m. From this day on until the end of the year, the performance duration curve falls and ultimately reaches a minimum of 3.141 kW with a head of 5,4 m.

Since the power plant was commissioned in 1951, the design discharge and effective head parameters can be considered obsolete. This leads to a degree of expansion that clearly exceeds that of modern power plants. However, a total production of ~ 1,5 GW was determined. In addition, it must be said that the power plan has been glossed over by setting the efficiency to 85 %. Therefore, it can be seen that the potential of this power plant has not been exhausted and that higher outputs can be generated after modernization.

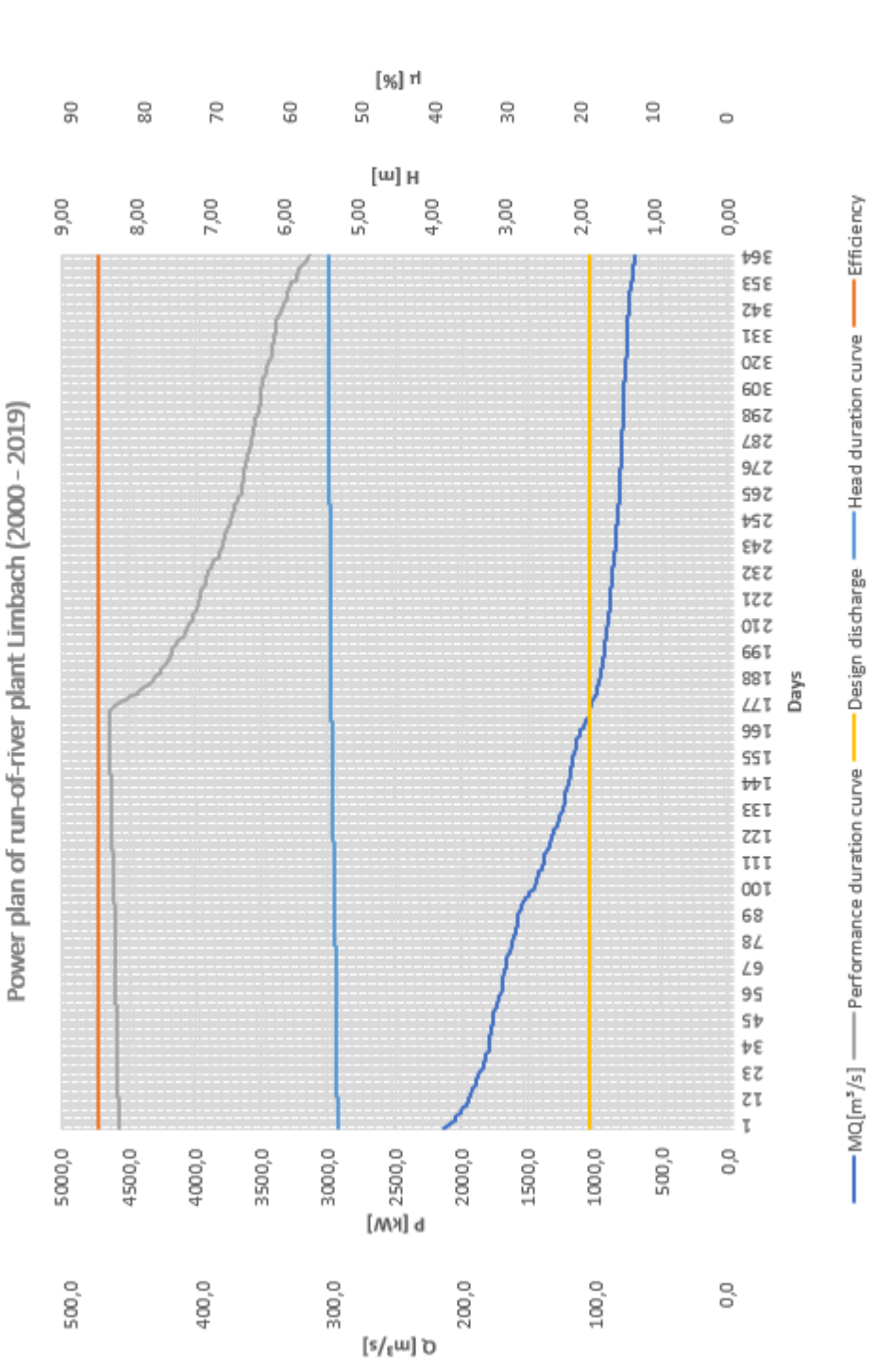

Figure 34 Power plan for run - of - river plant Limbach regarding the averaged water level and discharge within the present time period (2000 - 2019). Own figure

4.3 Climate Parameters in the Future

Hereinafter, the changes in global radiation, temperature, wind speed and discharge up to the time period 2071 – 2090 compared to the reference period 1991-2010 have been considered. The results indicate a possible mean state of the future climate which depends on the selected emission scenario RCP 8.5. Regarding the climate within the modelled area and after analysing the data, it could be generally stated that an increase in global radiation and temperature and a decrease in wind speed and discharge will occur.

The model member ‘kbu’ was chosen as the reference member, due to the fact, that its global radiation for the reference period 1991 – 2010 was the average out of all 50 members. The members ‘kcm’ (maximum) and ‘kbm’ (minimum) were displaying the maximum and minimum global radiation in the reference period. The two remaining members ‘kba’ (dry) and ‘kbk’ (wet) illustrated a dry or rather a wet scenario, due to its minimum or rather maximum in discharge in the future period. As mentioned in chapter *‘Identification of Future Climate Parameters’* the members symbolised different initial conditions described in a form of a code.

In the following subchapters, the climate parameters of 11 catchment areas out of 14 displayed in figure 18 were evaluated for each individual scenario. The reason for the exclusion of three catchment areas is that either no regenerative energy systems were installed within the excluded catchment areas or the catchment areas were outside of the study area. The climate diagrams presented here refer to the catchment area Würzburg due to its central location within the study area. Hence, the parameters global radiation, wind speed, temperature, and discharge were represented by two different illustration patterns:

1. Comparison of reference period (1991–2010) and future period (2071–2090) in the course of the year. The determined climate values were area–weighted and monthly averaged.
2. Comparison of both periods (reference and future) in a respective 20 – year cycle. As in point 1 - the determined climate values were area–weighted and monthly averaged.

4.3.1 Global Radiation (Future Period)

1. The imaging pattern 35 shows the average monthly global radiation of the reference period (blue) compared to the future period (orange) for the five selected members. It was noticeable, that in the winter (December and January) the radiation of the reference period was above the one of the future period. However, in the average course of the year it could be seen that the parabola of the future radiation would expand. From the second half of the year on to the month of November higher global radiations than at the reference period were determined. This applies to all five scenarios. The maximum radiation in the future period was displayed at member 'kcm' and was amounted to 179,9 kWh / m² in July. The minimum radiation had a value of 15,2 kWh / m² in December and occurred at the member 'kbk'.

2. In terms of global radiation in a 20-year cycle, both periods illustrated a periodic fluctuation with no clear recognizable trend. Regarding the future period, the radiation of the members 'kbu',' kcm' and 'kba' increased slightly and decreased for the member 'kbm' and 'kbk'. However, when comparing both periods, except of 'kbk', a slightly increase could be determined (figure 36).

Apart from the member 'kbk', the average monthly and yearly radiation increased comparing both periods, with a maximum increase of 2,3 kWh/m² per month ('kbm') and an increase of 29,4 kWh/m² per year ('kba'). The member 'kbk', contrarily, showed a reduction in global radiation, both in a monthly and in a year-on-year comparison.

Using the Pearson correlation coefficient (r), the monthly comparison of both periods (1) stated an absolute positive correlation for all 5 members (r_1 = +1). By contrast, no clear statement could be made for the 20-year cycle (2). In general, almost no correlation was detected (except for member 'kcm') averaging r_2 = - 0.24 (table 8).

Table 8 Comparison of parameters and members including the Pearson correlation coefficients regarding global radiation. Source: Own table

Period	***Member***	***Ø Gr_Month [kWh/m²]***	***Ø Gr_Year [kWh/m²]***	***r_1***	***r_2***
Reference	Kbu	89,3	1070,3		
				+1	-0,12
Future	Kbu	90,8	1090		
Reference	Kcm	90,6	1087		
				+1	+0,11
Future	Kcm	91,6	1099,1		
Reference	Kbm	88,8	1065,2		
				+1	-0,09
Future	Kbm	91,1	1093,3		
Reference	Kba	90,2	1082,1		
				+1	-0,06
Future	Kba	91,8	1101,5		
Reference	Kbk	90,5	1085,4		
				+1	-0,42
Future	Kbk	89,5	1074,5		

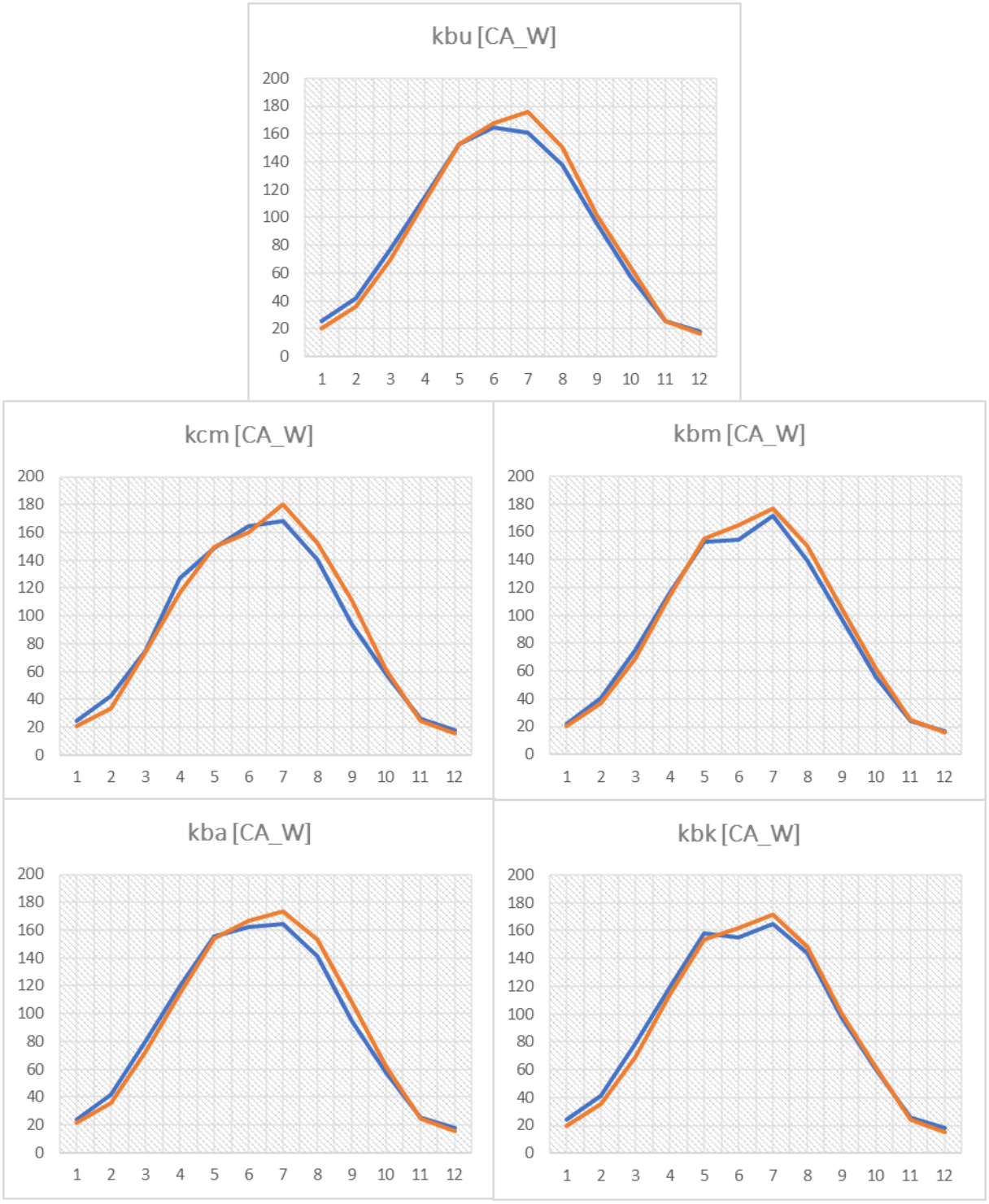

Figure 35 Differences between the selected climate model members in global radiation. Values were determined based on a monthly average within the reference period 1991-2010 (blue) and the future period 2071-2090 (orange) in the course of a year. The pattern is based on the climate catchment area of Würzburg. Source: Own figure based on (Leduc et al., 2019).

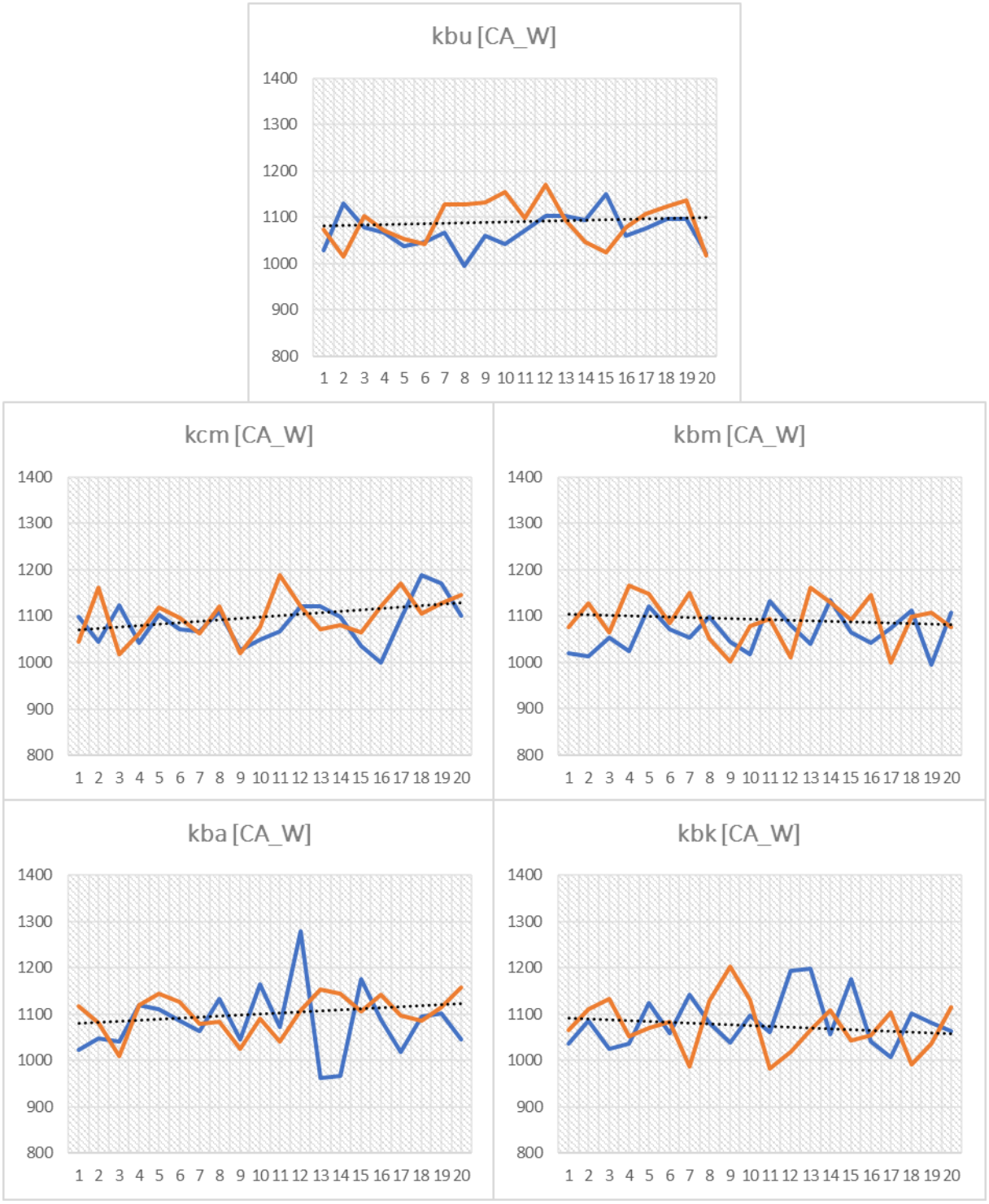

Figure 36 Differences between the selected climate model members in global radiation. Values were determined based on a monthly average within the reference period 1991-2010 (blue) and the future period 2071-2090 (orange) in a 20–year cycle. The pattern is based on the climate catchment area of Würzburg. Source: Own figure based on (Leduc et al., 2019).

4.3.2 Wind Force (Future Period)

1. Regarding the comparison of both periods during the course of a year, it was significant that the wind speed slightly decreased for all members, except at member ‘kcm’. In form of a parabola, the wind speed reached its maximum in the winter and early spring and had its minimums in the late summer months. Referring to the extrema in the future period, the member ‘kcm’ displayed the maximum (2,63 m/s in March) as well as the minimum (1,5 m/s in September) in average wind speed (figure 37).

2. In terms of a 20–year cycle, despite a fluctuation, no significant trend could be determined. Regarding the future period, the wind speed of the member ‘kcm’ increased slightly and decreased for the remaining members. Thereby, in terms of the extrema in the future period, the member ‘kcm’ stated a maximum in wind speed (2,3 m/s) in the year 2088, while the member ‘kbm’ displayed a minimum (1,77 m/s) in 2086 (figure 38).

It was noticeable, that there will be a slight decrease in wind speed in the future period. The biggest speed difference was analysed regarding member ‘kba’ with $\Delta = 0{,}11$ m/s. Using the Pearson correlation coefficient (r), the monthly comparison (r_1) of both periods stated a positive correlation close to 1. In terms of the 20–year cycle (r_2) no clear correlation could be deduced. It could be recognized that the members ‘kcm’ and ‘kbk’ showed a weak negative correlation, while the members ‘kbu’, ‘kbm’ and ‘kba’ showed a positive one. The average Pearson correlation was determined to r_2 = 0,1 (table 9).

Table 9 Comparison of parameters and members including the Pearson correlation coefficients regarding wind speed. Source: Own table

Period	***Member***	***Ø Wind [m/s]***	***r_1***	***r_2***
Reference	Kbu	2,02		
			0,91	0,36
Future	Kbu	2,01		
Reference	Kcm	2,03		
			0,94	-0,09
Future	Kcm	2,04		
Reference	Kbm	2,09		
			0,97	0,17
Future	Kbm	2,04		
Reference	Kba	2,09		
			0,95	0,22
Future	Kba	1,98		
Reference	Kbk	2,06		
			0,93	-0,14
Future	Kbk	2,02		

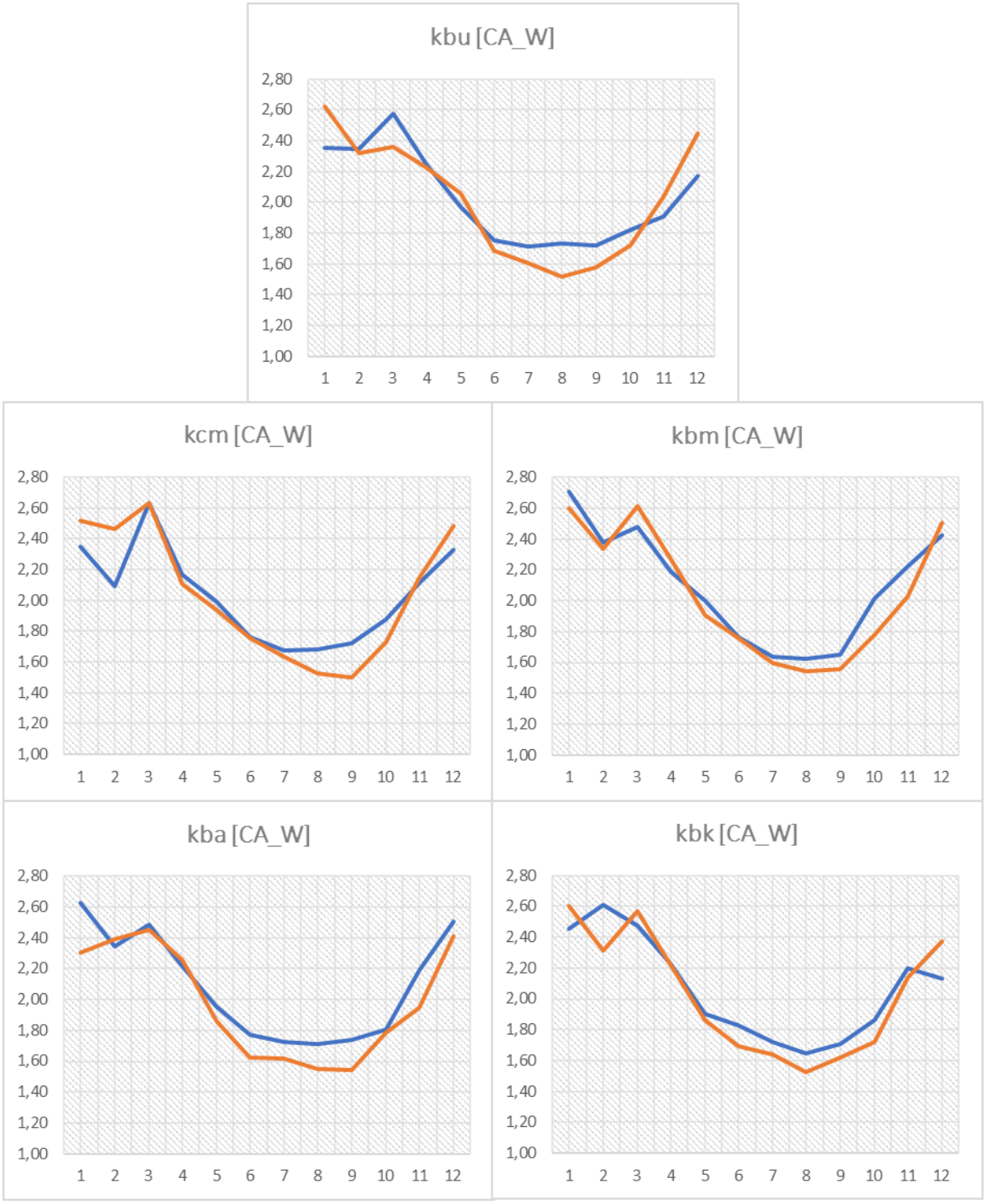

Figure 37 Differences between the selected climate model members in wind speed. Values were determined based on a monthly average within the reference period 1991-2010 (blue) and the future period 2071-2090 (orange) in the course of a year. The pattern is based on the climate catchment area of Würzburg. Source: Own figure based on (Leduc et al., 2019)

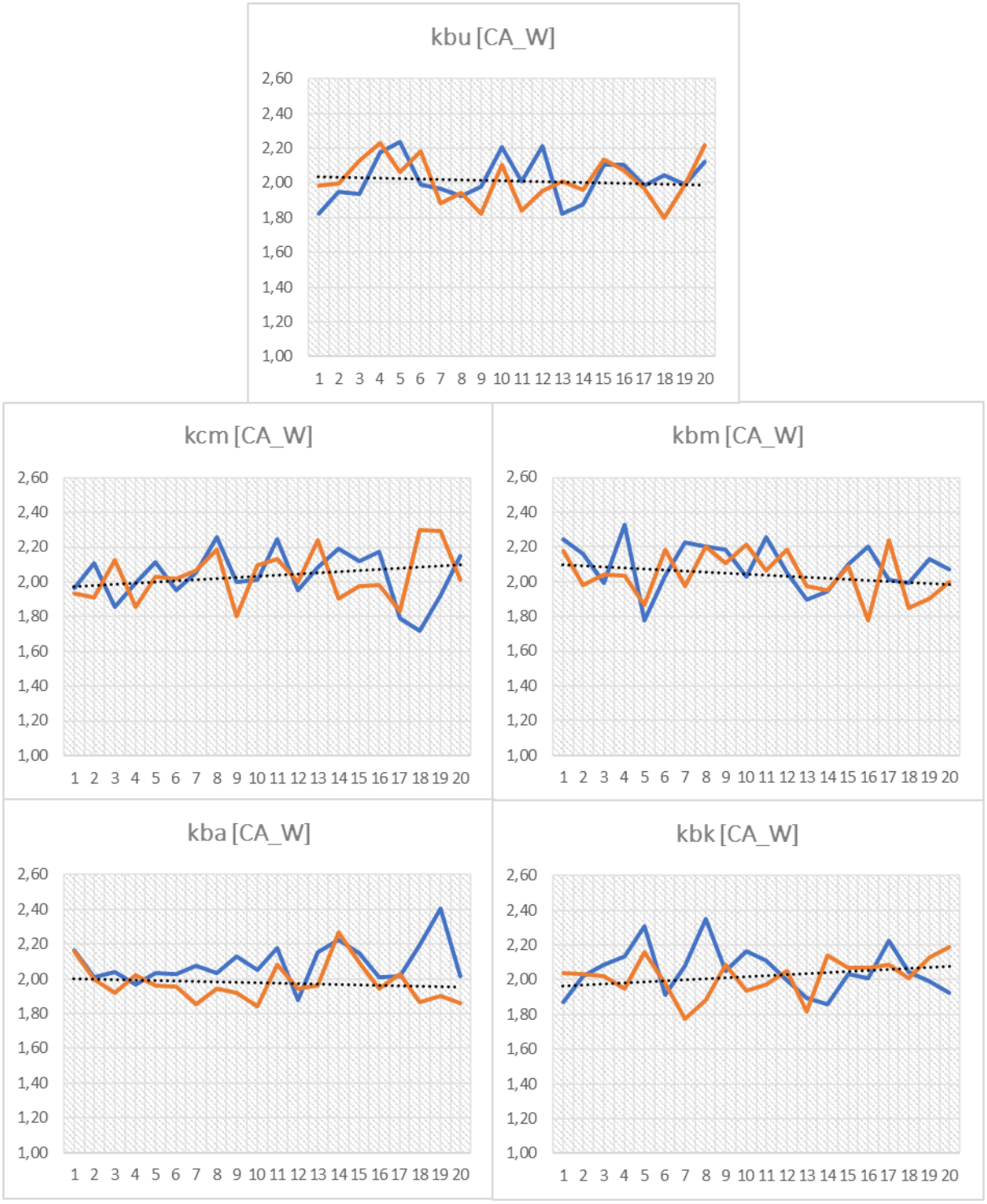

Figure 38 Differences between the selected climate model members in wind speed. Values were determined based on a monthly average within the reference period 1991-2010 (blue) and the future period 2071-2090 (orange) in a 20–year cycle. The pattern is based on the climate catchment area of Würzburg. Source: Own figure based on (Leduc et al., 2019)

4.3.3 Temperature (Future Period)

1. Within the course of a year, a significant difference could be determined in comparing both periods. The averaged monthly temperature within the time period 2071–2090 exceeded the values within the reference period. Therefore, a usual temperature parabola could be seen, with the minimum in winter and the maximum in the summer months. Out of the selected members and with regard to the future period, the member ‘kba’ displayed the maximum with an averaged monthly value of 25,3 °C in August, whereas the minimum of -0,1 °C is shown by the member ‘kbu’ in January (figure 39).

2. The same statement as for 1 could be made for the 20–year cycle. The averaged yearly temperature values of the future period exceeded the ones of the reference period. The maximum was determined regarding member ‘kbk’ in 2090 (15,7 °C) and the minimum at member ‘kba’ in 2073 (11,3 °C). For all members a significant trend could be determined. Furthermore, between both time periods a linear increase existed (figure 40).

The biggest difference in temperature was shown by the member ‘kbu’ with Δ = 4,4 °C, but also the other remaining members were showing a temperature difference of at least Δ 3,9 °C. Using the Pearson correlation coefficient again, the monthly comparison of both periods had an absolute positive correlation, while no clear statement could be given by comparing both periods in a 20-year cycle. Whereas the members ‘kbu’ and ‘kbk’ stated a positive correlation, a weak correlation occurred at the remaining members, with an average of r_2 = + 0,29 (table 10).

Table 10 Comparison of parameters and members including the Pearson correlation coefficients regarding temperature. Source: Own table

Period	***Member***	***Ø T [°C]***	***r_1***	***r_2***
Reference	Kbu	9,1		
			0,99	0,51
Future	Kbu	13,5		
Reference	Kcm	9,3		
			0,99	-0,17
Future	Kcm	13,4		
Reference	Kbm	9		
			0,99	0,18
Future	Kbm	13,3		
Reference	Kba	9,3		
			0,99	0,24
Future	Kba	13,2		
Reference	Kbk	9,3		
			0,99	0,71
Future	Kbk	13,3		

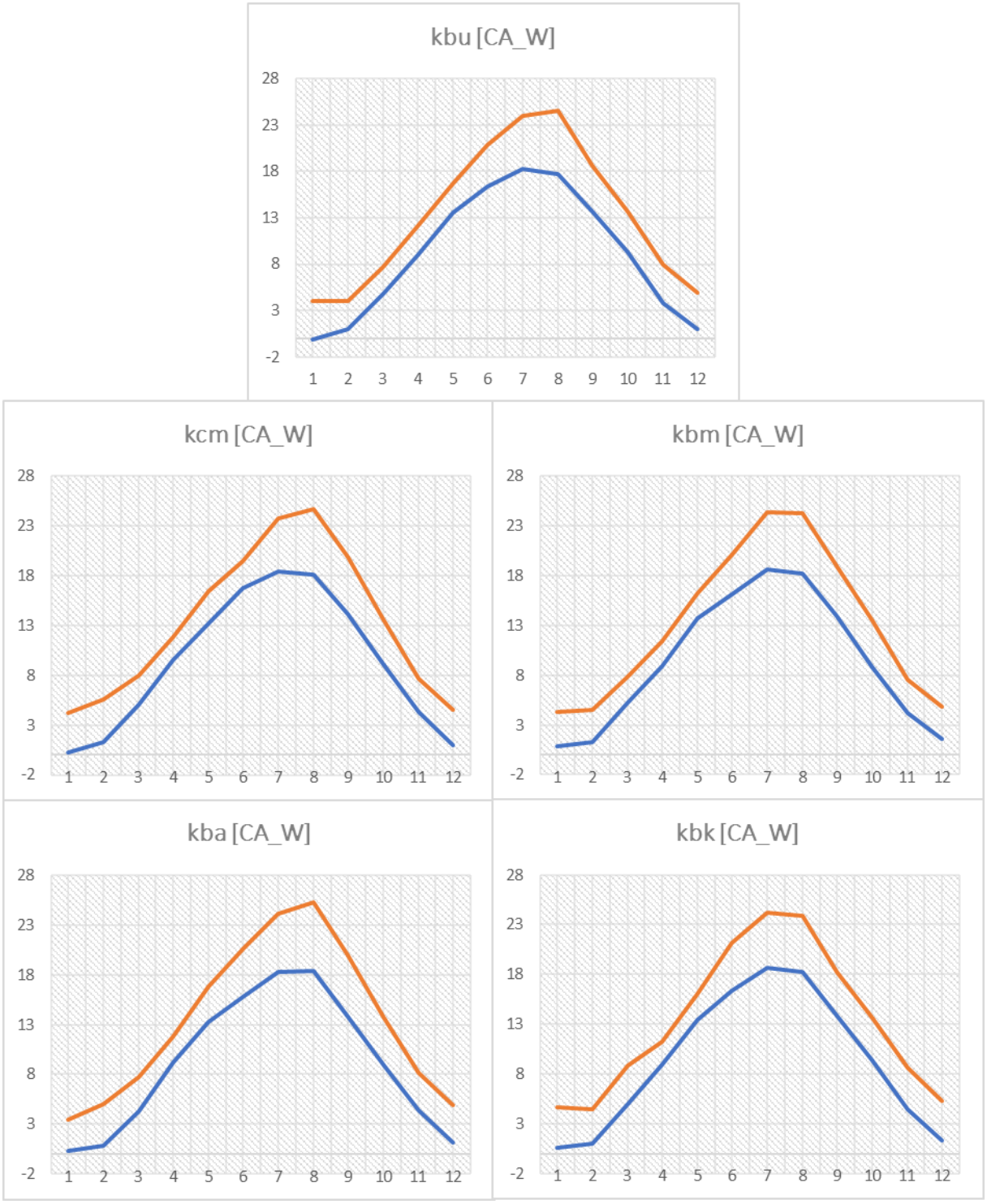

Figure 39 Differences between the selected climate model members in temperature. Values were determined based on a monthly average within the reference period 1991-2010 (blue) and the future period 2071-2090 (orange) in the course of a year. The pattern is based on the climate catchment area of Würzburg. Source: Own figure based on (Leduc et al., 2019)

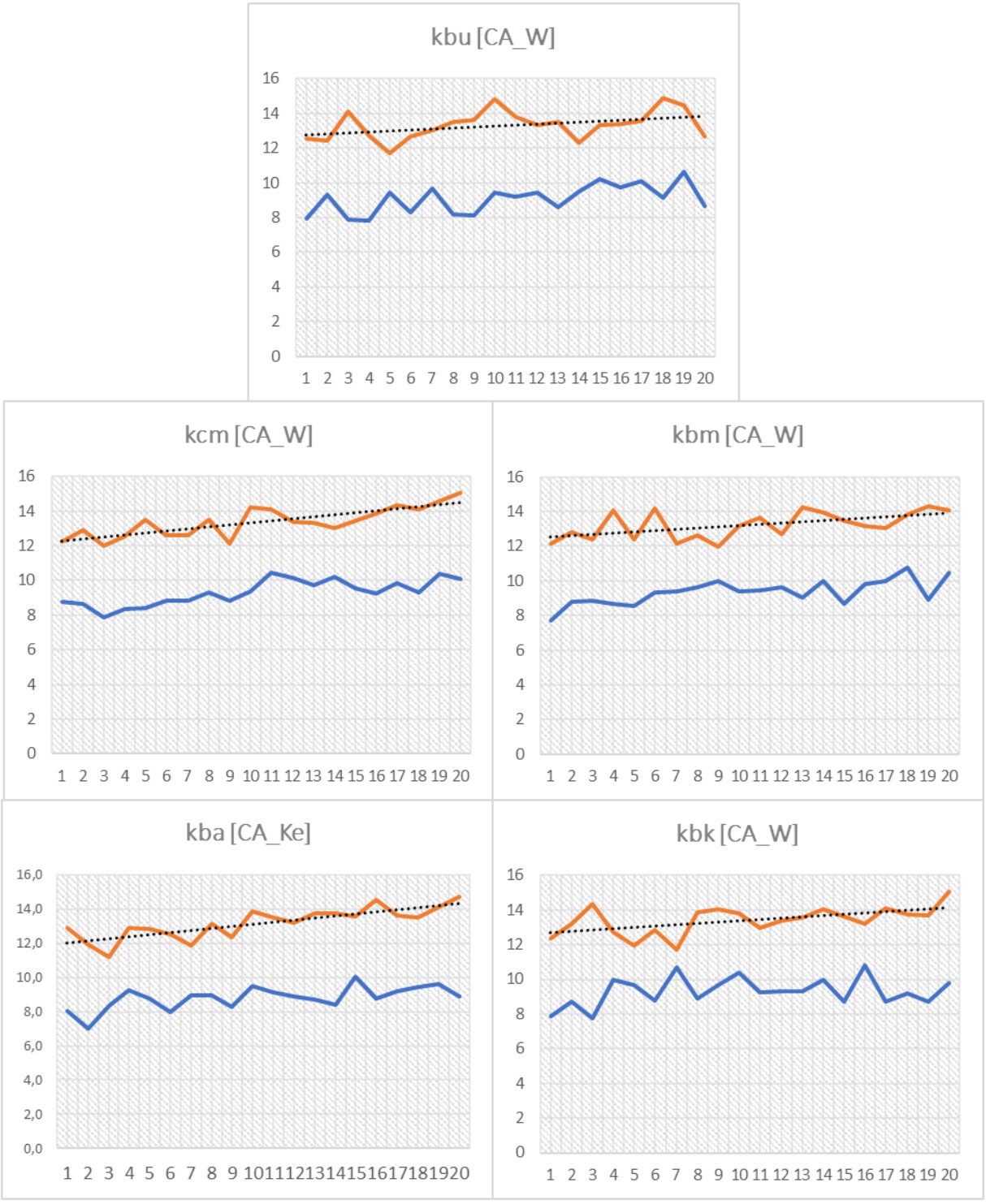

Figure 40 Differences between the selected climate model members in temperature. Values were determined based on a monthly average within the reference period 1991-2010 (blue) and the future period 2071-2090 (orange) in a 20–year cycle. The pattern is based on the climate catchment area of Würzburg. Source: Own figure based on (Leduc et al., 2019)

4.3.4 Discharge (Future Period)

1. In terms of monthly averaged discharges in the course of a year between both periods, significant differences between the members and could be pointed out. Regarding member ‘kbu’. From January until July the lines of mean discharges were coexisting, followed by a drop of the discharge line in the future period. The biggest decrease happened in September with a mean discharge difference of Δ = 50,3 m³/s. Regarding member ‘kcm’, the discharge of the future period exceeded the one of the reference period from February until July. However, from July until the end of the year the discharge of the future decreased below the one of the reference period. Referring to member ‘kbm’, the mean discharge of the future period was below the one of the reference period for the entire course of the year. The biggest difference in discharge between both periods was in late summer in September with Δ = 42,5 m³/s. Member ‘kba’ behaved almost the same as member ‘kbm’, with the difference that the discharge of the future, period exceeded slightly the one of the reference period in May. In terms of member ‘kbk’, from January to April the mean discharge of the reference period exceeded the one of the future period, followed by an intersection and a higher discharge in the future compared to the reference until June. From June on a drop of the future discharge took place again, which fell below the reference period. The maximum (192 m³/s) and minimum mean discharge (45,4 m³/s) were displayed by member ‘kcm’ in March and October (figure 41).

2. In terms of a 20-year cycle, no clear statement could be given. In most of the years the mean future discharge is below the one of the reference period. However, in some months it peaked through and exceeded the mean reference discharge. Regarding the future period in the 20 – year cycle, except of member ‘kbk’, a decrease in the mean discharge could be determined (figure 42).

It was noticeable that throughout a year and in the course of a 20–year cycle the averaged discharges of the future period were below the ones of the reference period. Thereby, member ‘kbm’ displayed the largest difference between both periods stated in a ΔQ = 48,3 m³/s. While the comparison between averaged monthly values of both periods had a strong correlation, almost no correlation took place regarding averaged yearly values in the 20–year cycle (table 11).

Table 11 Comparison of parameters and members including the Pearson correlation coefficients regarding discharge. Source: Own table

Period	***Member***	***Ø Q [m³/s]***	***r_1***	***r_2***
Reference	Kbu	128,2		
			0,9	0,08
Future	Kbu	112,5		
Reference	Kcm	119,6		
			0,94	-0,02
Future	Kcm	107,9		
Reference	Kbm	150,8		
			0,73	0
Future	Kbm	102,5		
Reference	Kba	142,5		
			0,76	-0,07
Future	Kba	98,5		
Reference	Kbk	131,5		
			0,9	-0,11
Future	Kbk	123,4		

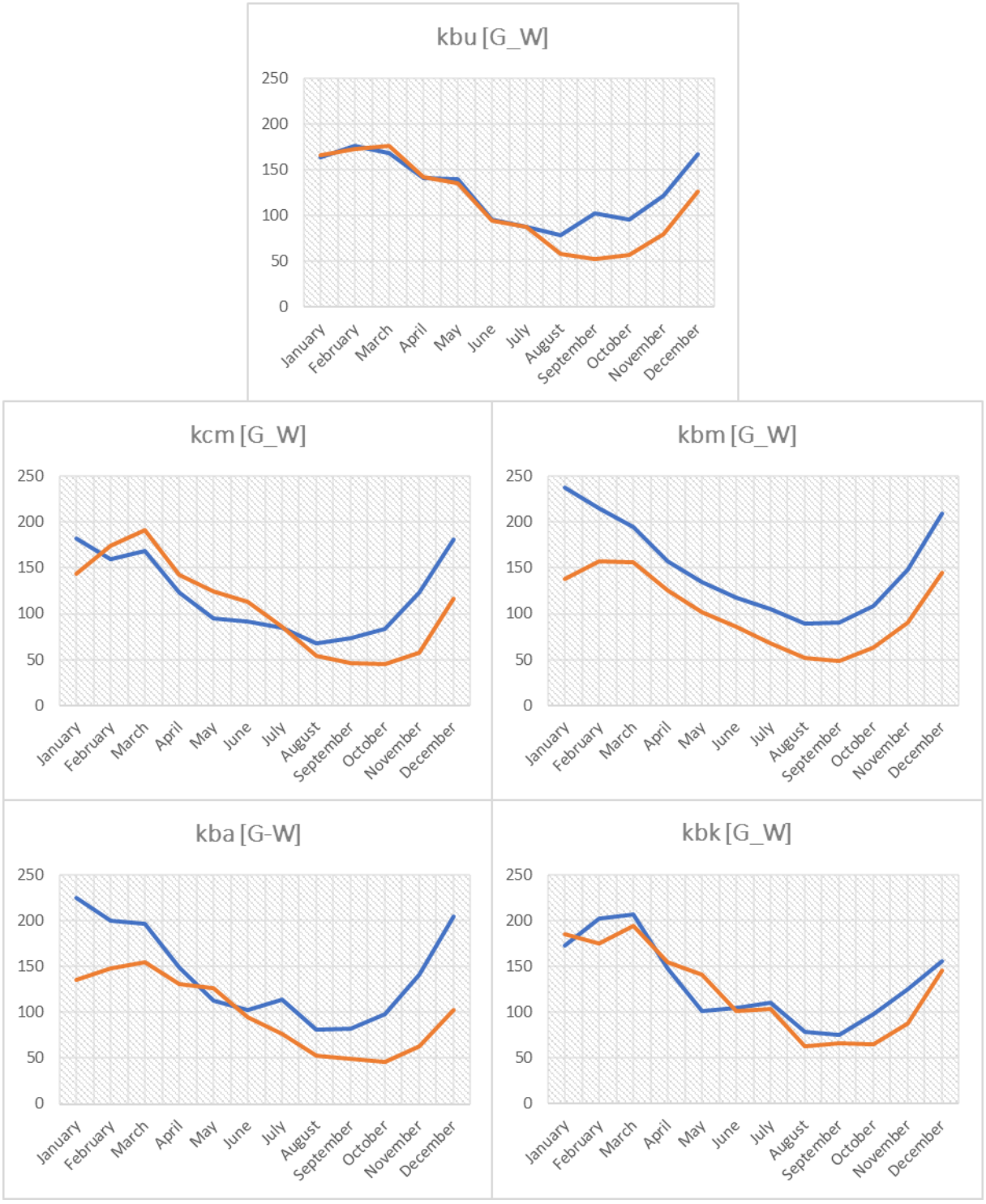

Figure 41 Differences between the selected climate model members in discharge. Values were determined based on a monthly average within the reference period 1991-2010 (blue) and the future period 2071-2090 (orange) in the course of a year. The pattern is based on the climate catchment area of Würzburg. Source: Own figure based on (Leduc et al., 2019)

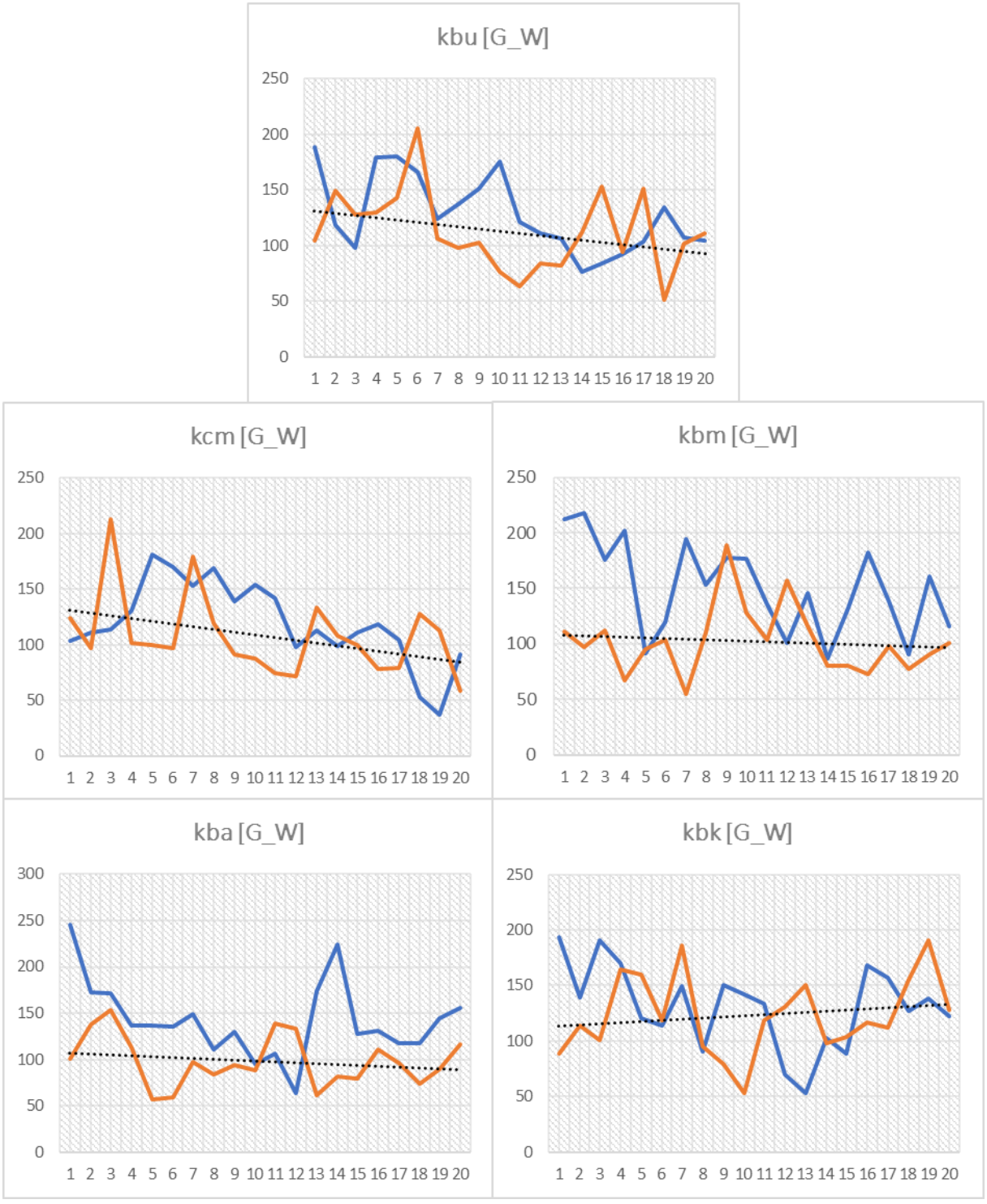

Figure 42 Differences between the selected climate model members in discharge. Values were determined based on a monthly average within the reference period 1991-2010 (blue) and the future period 2071-2090 (orange) in a 20–year cycle. The pattern is based on the climate catchment area of Würzburg. Source: Own figure based on (Leduc et al., 2019)

4.4 Comparison between Present (DWD) and Future Climate (CanESM2)

Having a closer look on the analysed climate parameters, significant differences could be figured out. For the comparison between the periods, uniform catchment areas and the model member 'kbu' were considered. Table 12 illustrates the differences between the different forms of evaluation for climate variables. The climate parameters were averaged on a monthly basis and displayed on a yearly mean. Regarding monthly analysis of each climate parameter, a strong correlation between all periods was determined ($r > 0,5$).

Table 12 Comparison of climate parameters between the different time periods. Source: Own table

Parameter/Period	***Present (2000 – 2019)***	***Reference (1991 – 2010***	***Future (2071 – 2090)***
Global radiation [kWh/m²]	1114	1046,2	1065,5
Temperature [°C]	9,7	8,9	13,1
Wind [m/s]	2,81	2,11	2,1
Discharge [m³/s]	122,1	128,4	111,3

It was noticeable that with regard to the temperature and the outflow, the values of the present period lay within the reference period and the future period. Regarding global radiation and wind force, however, the values of the present period exceeded the values of the reference and the future period. This is due to the fact that different approaches are obtaining climate parameters. While the derived parameters within the present period (2000–2019) depend on the observations provided by the DWD, the parameters within the reference and future period were obtained by the climate model CanESM2. As mentioned in chapter *'Identification of Future Climate Parameters'*, the earth system was subdivided into pixels in which the physical conditions and the exchange of mass and energy with the adjacent pixel were calculated. Climate models describe the state of the climate system over many decades as a trend by statistical approaches with associated uncertainties. Therefore, this leads to limitations in the interpretation of the result. Because of the displayed differences (table 12), the delta method (formula 35) was applied for giving reliable statements about the energy generation of the renewable energy systems.

4.5 Energy Generation in the Future regarding Regenerative Energy System

With the creation of uniform climate conditions regarding climate districts and catchment areas, and the establishment of uniform annual cycles of 20 years, based on the reference period, present period and future period, it became possible to use the delta methodology according to subchapter '*Relation between Present and Future Climate'*. Hence, future climate values used for the calculations of different energy systems, were ascertained after formula 35 and based on the climate model member 'kbu', as this one is used as the reference initial condition. Giving a statement about the change in energy output between both mentioned periods, it was assumed that the installed regenerative energy systems stayed the same, regarding distribution and characteristics.

4.5.1 Future Energy Generation by PV-Systems

Regarding the seasons winter and spring (December–April), the averaged global radiation of the reference period was above the one of the future period. Nevertheless, from summer on until autumn (June–October) the diffuse radiation of the future period exceeded the one of the reference period. Hence, by applying the delta method, a total increase of ~ 19,7 kWh/m² per year ('kbu') could be shown within the study area (figure 43). Regarding the five selected members, an averaged increase of ~ 13,7 kWh/m² per year could be determined.

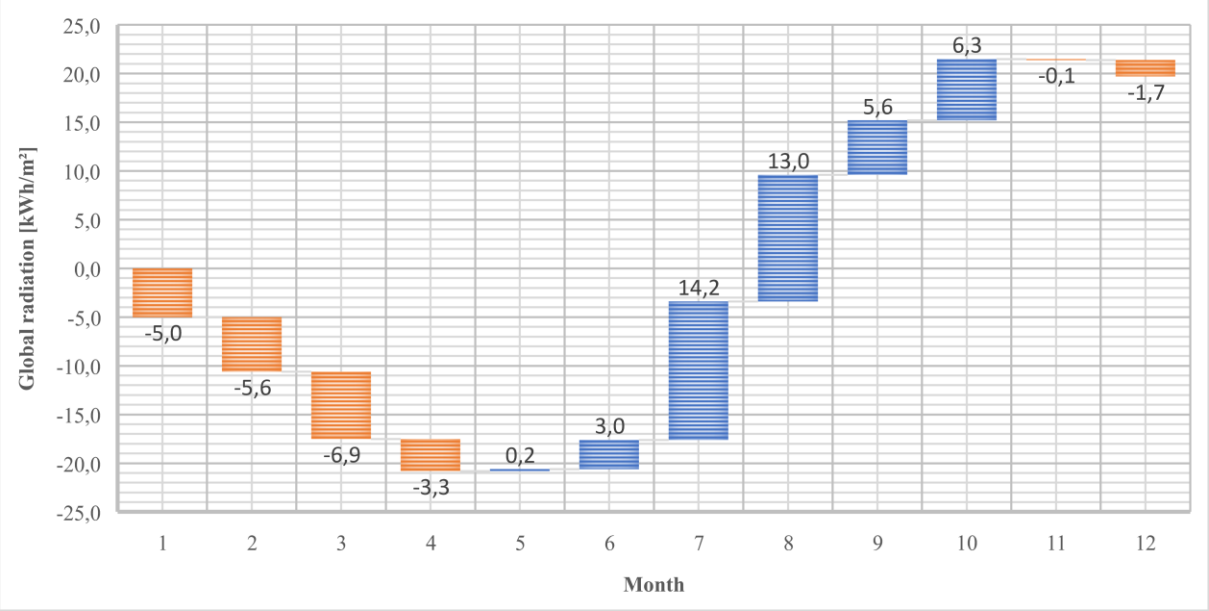

Figure 43 Change in global radiation in the future period (2071-2090) by applying the delta method. Source: Own figure

After adding the determined delta values on the global radiation of the present state, a change in the electrical energy output of the installed PV–modules within the adapted solar districts occurred. Based on this, the total theoretic power generation was calculated to ~ 496,3 GWh/a per year within the period 2071-2090. The performance ratio of real (regarding the present state) and theoretic (regarding the future state) electricity production amounted ~ 86 % on average.

According to chapter '*Solar energy*', the module temperature needed to be considered. Therefore, the delta of air temperature between reference and future period was added up to the temperature from the present sate. The obtained data was distributed according to the created and modified 11 catchment areas. By applying formula 13, it could be mentioned that indeed a chance of overheating will exist, which decreases the performance of a PV–module. With every degree above 25 °C the performance of a PV–module decreases around ~ 0,47 %. Except of the area Wolfsmünster, every catchment area will exceed the 25 °C-line (STC Conditions) in June, July and August. The area of Würzburg (T_M = 29,5 °C) illustrated the highest exceedance of up to Δ = 4,5 °C (figure 44).

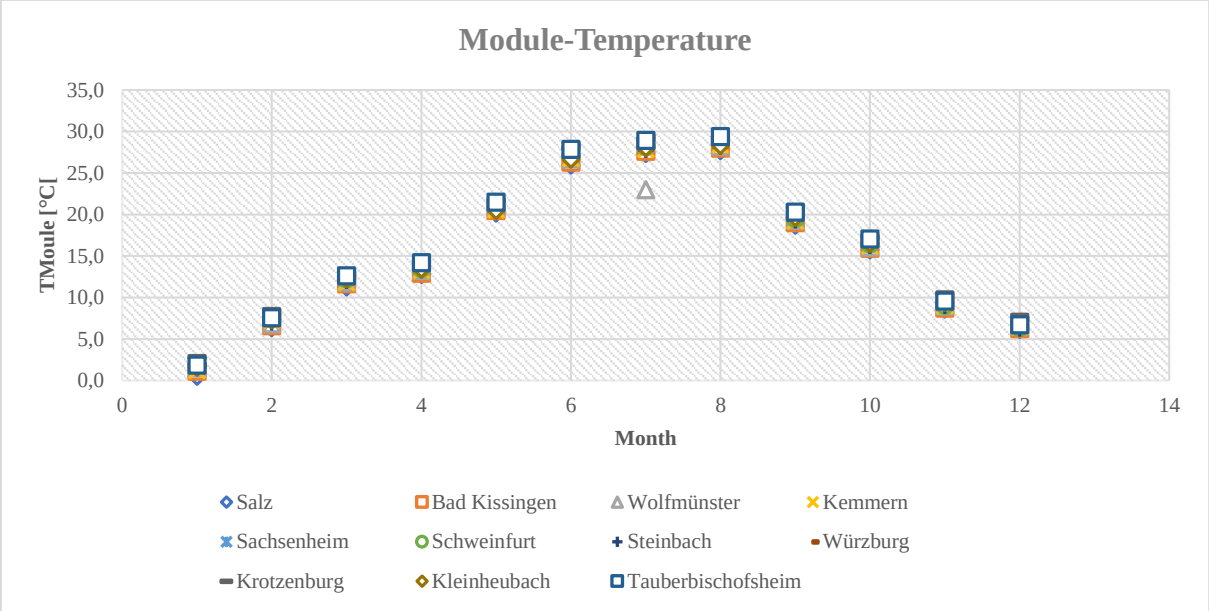

Figure 44 Chance of overheating of the PV - modules in the future period within the study area. Source: Own figure

By considering the power reductions, a different picture of the total and average power generation emerges. The 216 open-air plants would produce a total power generation of ~ 492,7 GWh/a. This corresponds to a power reduction caused by overheating of ~ 0,7% or ~ 3,6 GWh/a.

Having a more precise look on a single system, the effects of overheating and the distribution of the electricity production could be illustrated more detailed. The system is located in Aschaffenburg (49 ° 56 '38,9' 'N - 9 ° 6' 16,6 " E) within the catchment area Krotzenburg (ID_12). With an installed system of 321,3 kWp an electricity production of ~ 367,2 MWh per month could be generated, after power reduction by overheating. The peak of the energy generation corresponds to the maximum of global radiation within the course of a year and occurs in June. Within the months June (T_M = 28 °C), July (T_M = 29,1 °C) und August (T_M = 29,3 °C) the temperature of the module will lie above the 25 °C limit, which leads to a decrease in electricity production by ~ 1,41 % in June, by ~ 1,9 % in July and by ~ 2 % in August (figure 45).

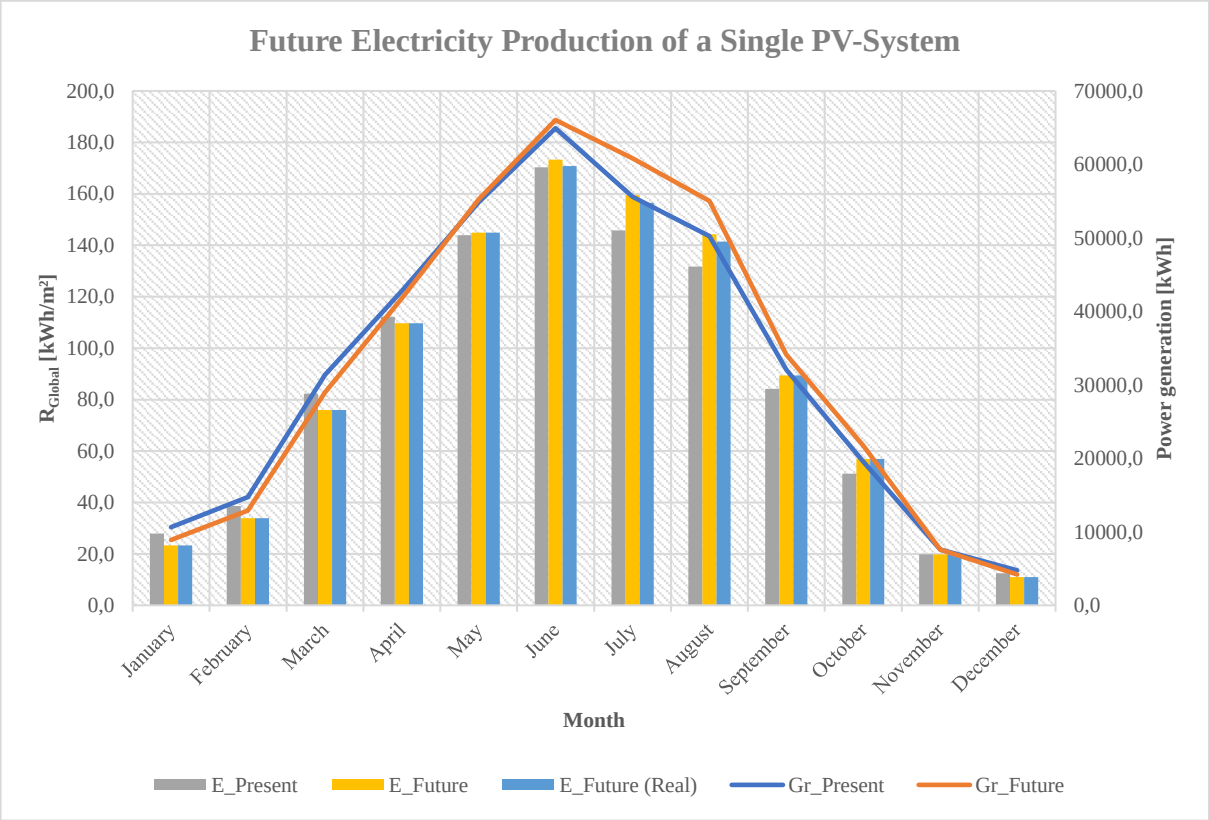

Figure 45 Distribution of global radiation and electric energy generation of a single PV-system located in Aschaffenburg. The colours blue and orange were defined as the global radiation in the present and future period. The colours of the bars grey, yellow and light blue were defined as the electric energy production of the present period (grey), the future period (yellow) without considering module overheating and the real future period (light blue) considering the chance of overheating. Source: Own figure

4.5.2 Future Energy Generation by Wind Turbines

Comparing both periods (reference and future), the wind speed rather slightly decreases. By observing the monthly individual values and applying the delta method, it was reflected that in the months November-February the wind speed of the future period is above the reference period and the present period. In the other months (February–October, except of May), however, a reduction was determined in this regard. Figure 46 shows the monthly increases and decreases according to the Delta method. For climate model member 'kbu', a future total decrease in wind speed of ~ - 0,22 m/s per year was determined. Based on all 5 selected members, the future averaged reduction is ~ 0,04 m/s.

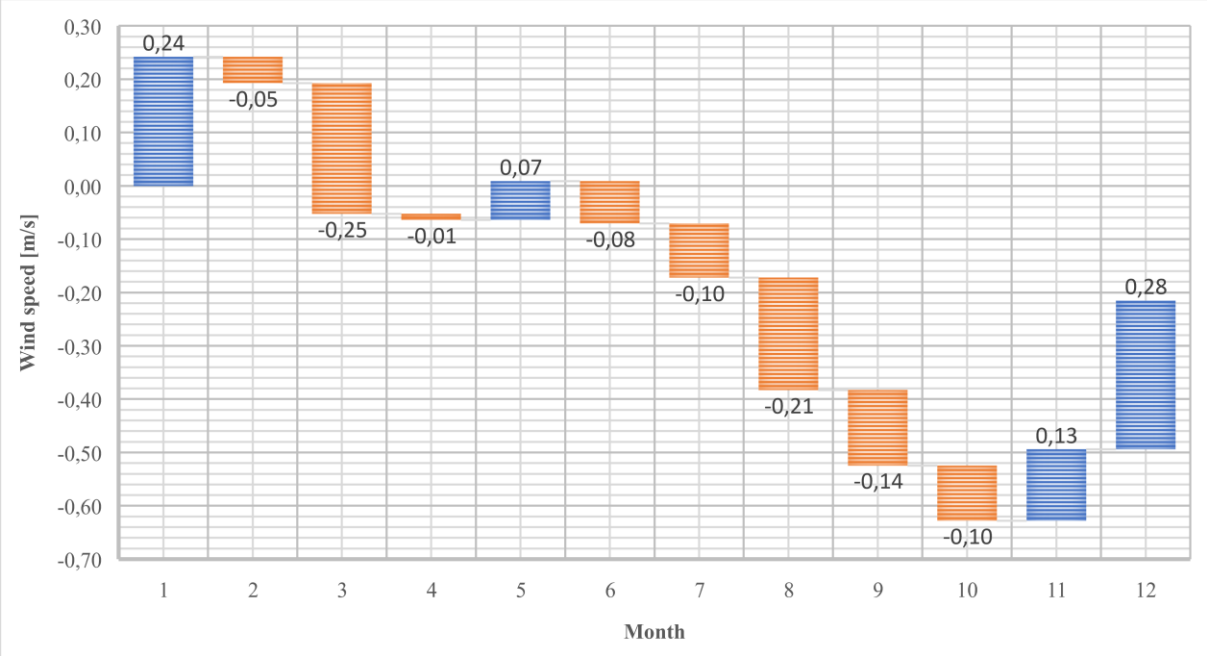

Figure 46 Change in wind speed in the future period (2071-2090) by applying the Delta method. Source: Own figure

After adding the determined delta values on the wind speed of the present state within the wind districts, a change in the energy output of the installed wind turbines will occur. Based on the calculated wind speeds in the different districts, the total theoretic power generation will be ~ 643,8 GWh/a within the time period 2071–2090.

In the subchapter '*Wind Turbines'*, a case study for a wind turbine (Maßbach) was executed based on wind speed parameters from the present state. Then, the same procedure according to the established power plan was executed, based on the calculated wind speed parameters for the future period. Therefore, the averaged wind speed per year was determined to ~ 2,88 m/s. By considering the turbine characteristics remain the same, except of the wind speed, there will be a slightly change in the relative and cumulative frequency regarding the wind speed distribution at the third decimal place, which directly affects the time the wind turbine is running in the course of the year (figure 47).

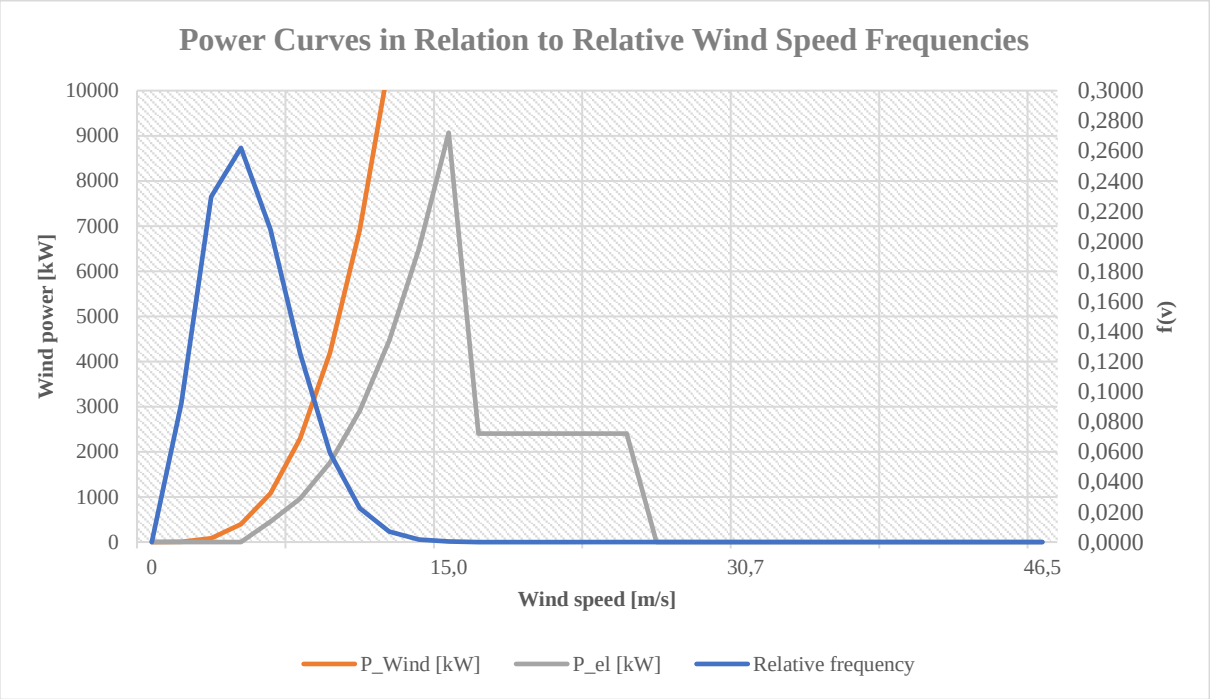

Figure 47 Wind power (P_Wind), extracted wind power (P_el) and relative frequency at a single wind turbine located in Maßbach with a hub height of 141 m, rotor diameter of 117 m and an installed capacity of 2400 kW in the future period (2071 - 2090). Source: Own figure

However, this will not have any impact on the wind power within the rotor area (extracted from the wind) and on the yielded electrical power, which was determined to ~ 9.069 kW (figure 48). Due to the change in relative frequency, the yielded accumulated energy will change over the course of the year. Hence, the annual energy output was determined to ~ 3.769 MWh/a (present period: 3.860 MWh/a), while the load factor does not change (figure 49).

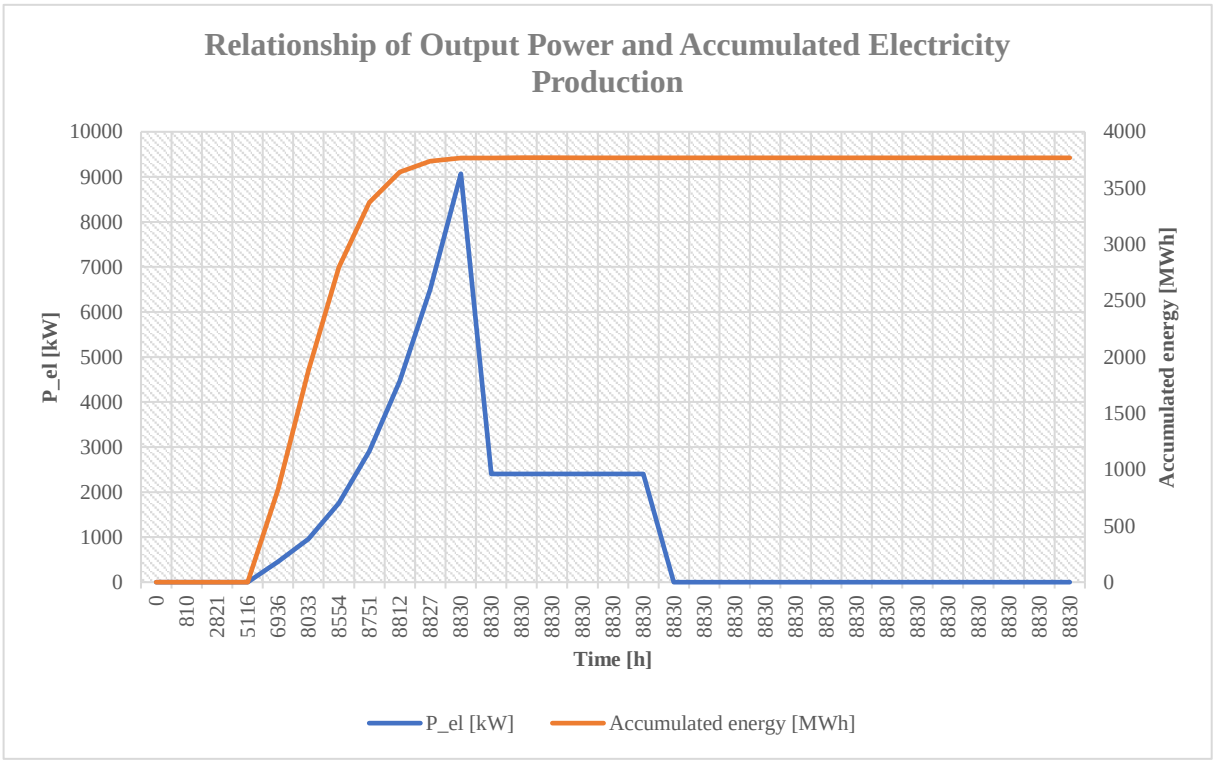

Figure 48 Extracted wind power and accumulated energy of the installed wind turbine located in Maßbach in the course of a year within the future period (2071 – 2090). Technical properties are the same as described in figure 47. Source: Own figure

Wind resource at location			**Wind resource at hub height**			**Wind turbine data**			**Power generation**	
v(mean) [m/s]	2,88		ref.Height) [m]	10		rotor dia [m]	117		rated capacity [kW]	2400
k	2		hub height [m]	141		cut-in speed [m/s]	4		production [MWh/a]	3769
A	3		roughness length [m]	0,1		design speed [m/s]	15		load factor [-]	0,179273195
			air density [kg/m³]	1,2		cut-out speed [m/s]	25			
						cp real	0,42			

speed at ref. Height	relative frequency	cumulative frequency	speed at hub height	P_wind [kW]	P_el [kW]	cp	time [h]	energy [MWh]	accumulated time [h]	accumulated energy [MWh]
0	0	0	0	0	0	0	0	0	0	0
0,5	0,09	0,02	0,8	3	0	0,00	810,1	0	810	0
1,5	0,23	0,19	2,4	85	0	0,00	2011,0	0	2821	0
2,5	0,26	0,45	3,9	394	0	0,00	2294,9	0	5116	0
3,5	0,21	0,69	5,5	1080	454	0,42	1820,3	826	6936	826
4,5	0,13	0,85	7,1	2295	964	0,42	1097,2	1058	8033	1883
5,5	0,06	0,94	8,7	4190	1760	0,42	520,3	916	8554	2799
6,5	0,02	0,98	10,2	6916	2905	0,42	197,4	573	8751	3372
7,5	0,01	1,00	11,8	10625	4462	0,42	60,5	270	8812	3642
8,5	0,00	1,00	13,4	15466	6496	0,42	15,1	98	8827	3740
9,5	0,00	1,00	15,0	21592	9069	0,42	3,1	28	8830	3768
10,5	0,00	1,00	16,5	29154	2400	0,08	0,5	1	8830	3769
11,5	0,00	1,00	18,1	38302	2400	0,06	0,1	0	8830	3769
12,5	0,00	1,00	19,7	49188	2400	0,05	0,0	0	8830	3769
13,5	0,00	1,00	21,3	61963	2400	0,04	0,0	0	8830	3769
14,5	0,00	1,00	22,8	76778	2400	0,03	0,0	0	8830	3769
15,5	0,00	1,00	24,4	93784	2400	0,03	0,0	0	8830	3769
16,5	0,00	1,00	26,0	113131	0	0,00	0,0	0	8830	3769
17,5	0,00	1,00	27,6	134973	0	0,00	0,0	0	8830	3769
18,5	0,00	1,00	29,1	159458	0	0,00	0,0	0	8830	3769
19,5	0,00	1,00	30,7	186739	0	0,00	0,0	0	8830	3769
20,5	0,00	1,00	32,3	216967	0	0,00	0,0	0	8830	3769
21,5	0,00	1,00	33,9	250292	0	0,00	0,0	0	8830	3769
22,5	0,00	1,00	35,4	286866	0	0,00	0,0	0	8830	3769
23,5	0,00	1,00	37,0	326840	0	0,00	0,0	0	8830	3769
24,5	0,00	1,00	38,6	370365	0	0,00	0,0	0	8830	3769
25,5	0,00	1,00	40,2	417592	0	0,00	0,0	0	8830	3769
26,5	0,00	1,00	41,7	468672	0	0,00	0,0	0	8830	3769
27,5	0,00	1,00	43,3	523757	0	0,00	0,0	0	8830	3769
28,5	0,00	1,00	44,9	582997	0	0,00	0,0	0	8830	3769
29,5	0,00	1,00	46,5	646543	0	0,00	0,0	0	8830	3769

Figure 49 Power plan of a single wind turbine located in Maßbach in the course of a year within the future period (2071 - 2090). Source: Own figure

4.5.3 Future Energy Generation by Run-of River Plants

As mentioned in subchapter '*Discharge*' differences in discharge between the single members occurs. With reference to the climate model member 'kbu' displaying the averaged delta between reference and future period of all catchment areas, through which the river Main runs, a significant decrease of discharge became recognizable throughout the year. The total decrease was determined to ~ 269,9 m³/s per year. By considering all 5 members an average future decrease of ~ - 40,5 m³/s was calculated (figure 50).

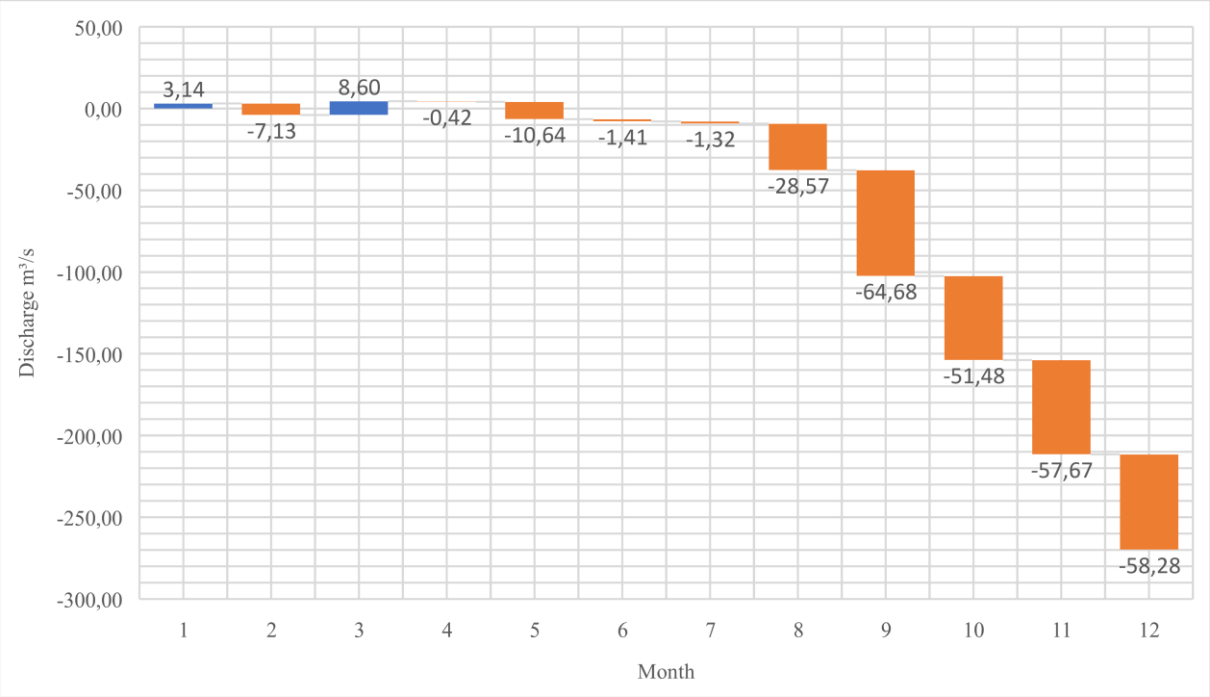

Figure 50 Changes in discharge in the future period (2071 - 2090) by applying the delta method. Source: Own figure

As for the other climate parameters, the delta between reference and future period was added up to the present discharge (2000–2019). This leads to an obvious change in the energy output of the installed run–of river plants (installed capacity > 1 MW) along the river Main, which were statistically analysed by a differentiation as in the chapter '*Run-of-River Plants'*. Except of the discharge and water level values, the properties of the existing hydro power plants remained the same.

1. General power generation per year within the future period 2071-2090 of the 28 run of river plants
2. Power generation per year within future period of five selected run–of–river plants
3. Power plan of the run–of–river plant Limbach (future period)

1. General power generation

It could be assumed that there will be numerous modernizations of existing run-of-river hydropower plants or new buildings in the next 52 years. Therefore, the average existing efficiency of ~ 66 % is neglected and the power and energy generation was presented based on an efficiency of ~ 85 %. Thus, based on the future runoff and water level according to the delta method and the existence of the usable fall height, a total power of ~ 134,6 MW/a and a total power generation of ~ 913 GWh/a will be obtained.

2. Power generation of selected run – of – river plants

Figure 51 shows the averaged power output of the selected run–of–river plants assuming an efficiency of 85 % within the time period (2071–2090), displaying a similar picture as for the power output according to present climate variables with maximum runoff in winter and minimum runoff in summer. It was noticeable that the power generation in the month of September drops again. The overall maximum and minimum occur at the hydro power plant Klingenberg. Thereby, the maximum appears in January with a power of ~ 10,1 MW and the minimum arises in September with a power generation of ~ 838 kW.

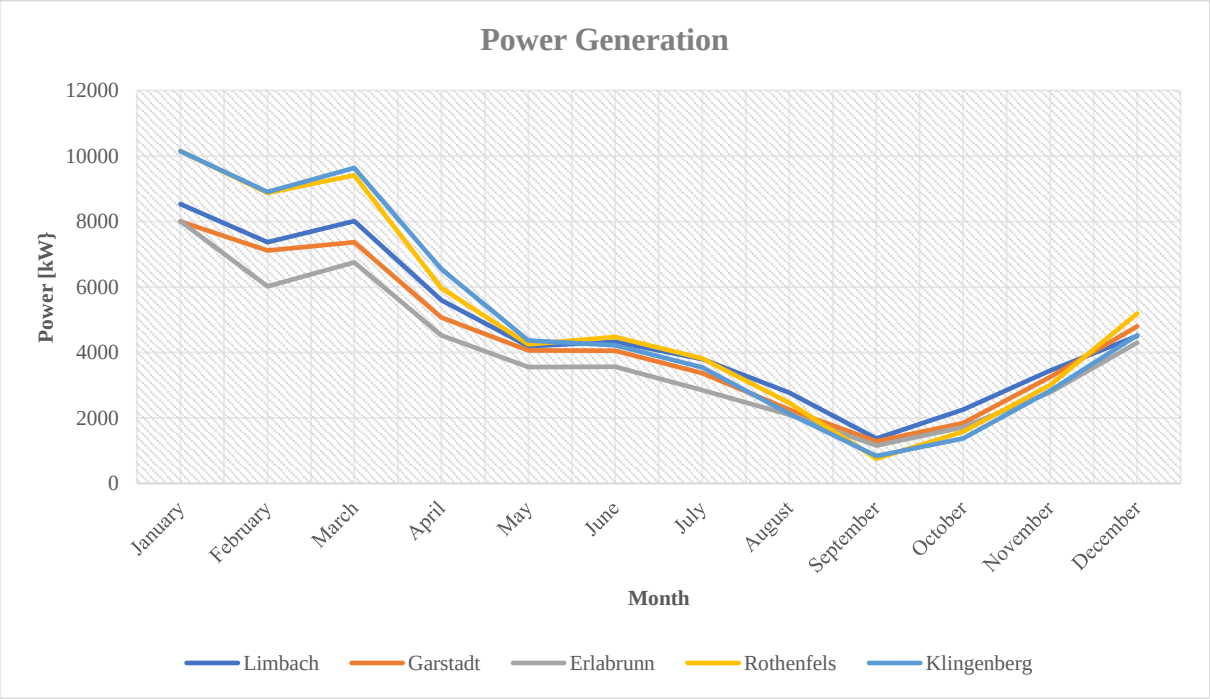

Figure 51 Power generation of the five selected run-of-river plants along the river Main in the future period (2071-2090). Source: Own figure

Figure 52 illustrates the yearly performance in the future for the five selected run–of–river plants. Beside the climate parameters, the properties of the hydro power plants remained the same. A total performance output of ~ 22,8 MW/a and a total energy generation of ~ 157,6 GWh/a could be determined.

Run of river plant	Gauging station	Head [m]	load hours [h]	Performance_future (μ=0,85) [kW]	Energy generation_future (μ=0,85.) [GWh]
Limbach	Trunstadt	5,36	6730	4682	31,5
Garstadt	Schweinfurt	4,69	5897	4373	25,8
Erlabrunn	Würzburg	4,15	7296	3881	28,3
Rothenfels	Steinbach	5,26	7214	4994	36,0
Klingenberg	Kleinheubach	4	7300	4920	35,9
Mean			***6888***		
Total				**22,8 MW**	**157,6 GWh**

Figure 52 Performance and electric energy generation of the five selected run-of-river plants within the future period (2071 - 2090). Source: Own figure

3. Case study - Run–of–river plant Limbach

Figure 53 displays the theoretical power plan of the run–of–river plant Limbach in the future period (2071–2090) assuming that, except of the discharge and water level, the design values, as design discharge and design head of the hydro power plant remained the same. The hydro power plant is located in the catchment area Schweinfurt and the regarding data for discharge provided by the climate model, or rather by the water balance model, was averaged on a daily basis within the future period. By applying the delta method between reference and future period and adding the difference on the present water level, following statements regarding the future could be made: The mean discharge ranges between 267,4 – 0 m³/s, whereas the mean water level will have a range between 279 – 0 cm. The water bed of both, upstream and downstream, calculated after Manning-Strickler (Jirka, 2007) (formula 41), remained the same, because of unchanged conditions in width and slope. The tailwater level downstream will range between 31 – 0 cm. Regarding the effective head of the power plant, the head duration curve runs between 5,23 – 5,53 m. A performance duration curve could be determined with a range between 4678 – 0 kW.

Regarding these observations, the design discharge will be exceeded for 147 days in the course of a year. On this day the maximum power will be generated, which could be determined to 4.678 kW. By the end of a year, the water level decreased to 0 kW, which leads to the assumption that no power could be generated anymore.

By comparing both power plans within the periods 2000–2019 and 2071–2090, significant differences could be noticed. Within the course of a year, the river Main carries more water in the beginning, which could be seen in the higher discharge, water level and tailwater level in the first days. However, throughout the year these parameters will decrease faster, with the result, that the degree of expansion will be reached earlier than in the present period (present period 174 days > future period 147 days). This statement is accompanied by the fact that the average outflow will decrease in the future. Despite the fact that in peak times more power could be generated comparing both periods (future period ~ 4.678 KW > present period 4.647 KW), no discharge will occur on day 365, resulting in a dried out river-bed. A total production of ~ 1,3 GW was determined. It must be mentioned that the current efficiency of the installed run–of–river plant was determined to a mean of ~ 68 %. Since it can be assumed that the existing plants will be modernised in future, the efficiency of the Limbach run-of-river power plant was set at 85 %. Otherwise, the generated power would be smaller in peak and average.

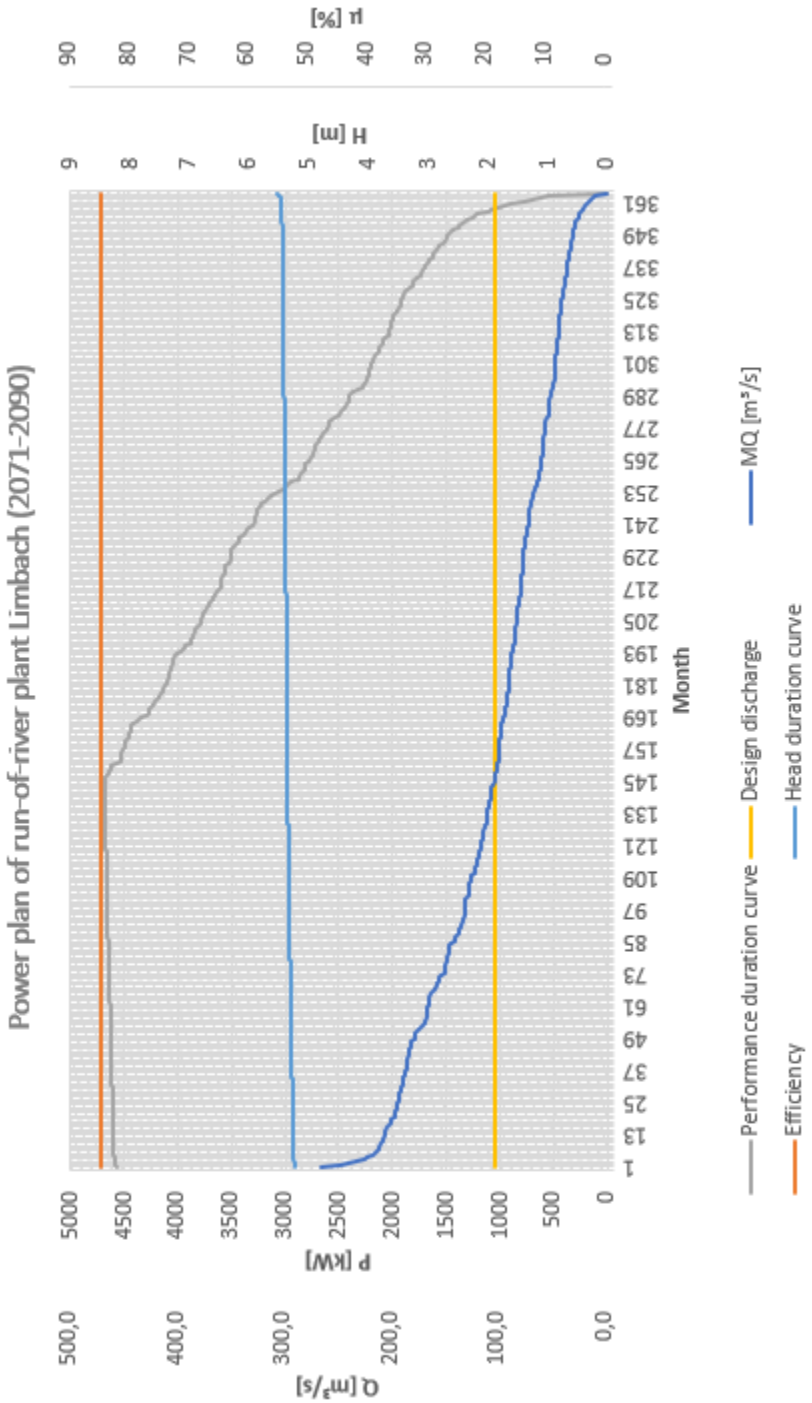

Figure 53 Power plan of the run-of-river plant Limbach in a year (exceedance lines) in the future period (2071-2090). Source: Own figure

4.6 Comparison of Electric Energy Generation between Present State and Future State

Within this chapter, the power generation of the three selected regenerative energy sources were compared regarding the present period and the future period. As mentioned, it was assumed, that the technological properties of the systems remained the same. Therefore, the most important variable factor were the climate parameters. Displayed in table 13, following systems were considered within the study area. 216 open–space PV–modules, 261 wind turbines and 28 run–of–river plants of more than 1 MW installed capacity.

Table 13 Change in electric energy generation of the three selected regenerative energy systems (PV, Wind and hydro power) between the present period (2000 – 2019) and the future period (2071 – 2090). Source: Own table

System	***Present period***	***Future period***
PV–modules [GWh]	489,3	492,7
Wind turbines [GWh]	645,2	643,8
Run–of–river plants [GWh]	1059,2	913

Despite of the fact that overheating of the PV–modules will occur (particularly in the summer months), open-space PV–systems will yield an overall increase of ~ 3,4 GWh/a in electricity production in the future, resulting in change of ~ 0,7 %. This calculated yield could be supported by the knowledge that the global radiation will also slightly increase in future. The distribution of the performance of a PV–module is according to the global radiation in the course of a year. This finding is supported by having a look on single system. Comparing the individual PV–systems located in Aschaffenburg with an installed capacity of 132,3 kWp, a decrease of electricity production of ~ 4,6 MWh/a occurs within both periods (present and future). This results in a production change of ~ 1,3 %. The distribution of global radiation and performance remains the same with a peak in June and minimums in the winter months.

Regarding wind turbines within the study area, a decrease of ~ 1,4 GWh/a in electrical energy generation will occur in total, resulting in a change of ~ 0,2 %. This determined fact goes along with the knowledge of a slight decrease in wind speed in the future. Concerning the comparison between both periods of a single wind turbine in Maßbach with unchanged technical conditions, a decrease in electricity production of ~91 MWh/a could be determined. This results in a production change of ~ 2 %

The highest change in electrical energy generation was investigated for run–of–river plants. Comparing both periods a decrease of ~ 146,2 GWh/a will occur which supports the fact of a strong decrease in discharge in the future. The decrease in total electricity production results in change of ~ 14 %. Having a look on the run–of–river plant at Limbach a decrease in total production of ~ 190,6 MW/a occurs, resulting in change of ~ 13 %.

After all, it could be stated, that overall a slight increase of ~ 0,7 % in electricity production by PV–systems will occur, whereas a reduction of ~ 0,2 % in wind electricity and ~ 14 % in hydroelectricity was determined.

5 Conclusions and Forecast

In today's political discourse, the issue of climate change is attracting a high attention. In order to achieve the self-imposed goals for global warming, a rethinking in the production and consumption of energy is needed, which is now described as the ‘Energiewende’.

The aim of this paper was to analyse and describe the relationships between climate variables and renewable energy systems. For this purpose, the administrative district of Lower Franconia was used as the study area. Climate variables were described in a 20-year cycle within three different periods. On the one hand, climate measurements by the DWD and the HND were used to break down the study area and divide it into different catchment areas, depending on their geographical, climatological and energetic attributes. Based on this, performance plans were drawn up to break down and evaluate the energy production from solar power, wind power and hydropower in detail. On the other hand, the climate model CanESM2 was used to represent a future climate projection. It was noticeable that the calculated climate variables of both methods differed, which can be traced back to the different approaches and uncertainties. By adapting the climate catchment areas of both approaches, a delta method could be used to apply the future climate parameters to the already installed regenerative energy systems. A comparison of the present and future energy production could then be made. In general, it could be found that climate variables change locally and cannot be generalized regionally. Overall, there will be an increase in global radiation and temperature in the future period (2071-2090). This has a positive effect on the yield of PV systems in terms of electricity production. The production increases by ~ 0,7 % compared to today, despite the possible reduction in output due to overheating of PV modules. The wind force, on the other hand, stagnates or even weakens slightly. This is reflected in a reduction of the output of ~ 0,2 % for the wind turbines, which are already installed. A drastic reduction can be assumed with regard to the runoff and the associated water level. This would be accompanied by a ~ 14 % reduction in hydroelectricity generation. As there are 52 years between the two examined periods, these calculated values must be viewed objectively. It can be assumed that the technologies of renewable systems will develop further in the future.

PV-Systems:

The generation of electricity by PV systems significantly depends on two factors: on the one hand the location and inclination of the installation with regard to incoming global radiation, and on the other hand on the properties of the module cells. Already installed systems are usually optimal, as far as the conditions allow, aligned to the south or east at an angle of ~ 30 degrees. However, there is still potential in electricity production by solar cells. The most common cell technology is based on silicon layers which, depending on the type (polycrystalline or monocrystalline), have an average efficiency of ~ 18 %. Technological progress should make it possible to increase efficiency in the future. Researchers at the ‘*Fraunhofer Institute for Solar Energy Systems’* are already researching a quadruple solar cell that makes it possible to convert ~ 46 % of the radiation into energy (Deutsche Handwerkszeitung, 2015). This consists of a combination of different semiconductor materials, such as gallium indium phosphide, gallium indium arsenide and germanium. The use of new technologies is usually associated with economic profitability. If solar cells can be produced cost-effectively with more effective radiation conversion, the potential yield of a PV-module could increase further. In addition to efficiency, module temperature also plays an important

role in such systems. As mentioned above, a module temperature above 25 °C leads to a reduction in performance. This is also where research could begin. Ventilation systems below modules, for example, could reduce the temperature on a module caused either by heat accumulation or high air temperatures.

Wind turbines:

The energy yield of a wind turbine depends to a large extent on the location and properties of the turbine. The locality is decisive for the occurring and useable wind speeds, with regard to geographical and topographical location. In addition to the climate parameter, however, the energy generation is also related to the size of the turbine erected. Wind speeds increase with altitude and it is therefore logical that higher turbines can also guarantee higher energy production. In addition to the hub height, the rotor diameter also plays an important role. As the diameter of the rotor blades increases, the collecting surface increases, which can be used to withdraw energy from the wind and convert it into power. In addition to the components mentioned, the amount of energy generated also depends on the parameters for which the turbine is designed, such as the design-speed. If the design-speed of a turbine is set higher as the used design speed of 15 m/s within this work, a higher electrical output could be generated. Beside these facts, the efficiency rate of a turbine could be increased by improving the converter technologies. Although the technical prerequisites to increase the performance are in place, the construction of new wind turbines or larger plants depends to a large extent on the political plan and the involvement of the society. Based on citizens' decisions and lawsuits, a plan will be adopted in the near future which foresees that wind turbines may only be erected at a minimum distance of 1.000 m to the nearest village. This would have the consequence that the planning areas could be reduced by 20-50 % and the construction of new wind turbines would probably stagnate (Ostendorf, 2019).

Run–of–river plants:

Hydropower plants depend to a large extent on three variables: the discharge, the effective head and the efficiency. The discharge of a river is influenced by a number of complex systems. On the one hand, there are climate parameters such as effective precipitation and evaporation, on the other hand there is the river catchment area where characteristics, such as geological, geographical, and topographical ones, must be taken into account. The discharge and the accompanying water level are also reflected in the effective head. However, the effective head also depends on the construction method of a hydroelectric power plant. Up to a certain point, a higher head is characteristic for a higher energy generation. The river Main is mostly home to older hydropower plants. These are based on a design runoff and water level of earlier times, since the prediction possibilities were limited at that time. Likewise, the efficiency is usually very low compared to more modern hydropower plants (80-90 %). Due to the outdated design parameters, the following approaches could be used to counteract this reduction in output: the efficiency could be increased by modernising existing hydropower plants which would lead to higher energy generations. It would be possible as well to transform existing transverse structures into hydropower plants to exploit the existing potential of the river. Further options were an increase in the water retention target and the increase in the degree of expansion. However, these possibilities heavily depend on governmental agencies, society, and especially on environmental agencies. A not negligible fact is the future reduction of runoff. In the future projections it could be seen that the discharge in the summer months is strongly reduced what leads to low water phases. If a river leads little water, this can have effects on both: the ecology,

concerning flora and fauna, and on the economy, concerning transport and hydroelectricity generation. As illustrated in the power plan of the run–of–river plant Limbach, one day per year the river does not carry any water.

High fluctuations in wind power and PV yields are currently a problem for the basic supply. Only hydropower plants, depending on the type, in the renewable energy sector would be able to handle a base load, but this would not be sufficient for the entire energy consumption. This thesis showed that wind and sun are to a certain extent balanced out in terms of fluctuations, i.e. there is a negative correlation between the respective offers. As already mentioned, the yield of both systems (PV and wind) depends strongly on regional factors. Strong wind fluctuations occur more frequently in the winter months, resulting in higher expected yields at this time of the year. Strong deviations related to the average yields of PV–systems occur mostly in summer. However, despite the negative correlation, there might be strong fluctuations in the sum of wind power and solar power. Regarding hydro power, higher discharges will occur in spring when the snow is melting at higher topographies and lower discharges appear in late summer and autumn. Beside the temporal variations, the energy supply of these regenerative systems is also subject to spatial fluctuations. Due to the greater proximity to the equator, higher global radiation occurs in the south of the study area than in the north. The wind is also spatially influenced depending on the topography. To counteract these fluctuations, electricity storage facilities would be unavoidable to make full use of the provided potential (Grotz, 2012). If this is achieved, these forms of regenerative systems (PV, wind turbines and hydro power), could replace fossil fuels for the most part.

6 References

AGEB Arbeitsgemeinschaft Energiebilanzen (2015). *Bruttostromerzeugung in Deutschland ab 1990 nach Energieträgern.*

Basso, S., & Botter, G. (2012). Streamflow variability and optimal capacity of run-of-river hydropower plants. *Water Resources Research*, *48*(10).

Bayerische Staatsregierung. (2017). Energieatlas Bayern: Bayerisches Staatsministerium für Wirtschaft, Landesentwicklung und Energie. Retrieved from https://geoportal.bayern.de/energieatlas-karten/?wicket-crypt=v4_quvVNjy0

Bayerisches Landesamt für Umwelt (2018a). Auswirkungen auf die Wasserbilanz.

Bayerisches Landesamt für Umwelt (2018b). Das weiß-blaue Klima. Retrieved from https://www.lfu.bayern.de/wasser/klima_wandel/bayern/index.htm

BDEW Bundesverband der Energie- und Wasserwirtschaft (März 2018). *Installierte Wind und PV Leistung.*

Behrendt, J., Penda, E., Finkler, A., Heil, U., & Polte-Rudolf, C. (2011). *Beschreibund der Datenbasis des KKDZ.*

Blasy, L., & Overland, H. (2005). *Wasserhaushaltsmodell ASGI für das Flussgebiet Unterer Main.: Datenaufbereitung*. Eching.

Brasseur, G. P., Jacob, D., & Schuck-Zöller, S. (2017). *Klimawandel in Deutschland: Entwicklung, Folgen, Risiken und Perspektiven*: Springer.

Bundesministerium für Umwelt, Naturschutz und Reaktorsicherheit (2010). *Potentialermitlung für den Ausbau der Wasserkraftnutzung in Deutschland als Grundlage für die Entwicklung einer geeigneten Ausbaustrategie: Schlussbericht*. Aachen.

Burger, B. (2019, July 3). *Stromerzeugung in Deutschland im ersten Halbjahr 2019*. Freiburg.

Christoffer, J., & Ulbricht-Eissing, M. (1989). Die bodennahen Windverhältnisse in der Bundesrepublik Deutschland: Berichte des Deutschen Wetterdienstes.

Deutsche Handwerkszeitung (2015, January 14). Solarzelle - neue Entwicklung bricht Weltrekord beim Wirkungsgrad. *Deutsche Handwerkszeitung*.

Drews, A., Keizer, A. C., Beyer, H. G., Lorenz, E., Betcke, J., van Sark, W., . . . Toggweiler, P. (2007). Monitoring and remote failure detection of grid-connected PV systems based on satellite observations. *Solar energy*, *81*(4), 548–564.

Dubbel, H. (2013). *DUBBEL: Taschenbuch für den Maschinenbau*: Springer-Verlag.

DWD (1989). *Deutsches Meteorologisches Jahrbuch*. Offenbach a. Main.

DWD (2019). Wetter und Klima vor Ort: Würzburg. Retrieved from https://www.dwd.de/DE/wetter/wetterundklima_vorort/bayern/wuerzburg/_node.html.

DWD Climate Data Center (2019). FTP-Verzeichnis/ climate_environment/CDC: Observations germany. Retrieved from ftp://opendata.dwd.de/climate_environment/CDC/

Freydank, E. (2014). *150 Jahre staatliche Wetter-und Klimabeobachtungen in Sachsen: Ergänzungs- und Sondernetze, Messungen in der freien Atmosphäre*: Institut für Hydrologie und Meteorologie.

Fyfe, J. C., Derksen, C., Mudryk, L., Flato, G. M., Santer, B. D., Swart, N. C., . . . Arora, V. K. (2017). Large near-term projected snowpack loss over the western United States. *Nature communications*, *8*, 14996.

Gasch, R., & Twele, J. (2010). *Windkraftanlagen: Grundlagen, Entwurf, Planung und Betrieb*: Springer-Verlag.

Gebhardt, H., Glaser, R., Radtke, U., & Reuber, P. (2007). *Geographie: Physische Geographie und Humangeographie*: Elsevier.

Geoffrey, P., Hammond, P. J., & Pearson, M. (2013). *Energy Policy: Challenges of the transition to a low carbon, more electric future: From here to 2050.* (52nd ed.).

Gerstengarbe, F. W., & Peter, W. (2007). Der rezente Klimawandel.

Gewässerkundlicher Dienst Bayern (2019). Wasserstand Unterer Main. Retrieved from https://www.gkd.bayern.de/de/fluesse/wasserstand/main_unten

Giesecke, J., Heimerl, S., & Mosonyi, E. (2014). *Wasserkraftanlagen: Planung, Bau und Betrieb*: Springer-Verlag.

Goetzberger, A., & Stahl, W. (Eds.) (1985). *Global estimation of available solar radiation and cost of energy for tracking and non-tracking PV-systems.*

Google. (2019). Google Earth Pro: Google Earth.

Google Maps. (2019). *Route: Viereth - Krotzenburg: Höhendifferenz entlang des Main*: Google. Retrieved from https://www.google.de/maps/

Grotz, B. (2012). *Untersuchung der Korrelationen zwischen Wind - und Solarangebot mit spezieller Berücksichtigung von Extremwetterlagen* (Diplomarbeit).

Hasenfratz, E. (2006). *Die Rolle der Globalstrahlung im Klimasystem Südwestdeutschlands: vergleichende statistische Untersuchungen zu ihrer raumzeitlichen Variabilität.*

Heier, S. (2013). *Windkraftanlagen im Netzbetrieb*: Springer-Verlag.

Hellmann, G. (1915). *Über die Bewegung der Luft in den untersten Schichten der Atmosphäre (1. Mitt.)*: Meteorol.

Hochwassernachrichtendienst Bayern (2019). Pegel Meldestufen Unterer Main.

Hoff, A. M. (1987). *Ein analytisches Verfahren zur Bestimmung der mittleren horizontalen Windgeschwindigkeiten über zweidimensionalen Hügeln*: Institut für Meteorologie und Klimatologie der Univ.

Hörstmann-Jungemann, P. (2005). *Wie funktioniert eine Silizium Solarzelle: Solarbrief 2/05*. Aachen.

IPCC (2007). *Climate Change: The physical science basis.*

Jacobsson, S., & Lauber, V. (Eds.). (2006). *3. Energy Policy: The politics and policy of energy system transformation - explaining the German diffusion of renewable energy technology* (34th ed.): Elsevier.

Jirka, G. H. (2007). *Einführung in die Hydromechanik*: KIT Scientific Publishing.

Kaltschmitt, M. (2006). Regenerative Energien zur Stromerzeugung I. *Skriptum zur Vorlesung, Institut für Energiewirtschaft und Rationelle Energieanwendung, Universität Stuttgart, WS 00/01*.

Kleemann, M., & Meliß, M. (2013). *Regenerative Energiequellen*: Springer-Verlag.

Koethe, H. K. (1982). Practice of electric energy supply by solar and wind power. Praxis solar-und windelektrischer Energieversorgung.

Kuchling, H. (1994). *Taschenbuch der physik*: Fachbuchverl.

Leduc, M., Malihot, A., Frigon, A., Braun, M., Schmid, J., Sushama, L., . . . Ludwig, R. (Eds.) (2016). *The ClimEx Project: Dynamical downscaling of a GCM large ensemble at very high resolution for Bavaria and Quebec.*

Leduc, M., Malihot, A., Frigon, A., Martel, J., Luwig, R., Brietzke, G. B. [G. B.], . . . Braun, M. (2019). The ClimEx Project: a 50-member ensemble of climate change projections at 12-km resolution over Europe and Northeastern North America with the Canadian regional climate model (CRCM5). *Journal of Applied Meteorology and Climatology*, *58*(4).

Liu, B. Y., & Jordan, R. C. (1960). The interrelationship and characteristic distribution of direct, diffuse and total solar radiation. *Solar energy*, *4*(3), 1–19.

Meaden, G. T., Kochev, S., Kolendowicz, L., Kosa-Kiss, A., Marcinoniene, I., Sioutas, M., . . . Tyrell, J. (2007). Comparing the theoretical versions of the Beaufort scale, the T-Scale and the Fujita scale. *Atmospheric research*, *83*(2-4), 446–449.

Miller, K. A., & Yates, D. (2005). Climate Change and Water Resources: A Primer for Water Utilities.

Molly, P. J. (1990). *Windenergie: Theorie-Anwendung-Messung*: Muller.

Müller-Westermeier, G. (1995). Numerisc hes Verfahren zu Er stellung klimatologischer Karten. Bericht des Deutschen Wet-ter dienstes. *Offenbach am Main: Selbstverlag des Deutschen Wetterdienstes*.

Niebert, K. (2010). Den Klimawandel verstehen Eine theoriegeleitete und evidenzbasierte Entwicklung von Interventionen.

Niederberger, J. (2000). *Räumiche Interpolation von Niederschlag und Klimadaten* (Diplomarbeit). Albert-Ludwigs-Universität Freiburg i.Br., Freiburg.

Nordex (2019). Windenergieanlagen. Retrieved from http://www.nordex-online.com/de/produkte-service/windenergieanlagen.html

Ostendorf, S. (2019, November 16). Die Folgen von 1000 m Abstand. *Tagesschau*.

Pryor, S. C., & Barthelmie, R. J. (2010). Climate change impacts on wind energy: A review. *Renewable and sustainable energy reviews*, *14*(1), 430–437.

Pvamanarhan, V., Barksrrom, B. R., & Harruison, E. F. (1989). Climate and the Earth's radiation budget. *Physics Today*, 20.

Quaschning, V. (2008). *Erneuerbare Energien und Klimaschutz*: Hanser.

Quaschning, V. (Ed.). (2015a). *Regenerative Energiesysteme. Technologie - Berechnung - Simulation.*

Quaschning, V. (2015b). *Regenerative Energiesysteme: Technologie-Berechnung-Simulation*: Carl Hanser Verlag GmbH Co KG.

Quaschning, V., Geuder, N., & Ortmanns, W. (2002). Vergleich und Bewertung verschiedener Verfahren zur Solarstrahlungsbestimmung.

Ragheb, M. (2012). Wind shear, roughness classes and turbine energy production.

Raicu, A. (Ed.) (1992). *Realistic reporting conditions–RRC–for site-dependent energy rating of PV devices.*

Rapp, J. (2000). *Konzeption, Problematik und Ergebnisse klimatologischer Trendanalysen fur Europa und Deutschland*: Offenbach a. M.: Selbstverl. des Dt. Wetterdienstes.

Riahi, K., Krey, V., Rao, S., Cho, C., Chirkov, V., Fischer, G., . . . Rafaj, P. (2011). RCP 8.5—A scenario of comparatively high greenhouse gas emissions. *Climatic Change*, *109*(1-2), 33.

Rudolf, B., Hauschild, H., Reiss, M., & Schneider, U. (1992). Die Berechnung der Gebietsniederschläge im 2, 5-Raster durch ein objektives Analyseverfahren. *Meteorologische Zeitschrift*, 32–50.

Schaefer, H. (1994). Opportunities for and limits of renewable energy use; Moeglichkeiten und Grenzen der Nutzung regenerativer Energien.

Schiffer, H. (Ed.). (2019). *Energiemarkt Deutschland: Daten und Fakten zu konventionellen und erneuerbaren Energien*. Wiesbaden: Springer Fachmedien Wiesbaden.

Schröder, W., Euler, G., Schneider, F., & Knauf, D. (1982). *Grundlagen des Wasserbaus*: Werner.

Schubert, G. (2012). Modellierung der stündlichen Photovoltaik-und Windstromeinspeisung in Europa. *Graz, Austria, Feb*.

Schulla, J. (1997). *Hydrologische Modellierung von Flussgebieten zur Abschätzung der Folgen von Klimaänderungen.* ETH Zurich.

Schulla, J. (1998). *Modellbeschreibung WaSiM-ETH: unveröffentlicht.* ETH Zürich, Zürich.

Shell Solar (2006). *Shell SP140 Photovoltaik Solarmodul: Produktinformation*. Draft.

Shockley, W. (1953). Electrons and holes in semiconductors: with applications to transistor electronics.

Stocker, T. (2014). *Climate change 2013: the physical science basis: Working Group I contribution to the Fifth assessment report of the Intergovernmental Panel on Climate Change*: Cambridge University Press.

Strobl, T., & Zunic, F. (2006). *Wasserbau*: Springer.

Sze, S. M., & Ng, K. K. (2006). *Physics of semiconductor devices*: John wiley & sons.

Taylor, K. E., & Penner, J. E. (1994). Response of the climate system to atmospheric aerosols and greenhouse gases. *Nature*. (6483), 3–734.

Troen, I., & Petersen, E. (1989). *European wind atlas*: Risø National Laboratory.

Vischer, D., & Huber, A. (2013). *Wasserbau: Hydrologische grundlagen, elemente des wasserbaus, nutz-und schutzbauten an binnengewässern*: Springer-Verlag.

Wasser- und Schifffahrtsverwaltung des Bundes (Juni 2003). Daten und Fakten.

Wind power program (2019). Turbine characteristics: Wind turbine power output variation with steady wind speed.